JPL PUBLICATION 82-104

The Deep Space Network — A Radio Communications Instrument for Deep Space Exploration

N.A. Renzetti
C.T. Stelzried
G.K. Noreen
S.D. Slobin
S.M. Petty
D.L. Trowbridge
H. Donnelly
P.W. Kinman
J.W. Armstrong
N.A. Burow
M.K. Tam
J.W. Layland
A.L. Berman

July 15, 1983

NASA
National Aeronautics and
Space Administration

Jet Propulsion Laboratory
California Institute of Technology
Pasadena, California

JPL PUBLICATION 82-104

The Deep Space Network — A Radio Communications Instrument for Deep Space Exploration

N.A. Renzetti
C.T. Stelzried
G.K. Noreen
S.D. Slobin
S.M. Petty
D.L. Trowbridge
H. Donnelly
P.W. Kinman
J.W. Armstrong
N.A. Burow
M.K. Tam
J.W. Layland
A.L. Berman

July 15, 1983

National Aeronautics and
Space Administration

Jet Propulsion Laboratory
California Institute of Technology
Pasadena, California

The research described in this publication was carried out by the Jet Propulsion Laboratory, California Institute of Technology, under contract with the National Aeronautics and Space Administration.

PREFACE

This report is one in a series of four that have been published by the Jet Propulsion Laboratory to describe the capabilities of the Deep Space Network as of the early 1980s. The others are:

1) The Deep Space Network -- An Instrument for Radio Science Research (JPL Publication 80-93)

2) The Deep Space Network -- An Instrument for Radio Astronomy (JPL Publication 82-68)

3) The Deep Space Network -- An Instrument for Radio Navigation of Deep Space Probes (JPL Publication 82-102)

Those developments of the various elements that compose a Deep Space Communications Station and that have made it possible to increase communication capability from space to earth by a factor of 100 in the last ten years are presented. This remarkable performance increase is due in large part to a vigorous and imaginative research and technology development activity sponsored by the NASA Office of Space Tracking and Data Systems at the Jet Propulsion Laboratory.

Although the Network operates in the microwave region of the electromagnetic spectrum wherein the effects of the media between the spacecraft and Earth operating at distances to the edge of the Solar System are minimal, considerable research and development has been accomplished in understanding the effects of the atmosphere and charged particles of the ionosphere and interplanetary regions on the radio links.

ACKNOWLEDGMENT

R. C. Clauss, M. Koerner, and B. Buckles provided technical contributions. M. S. Tucker, B. A. White, and B. F. Larkin shared in the typing. D. Maple provided editorial assistance.

CONTENTS

CONTENTS (cont'd)

CONTENTS (cont'd)

ABSTRACT

The Deep Space Network is the National Aeronautics and Space Administration (NASA) telecommunications instrument for deep space exploration. Communications are provided between spacecraft and the various Network ground facilities. The uplink communications channel provides instructions or commands to the spacecraft. The downlink communications channel provides command verification and spacecraft engineering and science instrument payload data.

The Network evolved from the Microlock tracking and data acquisition system developed by JPL in support of the flight of the first U.S. earth orbiter, Explorer I, in 1958. In the last decade, spacecraft tracked by the Network have encountered all but the three outermost planets of our solar system. In the latter half of this decade, the Network will face the very exciting and exceedingly challenging task of supporting the Voyager 2 spacecraft as it flies by Uranus (1986) and Neptune (1989).

The Network consists of a sophisticated tracking network incorporating state-of-the-art large antennas, ultra-low-noise amplifiers, precision phase-locked receivers, transmitting equipment and telemetry error-correction systems. This report presents the history, theory, and implementation of each of these separate systems. Particularly emphasized is the history and theory of system performance in terms of the telemetry data rate and receiving system figure of merit. In addition, anticipated future Network capabilities are discussed. This includes arraying techniques with other very large non-NASA radio telescopes as necessary to support the Voyager Uranus and Neptune encounters, and the upgrade to X-band uplink and K_a-band telecommunications.

I. INTRODUCTION

N. A. Renzetti and C. T. Stelzried

A. PURPOSE

The primary purpose of the Deep Space Network (DSN) is to serve as a communications instrument for deep space exploration. It provides communications between the spacecraft and the ground facilities. The uplink communications channel provides instructions or commands to the spacecraft. The downlink communications channel provides command verification and spacecraft engineering and science instrument payload data (Refs. 1-1, 2 and 3).

B. HISTORY

The Network is a continuously evolving facility (Ref. 1-4). It grew out of the Microlock tracking and data acquisition system developed by JPL in support of the flight of the first U.S. earth orbiter, Explorer I, in 1958 (Ref. 1-5). This system was inadequate for communicating at lunar and planetary ranges and was supplanted by the TRAC(E) (Tracking and Communication, Extraterrestrial) receiving system later that year (Ref. 1-6). From that time, the Network has developed into a sophisticated telecommunications network incorporating state-of-the-art large antennas, low-noise amplifiers, receiving systems, and transmitting equipment (Refs. 1-1, 7).

The Network has played a crucial role in all deep space missions undertaken by the United States in addition to supporting the Apollo manned spacecraft project. In the past ten years, spacecraft tracked by the Network have encountered all but the three outermost planets of our solar system, and two of these will be encountered before 1990. The Network will support the Voyager 2 spacecraft as it flies by Uranus and Neptune in 1986 and 1989, respectively. References 1-8 through 1-12 give detailed accounts of past encounters.

Communicating with deep space probes requires extraordinary system performance since the amount of data that can be successfully received from a spacecraft decreases as the square of the distance between the spacecraft and the earth. For example, the range between a deep space probe at Saturn and

its ground station on Earth is greater than the range between a satellite in geosynchronous orbit and its ground station by a factor of about 4×10^4 - hence an improvement in performance of 1.6×10^9 is necessary to receive the same amount of data from Saturn as could be received from geosynchronous orbit. To enable reception of an adequate data rate at ranges greater than 1 billion kilometers, the Network has developed extremely sensitive and powerful instruments for deep space communications. Over the first twenty years of the existence of the Network, the figure-of-merit M (a measure of system sensitivity, see Section II) of the ground receiving stations has increased by a factor of 10^5 - an astounding increase averaging over 2 dB per year (Fig. 1-1). This improvement has been achieved through continual development of new, high performance equipment operating at ever-higher frequencies. Table 1-1 shows the operating frequency increase of Network receivers from 108 MHz in 1958 to 8415 MHz currently.

C. OVERVIEW

Network complexes are approximately equally spaced around the world so that probes far from earth are always in view of at least one complex as long as they remain near the equatorial plane of the earth. Each complex includes one 64-m-diameter parabolic dish antenna and several smaller antennas along with associated subsystems (Fig. 1-2). The combination of a particular antenna and its associated subsystems is referred to as a Deep Space Station (DSS).

Communications between the earth-based station and the spacecraft are classified as one of two processes: the uplink process, denoting the generation and communication of commands to the spacecraft, and the downlink process, or telemetering of data from the spacecraft. The Network is an integral part of both of these communication processes. In the uplink process, commands are generated by the flight project, processed by the Mission Control and Computing Center (MCCC) at JPL and relayed by the Ground Communications Facility (GCF) to the Network for transmission to the spacecraft (Fig. 1-3). Similarly, telemetry is received by Network antennas,

relayed over the GCF to MCCC for processing and sent to the flight project. Network operations and scheduling are handled by the Network Operations Control Center (NOCC) at JPL.

Both the uplink and the downlink processes require long strings of equipment operating in series. The successful operation of the communications process requires adequate performance from each of the components of the end-to-end system through which commands and data pass. In this document we are primarily concerned with those telecommunications processes that are carried out by the Network. In the following sections, we discuss the function of each part of the Network that operates in the communication link with a spacecraft.

REFERENCES

1-1. Renzetti, N. A., A History of the Deep Space Network, from Inception to January 1, 1969, Technical Report 32-1533, Jet Propulsion Laboratory, Pasadena, Calif. Sep. 1, 1971.

1-2. Renzetti, N. A., et al, "Communications at Planetary Distances," Presented at the International Convention on Radio Communications at Great and Very Great Distances," Roma-Pontecchio Marconi-Bologna, Italy, March 29, 1974.

1-3. Yuen, J. H., editor, Deep Space Telecommunications Systems Engineering, Publication 82-76, Jet Propulsion Laboratory, Pasadena, Calif., July 1982.

1-4. Corliss, W. R., "A History of the Deep Space Network", NASA Document CR-151915, May 1, 1976.

1-5. Rechtin, E., "Communication Techniques for Space Exploration," IRE Trans. Space Electron. Telem., Sep. 1959.

1-6. Brockman, M. H., et al., "Extra-Terrestrial Radio Tracking and Communication," IRE Proceedings, Vol. 48, No. 4, Apr. 1960.

1-7. Edelson, R. E., et al., "Voyager Telecommunications: The Broadcast from Jupiter," Science, Vol. 204, June 1, 1979.

1-8. Murray, B. C., and Burgess, E., Flight to Mercury, Columbia University Press, New York, 1977.

1-9. Carr, M. H., The Surface of Mars, Yale University Press, New Haven, 1981.

1-10 Morrison, D., and Samz, J., Voyage to Jupiter, NASA SP-439, U. S. Government Printing Office, Washington, D. C., 1980.

1-11 Morrison, D., Voyage to Saturn, NASA SP-451, U. S. Government Printing Office, Washington D.C., 1982.

1-12 Newell, H. E., Beyond the Atmosphere, NASA History Series. SP-4211, 1981.

Table 1-1. Deep Space Network Frequency First Usage History

Downlink frequency MHz	Receiver	Ground antenna diameter m	First spacecraft usage	Launch date
108	Microlock	a	Explorer I	January 1958
960	TRAC(E)	26	Pioneer III	December 1958
2295	Block I	26	Mariner IV	November 1964
8415	Block IV	64	Mariner X	November 1973

[a] Helical antenna

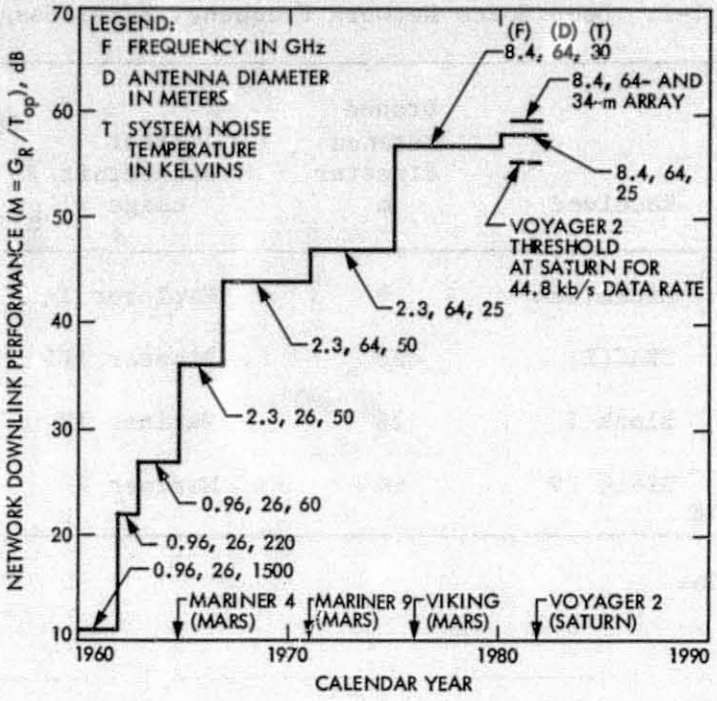

Fig. 1-1. Profile of the Deep Space Network downlink performance ($M=G_R/T_{op}$) from 1960 to 1982 (from Table 2-1)

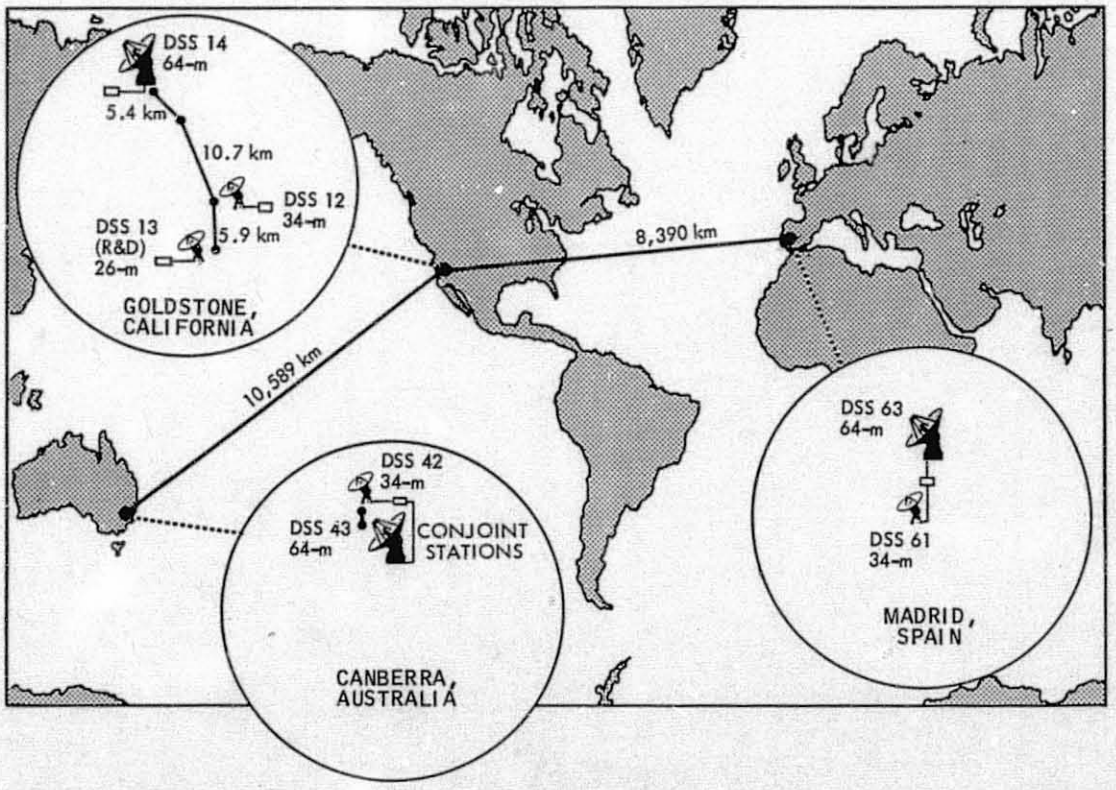

Fig. 1-2. 1982 Deep Space Network Complex configurations

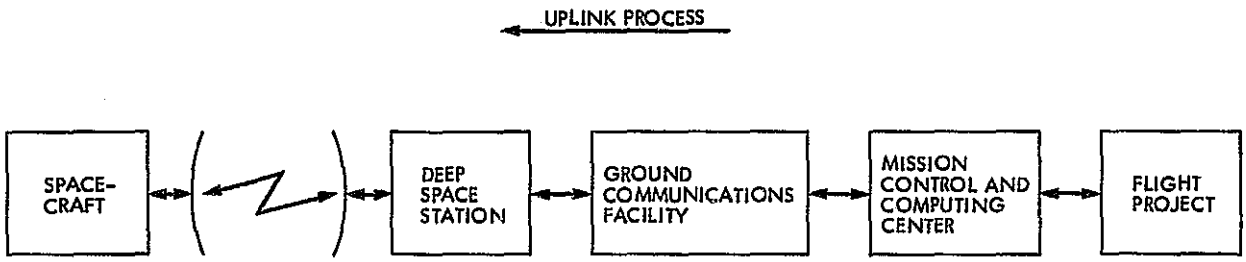

Figure 1-3. End-to-end flow of commands and telemetry to and from deep space

II. THE SYSTEM VIEW

G. K. Noreen and C. T. Stelzried

A. INTRODUCTION

This section provides an analysis of spacecraft-to-ground communications link performance and a description of the Deep Space Network system. Due to the tremendous distances involved in communicating between the spacecraft at the edge of our solar system and earth, communications link performance is stretched to the limit of theoretical predictions. This is required in order to return the maximum amount of data possible during critical events such as planetary flybys. The link analysis provides a basis for the initial link design before spacecraft launch and performance prediction and monitoring during spacecraft flight. Additionally, it indicates what performance upgrades are required for mission extensions and new missions. Performance can be improved through the use of a larger antenna collecting area, greater transmitter power, lower receiving system noise temperature and more sophisticated data coding schemes. Later in this section the performance of the Deep Space Station configuration which serves as the ground portion of the communications link is assessed. The Voyager 2 Saturn encounter link performance is analyzed to illustrate the relevant concepts. The following sections provide detailed descriptions of the Deep Space Station configuration, as well as the transmission media, and modulation and coding schemes appropriate to link performance characterization.

B. SPACECRAFT/EARTH LINK ANALYSIS

The objective of an analysis of the telemetry link is usually to determine the maximum bit rate that can be transmitted at a given time. Two conditions must be satisfied to ensure adequate reception of a particular data rate: the minimum received energy-per-bit-to-noise spectral density ratio (E_b/N_0, see Eq. 2-8) must be high enough to guarantee an acceptable bit error rate, and the received signal carrier-to-noise ratio must be high enough for the receiver to track the received signal carrier.

The required E_b/N_0 is dependent primarily on the type of coding used and on the maximum tolerable bit error rate (BER). For example, with an advanced Reed-Solomon/Viterbi concatenated code, an E_b/N_0 of 2.2 dB is sufficient to ensure a BER not exceeding 10^{-5} (Section VI) - assuming perfect carrier, subcarrier, and bit synchronization at the receiver.

Deep space telemetry is typically phase-shift-key modulated onto a squarewave subcarrier which is then phase modulated onto a carrier (Section VI). To demodulate the received signal, the receiver must first reconstruct the carrier and then use the reconstructed carrier to coherently demodulate the telemetry. Adequate performance of the demodulation process is thus crucially dependent on the ability of the receiver to track the carrier. This tracking function is performed by a phase-locked-loop (PLL) receiver (Section V).

In the following, it is shown that a useful figure of merit of a receiving system is given by $M = G_R/T_{op}$ (see Eq. 2-10). An expression is derived for the required figure of merit for a receiving system to support a given data rate. An example follows for the Voyager 2 1981 Saturn encounter; the required and actual receiving system figures of merits are compared and the performance margin is calculated.

1. Received Power

The first step in any telemetry link analysis is to calculate the received power.

$$P_R = P_T A_T A_R / L_{TR} (D\lambda)^2 \qquad (2\text{-}1)$$

where

P_R = received power, W

P_T = transmitted power, W

A_R = effective area of the receiving antenna, m^2

A_T = effective area of the transmitting antenna, m^2

D = distance between transmitter and receiver antennas, m

λ = carrier wavelength, m

L_{TR} = losses between the transmitter and receiver antennas (= 1 for an idealized system), ratio (≥ 1)

$= L_A L_P L_{POL}$

L_A = atmospheric loss (Section VIII), ratio (≥ 1)

L_P = pointing loss due to inaccurate pointing of the transmitting and receiving antennas, ratio (≥ 1)

L_{POL} = polarization loss due to the polarization mismatch between the transmitter and receiver antennas (Ref. 2-1), ratio (≥ 1)

2. Noise Spectral Density

Assuming that the noise in the receiving system has uniform spectral density (approximating white noise) in the frequency band containing the signal, the one-sided noise spectral density is

$$N_0 = kT_{op} \qquad (2\text{-}2)$$

where

N_0 = one-sided noise spectral density, W/Hz

k = Boltzmann's constant, 1.3806×10^{-23} J/K

T_{op} = system operating noise temperature, K

T_{op} includes (Ref. 2-2) contributions from the cosmic background radiation, atmosphere (Section VIII), ground radiation, transmission line losses, the low-noise maser amplifier (Section IV) and the follow-on receiver.

3. Carrier Margin

Carrier margin M_c on either the uplink or downlink is defined as

$$M_c = \frac{P_c}{2\ B_{LO}\ N_0} \qquad (2\text{-}3)$$

where

P_c = portion of received power in the residual carrier, W

B_{LO} = one-sided threshold loop noise bandwidth, Hz

P_c is calculated from P_R based on the modulation indices of the link.

The above definition of carrier margin was chosen because a phase locked loop receiver loses lock when P_c drops below $2\ B_{LO}\ N_0$ watts. Thus, $P_c = 2\ B_{LO}\ N_0$ defines carrier threshold. M_c is often defined in terms of

$$\text{Carrier SNR in } 2\ B_{LO} = \frac{P_c}{2\ B_{LO}\ N_0} \qquad (2\text{-}4)$$

However, this is a misnomer since $B_{LO}\ N_0$, not $2\ B_{LO}\ N_0$, is the noise power in a thresholding loop. So "Carrier SNR in $2\ B_{LO}$" equals one-half the carrier signal-to-noise ratio in a threshold loop.

The minimum acceptable carrier margin, in general, is greater than 1 and is usually greater than 10.

4. Telemetry Performance

The signal energy per bit per noise spectral density at the receiver input is given by

$$ST/N_0 \qquad (2\text{-}5)$$

where

S = portion of received signal power in the data modulation sidebands, W
  $= P_R \sin^2\theta$
θ = modulation angle, degrees (typically, $20^\circ < \theta < 80^\circ$)
T = time per bit, s
  = 1/R
R = data rate, bps

For system performance calculations, the signal energy per bit per noise spectral density at the receiver output is

$$ST/N_0L_s \qquad (2\text{-}6)$$

where

L_s = system losses, ratio (≥ 1)

System losses are due to suboptimal demodulation of the signal. They are caused by such degraded conditions as a low carrier margin, which makes coherent detection difficult.

Threshold ST/N_0L_s at the receiver output, or E_b/N_0, is determined by the maximum bit error rate that can be tolerated and by the error-correcting code(s) protecting the link, as noted earlier. With a Reed-Solomon/Viterbi concatenated code, the bit error rate will not exceed 10^{-5} as long as the signal energy per bit per noise spectral density receiver at the output, $ST/N\ L_s$, does not drop below 2.2 dB (assuming perfect synchronization), the threshold signal energy per bit per noise spectral density at the receiver output, E_b/N_0 (Fig. 6-4).

Thus the maximum data rate R that can be tolerated given that the carrier margin is adequate is

$$R \leq S/[N_0 L_s E_b/N_0] \tag{2-7}$$

where

E_b/N_0 = threshold signal energy per bit per noise power density, ratio

As an example, the maximum data rate is found from Eqs. (2-1) and (2-7).

$$R_{max} = P_T A_T A_R/[LkT_{op}(D\lambda)^2 E_b/N_0] \tag{2-8}$$

where

L = total telemetry link loss, ratio (≥ 1),
$= L_{TR} L_s L_M$

L_M = (P_R/S), ratio (≥ 1),
$= 1/\sin^2\theta$

5. Receiving System Figure of Merit

Equation (2-8) can be written

$$R_{max} = M\ P_T A_T/[4\pi kLD^2 E_b/N_0] \tag{2-9}$$

where

M[1] = figure of merit, ratio (≥ 1),
$= (G_R/T_{op})$

G_R = effective gain of the receiving antenna, ratio (≥ 1),
$= 4\pi A_R/\lambda^2$

---

[1] For an "optimized" array, with individual antenna figures of merit M_i, $M = \sum_{i=1}^{n} M_i$ (Ref. 2-3).

Alternately, the required figure of merit for the receiving system is given by

$$M = (G_R/T_{op}) \geq 4\pi kRLD^2(E_b/N_0)/P_T A_T \qquad (2\text{-}10)$$

The system operating noise temperature (defined at the same input reference plane as the antenna gain, typically at the maser input for the Network) is given by

$$T_{op} = T_C + T_{ATM} + T_{GD} + T_L + T_M + T_F \qquad (2\text{-}11)$$

where

T_C = noise temperature contribution of the cosmic background, K (≃ 2.7 K at 2.3 GHz)

T_{ATM} = noise temperature contribution of the atmosphere, K (≃ 4.9 K for Goldstone at 8.5 GHz, "90% weather" and 30° elevation)

T_{GD} = noise temperature contributed by the ground, K

T_L = noise temperature contribution of the transmission line components between the antenna and the first low noise amplifier (maser), K

T_F = noise temperature contribution of the follow-on receiver, K

The Network downlink performance figure of merit comprising both antenna gain (Section III) and system operating noise temperature (Sections IV and VIII) is tabulated in Table 2-1 from 1960 to 1982.

C. THE DEEP SPACE NETWORK

1. Introduction

The downlink communications process begins with the collection and formatting of data by the spacecraft data system. The spacecraft telecommunications system encodes, modulates, and transmits the data. The data are first encoded for efficient transmission, then used to phase modulate a square wave subcarrier which in turn phase modulates the carrier as discussed in Section VI. The resultant signal is amplified and transmitted. A simplified

block diagram of the telemetry processing flow is shown in Fig. 2-1. A low-noise traveling wave maser amplifies the signal received by the network antenna and routes it to a receiver, which tracks the carrier and translates the signal to an intermediate frequency coherent with the station reference. The Subcarrier Demodulator Assembly (SDA) translates the signal to baseband and demodulates the subcarrier. The output of the SDA is synchronized by the Symbol Synchronizer Assembly (SSA), and decoded by the Maximum Likelihood Decoder (MCD) if the spacecraft used a convolutional code. Finally, decoded data are formatted by the Telemetry Processor Assembly (TPA) and sent to JPL over the Ground Communications Facility (GCF).

The involvement of the Network in the uplink process begins with the reception of commands from the originating agency over the GCF. Commands are processed by the Command Processor Assembly, and used by the Command Modulator Assembly (CMA) to phase modulate a subcarrier. The subcarrier modulates a carrier in the Exciter Assembly prior to amplification and transmission to the spacecraft. The command process is described in detail in Section IX.

2. Network Complexes and Antennas

The Network has three complexes (Fig. 1-2) located at Goldstone, California (Fig. 2-2), Canberra, Australia (Fig. 2-3), and Madrid, Spain (Fig. 2-4), about 120° apart in longitude and at about 35° to 40° latitude - two in the northern hemisphere and one (Canberra) in the southern hemisphere. These locations provide continuous contact with spacecraft in deep space in or near the ecliptic plane.

Each complex has a 64-m antenna (Fig. 3-1) and a 34-m antenna (Fig. 3-6). The 26-m antennas (Fig. 3-3) and their supporting facilities were removed from the operational network in December 1981 as an economy measure. Goldstone has a 26-m research antenna (Station 13) used to support Network development.

The antennas and facilities at Goldstone are located in separate sites. At Canberra and Madrid, they are located about 200 to 400 meters apart and are supported from common facilities called conjoint stations.

The control console for the Goldstone 64-m antenna, Station 14 is shown in Fig. 2-5. During the process of a spacecraft tracking operation, the station is controlled from this console. The staff shown is representative of a routine tracking operation.

The complexes are connected by the Ground Communications Facilities (GCF) using NASCOM communication links to the Network Operations Control Center (NOCC) and the Mission Control and Computing Center (MCCC) at JPL located in the Space Flight Operations Facility (SFOF).

The Network control console in the JPL Space Flight Operations Facility is shown in Fig. 2-6. Consoles for individuals working with each of the active complexes are shown in the background. Also located in the SFOF are these facilities: (1) the Ground Communications Facility terminal providing the interface between the Control Center and the stations and (2) the Network Data Processing Area (NDPA) which has the equipment necessary to monitor, record, and validate data from the stations. Scheduling and tracking predicts are also supplied by the Processing Area.

Each station provides two-way phase coherent communications with the spacecraft at S-band (2.1 GHz uplink 20 kW, and 2.3 GHz downlink) and downlink only at X-band (8.4 GHz). In addition, the 64-m stations provide 100-400 kW RF power for uplink emergency spacecraft commanding and special open loop receivers (Section V) for radio science measurements.

The Goldstone 64-m antenna also has a sophisticated planetary radar capability for scientific measurements and for Network systems development and demonstration.

The Australian and Spanish stations each share a single control room in the conjoint configuration for the 34-m and 64-m antennas. The single control room at each of these complexes has individual sets of receiving, transmitting and tracking electronic equipment associated with each antenna. Some functions such as the hydrogen frequency based timing system are shared.

The function of the reflector antennas as used in the Network (Section III) is to capture a portion of the signal transmitted by the spacecraft. The antennas use subreflectors in a Cassegrainian configuration to focus this signal into the feed horn and maser amplifier located in the cone attached to the surface of the dish. A reflex feed system is used to provide simultaneous S- and X-band signal reception in separate receiving systems.

3. Masers

Low noise maser amplifiers (Section IV) and follow-on receiving systems (Section V) are used to amplify the signal received by the antenna with a minimum of noise contamination.

The cryogenically cooled maser solid state amplifiers produce extremely low noise amplification through the process of transforming energy from a radio frequency pump to the signal frequency. This is accomplished through a process of stimulated emission in a cooled ruby crystal material immersed in the proper magnetic field.

The Goldstone 64-m antenna S-band receiving system has achieved a system noise temperature of 13 K with a maser noise temperature contribution of about 2 K in a special low noise configuration. The present 64-m antenna systems typically have an X-band (8.4 GHz) system noise temperature of about 20 K at zenith with a maser noise temperature contribution of about 3.5 K.

4. Receivers and Exciters

Different types of follow-on receiver-exciters are used in the Network for various purposes. The exciter and the tracking receiver-exciter provide the capability, with other elements of the Network, to command the spacecraft and to receive telemetry and radio metric data. The major exciter and receiver assemblies for these functions are:

(1) Exciter. Generates a carrier, modulated with command and ranging signals, to drive the transmitter amplifier.

(2) Phase Tracking Receiver. Maintains phase lock with the spacecraft downlink carrier, generating a reference signal required to coherently detect telemetry and ranging modulation signals for telemetry and radio metric data processing.

(3) Doppler Extractor. Generates a doppler signal from the exciter reference and receiver signals.

(4) Subcarrier Demodulation Assembly (SDA). Coherently translates the telemetry subcarrier to baseband and demodulates the subcarrier for data extraction.

The block IV receiver subsystem incorporates Subcarrier Demodulator Assemblies as general-purpose, mission-independent devices capable of meeting the requirements of all projects at any Network station. This requires standardized subcarrier modulation schemes by the flight projects, such as the widely used bi-phase modulation with digital data (see Section VI). The subcarrier demodulator design handles high doppler rates with the use of a third-order tracking loop. The receiver intermediate frequency (IF) bandwidth required for a particular data rate is given by (Section V)

$$\text{Data Bit Rate (b/s)} = \frac{\text{Receiver Channel Bandwidth (Hz)}}{30 \text{ to } 150} \qquad (2\text{-}12)$$

Demodulation loss is related to symbol rate and E_b/N_0.

5. Symbol Synchronizer Assembly (SSA)

The function of the SSA is to perform symbol/bit synchronization and detection (conversion of the demodulated baseband analog signal to digital bits). The present SSA upper symbol rate capability is 250 K symbols/s. Since all other components of the Network receiving system can handle higher symbol rates, the SSA presently determines the upper limit on the Network data rate (125 Kb/s for rate 1/2 coding).

6. Maximum Likelihood Convolutional Decoders (MCD)

Coding schemes are used to reduce bit error probability in digital communications systems or to maintain the same bit error probability with reduced link capability compared to uncoded performance. Coding can improve system performance approximately 2 to 7 dB. This improvement is seen by plotting the bit error rate performance of coded and uncoded systems versus the energy per data bit to noise spectral density ratio (Section VI).

The cost to the communications system is in added bandwidth so that a higher channel rate in symbols/s is required as compared to the original data rate in bits/s. This requires greater hardware data handling capability as well as greater complexity of the decoding process.

An extremely powerful coding technique to be used for the Voyager 2 encounter of Uranus and Neptune and other future deep space missions is the "Reed-Solomon (block coding)/Viterbi (convolutional coding) concatenated code" (Section VI). In this scheme a Reed-Solomon outer code and a convolutional inner code are interleaved (Figs. 2-7 and 8). This technique combines the advantages of each coding method; the interleaving reduces the effect of "bursty" errors.

The function of the Maximum Likelihood Convolutional Recorder hardware is to decode the Viterbi (convolutional) code. The Reed-Solomon (block) decoding and de-interleaving are presently achieved in software by the flight project.

7. Telemetry Processing Assembly (TPA)

The function of the Telemetry Processing Assembly is to format the telemetry data in appropriate block sizes with the addition of the block serial number, time, header and ending. The block header contains such information as spacecraft identification number, destination code, etc. This data is then transferred via the Ground Communication Facility (GCF) to the Jet Propulsion Laboratory.

D. VOYAGER: COMMUNICATING TO SATURN

Communications for the successful 1979 Voyager Jupiter flyby have been described in Ref. 2-4. The August 1981 Voyager 2 (Fig. 2-9) Saturn flyby (Fig. 2-10) with a telemetry data rate of 44.8 kb/s provides the most recent example of the spacecraft-to-Network downlink telemetry performance capability. Imaging telemetry was transmitted at X-band (8.42 GHz) and was convolutionally coded to ensure a bit error rate less than 5×10^{-3}. The required receiving system figure of merit is 55 dB (using the parameter values for Eq. 2-11 tabulated in Table 2-3 with a DSS 64-m antenna). The actual receiving system figure of merit $M = G_R/T_{op}$ of about 58 dB (tabulated in Table 2-1 and plotted in Fig. 1-1) obtained with the 64-m antenna provided about 3 dB link performance margin. This link margin is based on mean parameter values; adequate planned margin is required for variations in the actual parameter values - particularly the system noise temperature as a function of weather conditions.

Future (Section X) Uranus and Neptune flybys will require arraying techniques to obtain the total figure of merit required for the desired data rates at those distances. A Network array was demonstrated during the Voyager 2 Saturn flyby using a 64-m antenna and a 34-m antenna (Table 2-1 and Fig. 1-1). This resulted in a measured average increase in signal-noise ratio of about 0.6 dB relative to the 64-m antenna only (Ref. 2-5). Assuming 50% efficiency for both antennas and no array losses, the potential improvement was about 1.1 dB (Fig. 1-1). Future refinements of the array techniques should reduce the implied approximate 0.5 dB average loss.

REFERENCES

2-1. Hartop, R., Power Loss Between Arbitrarily Polarized Antennas, Technical Report 32-457, Jet Propulsion Laboratory, Pasadena, Calif., Sep. 1, 1964.

2-2. Stelzried, C., The Deep Space Network - Noise Temperature Concepts, Measurements, and Performance, Publication 82-33, Jet Propulsion Laboratory, Pasadena, Calif., Sep. 15, 1982.

2-3. Stelzried, C., Berman, A., and Noreen, G., "Antenna Arraying Performance of a Deep Space Telecommunications Systems," TDA Progress Report 42-72, Jet Propulsion Laboratory, Pasadena, Calif., Feb. 15, 1983.

2-4. Edelson, R. E., et al., "Voyager Telecommunications: The Broadcast from Jupiter," Science, Vol. 204, June 1, 1979.

2-5. Bartok, C. D., "Performance of the Real-Time Array Signal Combiner During the Voyager Mission," TDA Progress Report 42-63, Jet Propulsion Laboratory, Pasadena, Calif., June 15, 1981.

Table 2-1. Tabulation of the Deep Space Network operational measured downlink performance figure of merit ($M = G_R/T_{op}$) from 1960 to 1982

Parameter	Calendar Year								
	1960	1962	1963	1965	1967	1971	1975	1980-1982	
Frequency f, GHz	0.96	0.96	0.96	2.30	2.30	2.30	8.42	8.42	
System noise temperature T_{op},[a] K	1500	220	60	50	50	25	30	25	
Antenna diameter D_R, m	26	26	26	26	64	64	64	64	
Antenna gain G_R, dB	43	45	45	53	61	61	72	72	
Figure of merit ($M = G_R/T_{op}$), dB	11	22	27	36	44	47	57	58	59[b]

[a] Assumes "90% weather" (see Section VIII) and 30° elevation angle.

[b] Assumes arrayed network 64- and 34-m antennas.

Table 2-2 Qualitative comparison of block and convolutional coding techniques

Characteristics	Coding	
	Block	Convolution
Data	Sequential (quick-look advantages)	Nonsequential
Performance	Closed form	Difficult (generally requires computer simulation)
Performance quality		Generally superior
Implementation		Generally simpler

Table 2-3 Tabulated Voyager 2 spacecraft Saturn fly-by (August 1981) X-band (8.42 GHz) downlink parameters

Parameter	Value
Transmitter power (P_T),	21.3
Spacecraft antenna effective area (A_T), m^2	5.4
Distance (D), m	1.557×10^{12}
Total link loss (L), ratio	1.1
Data rate (R), b/s	4.48×10^4
Threshold signal to noise ratio for 5×10^{-3} BER $(E_b/N_o)_T$, ratio	1.8
Threshold figure of merit calculated from Eq. 2-11, (M_T),dB	55

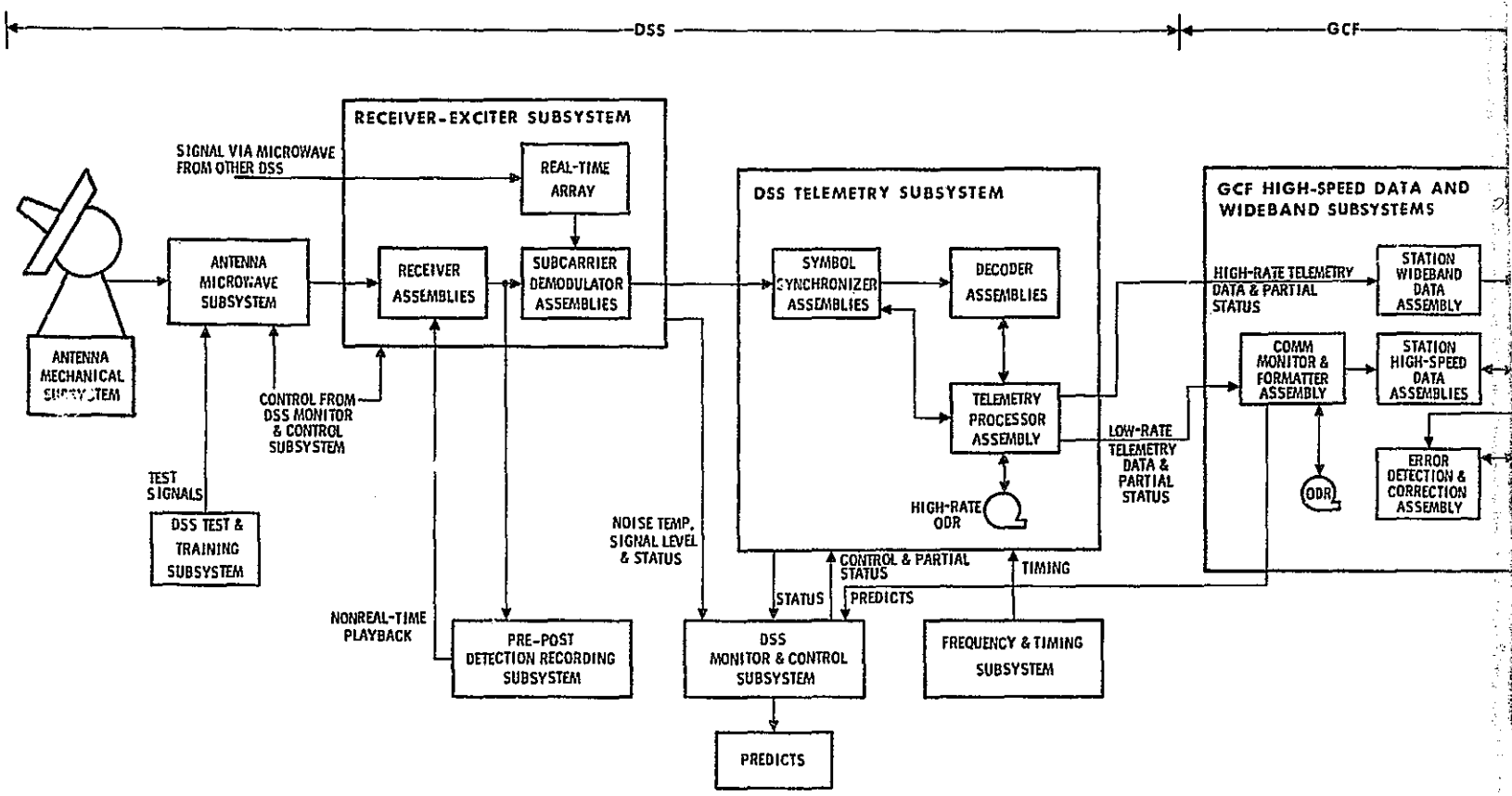

FOLDOUT FRAME

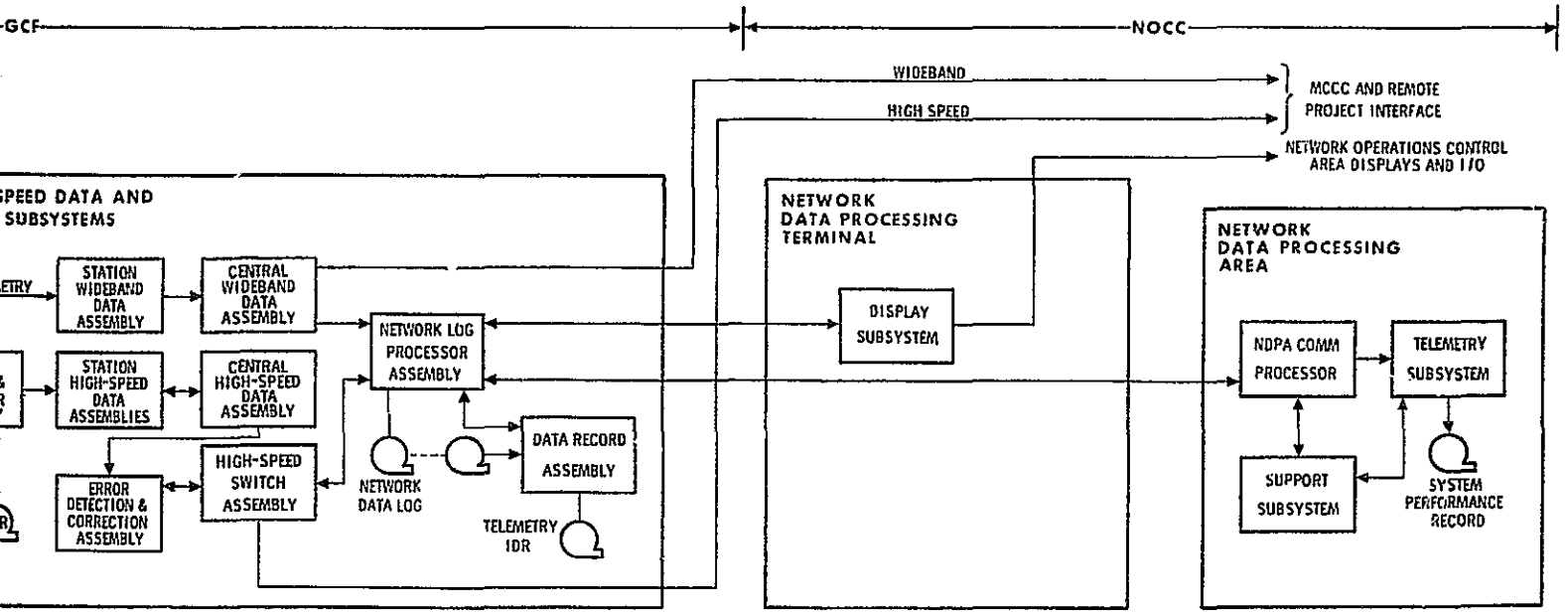

Fig. 2-1. Block diagram of the Network MK III telemetry system

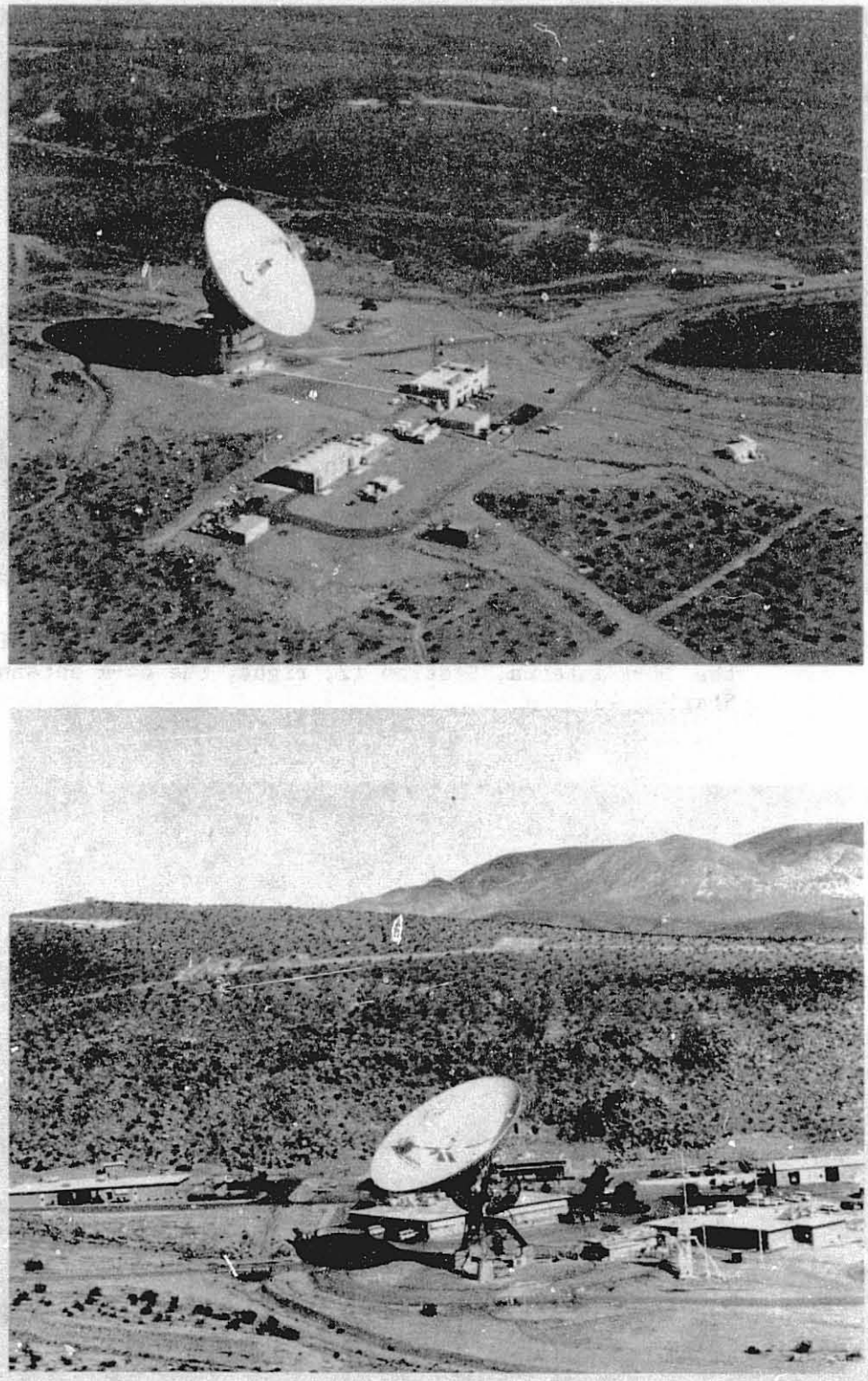

Fig. 2-2. Photographs of the Goldstone, California, Network Complex: top, the 64-m antenna, Station 14; bottom, the 34-m antenna, Station 12

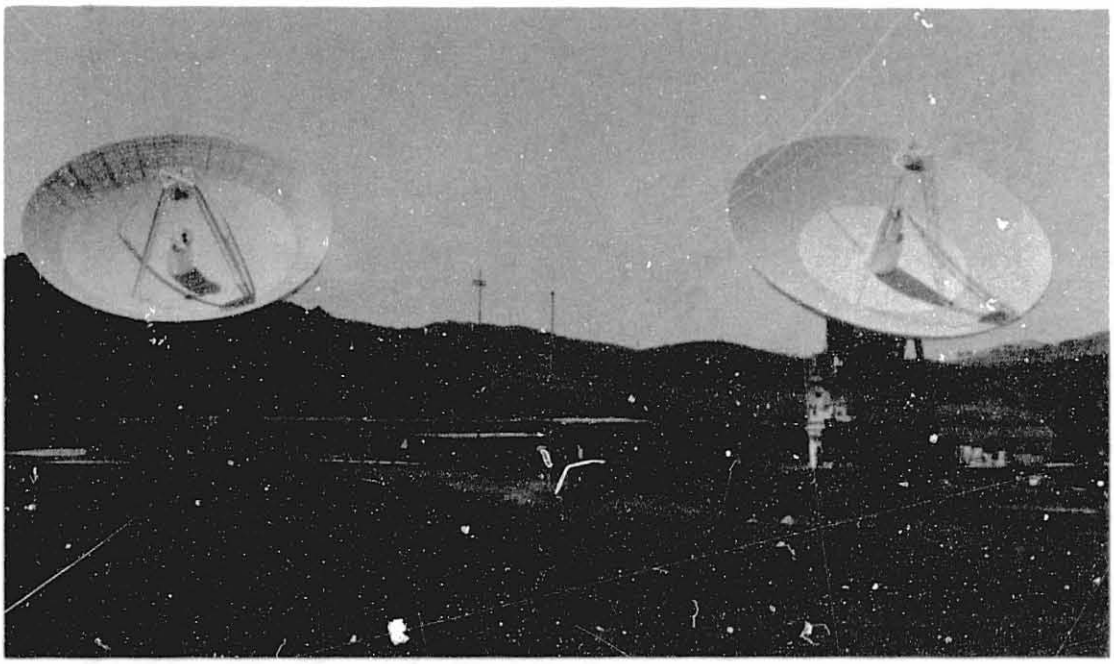

Fig. 2-3. Photograph of the Canberra, Australia, Network: left, the 34-m antenna, Station 12, right, the 64-m antenna, Station 43

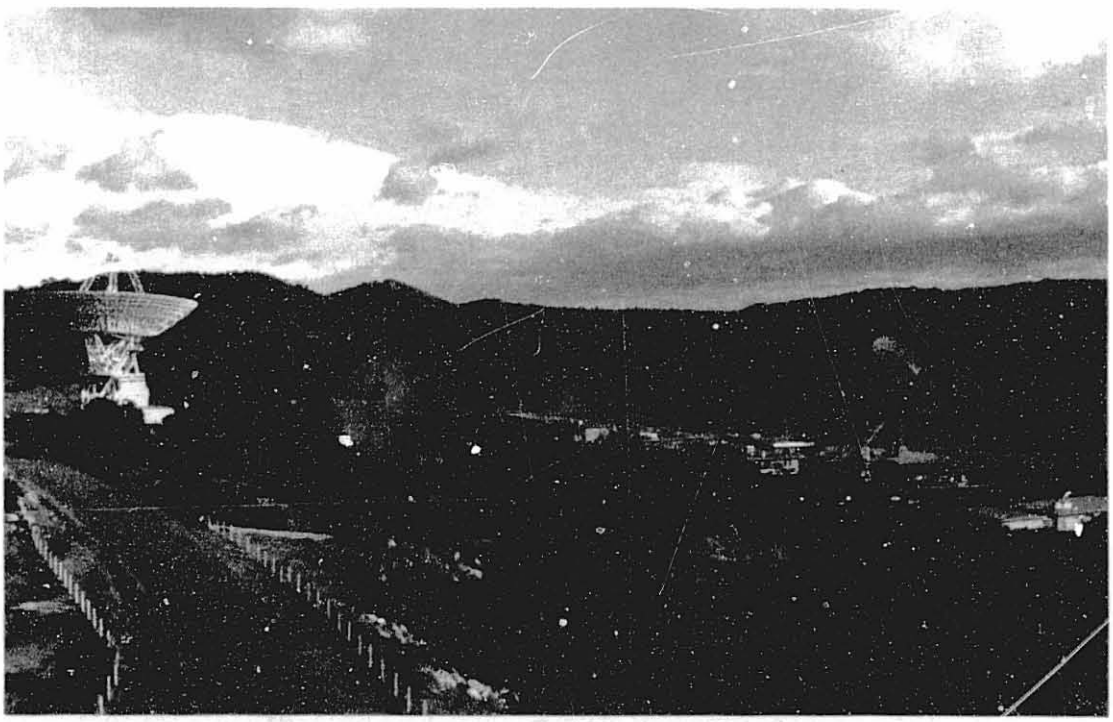

Fig. 2-4. Photograph of the Robledo, Spain, Network Complex: left, the 64-m antenna, Station 63; right, the 34-m antenna, Station 61

Fig. 2-5. Photograph of the Goldstone, California, 64-m antenna, Station 14 control console

Fig. 2-6. Photograph of the Deep Space Network control console in the JPL Space Flight Operations Facility

Fig. 2-7. Typical implementation of a concatenated coding scheme: outer encoder with block coding and inner encoder with convolutional coding.

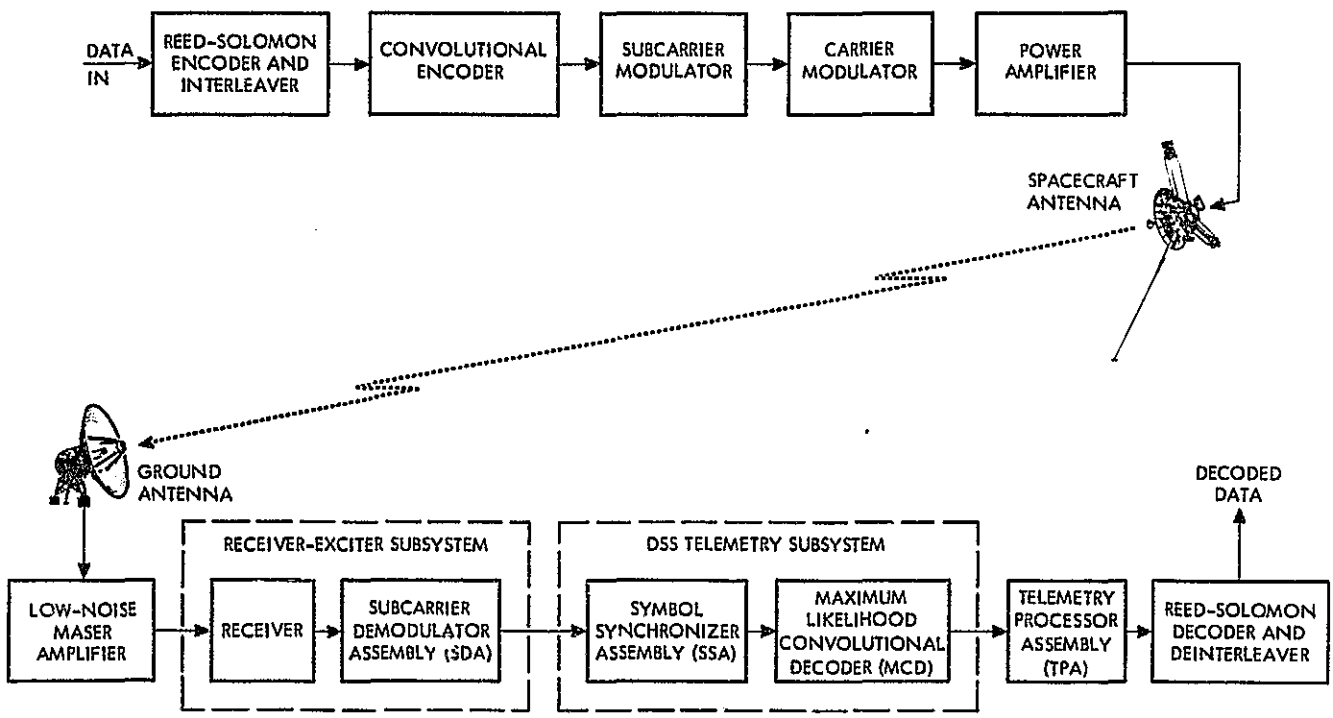

Fig. 2-8. Spacecraft-to-ground communications link with typical inner and outer coding/decoding implementation

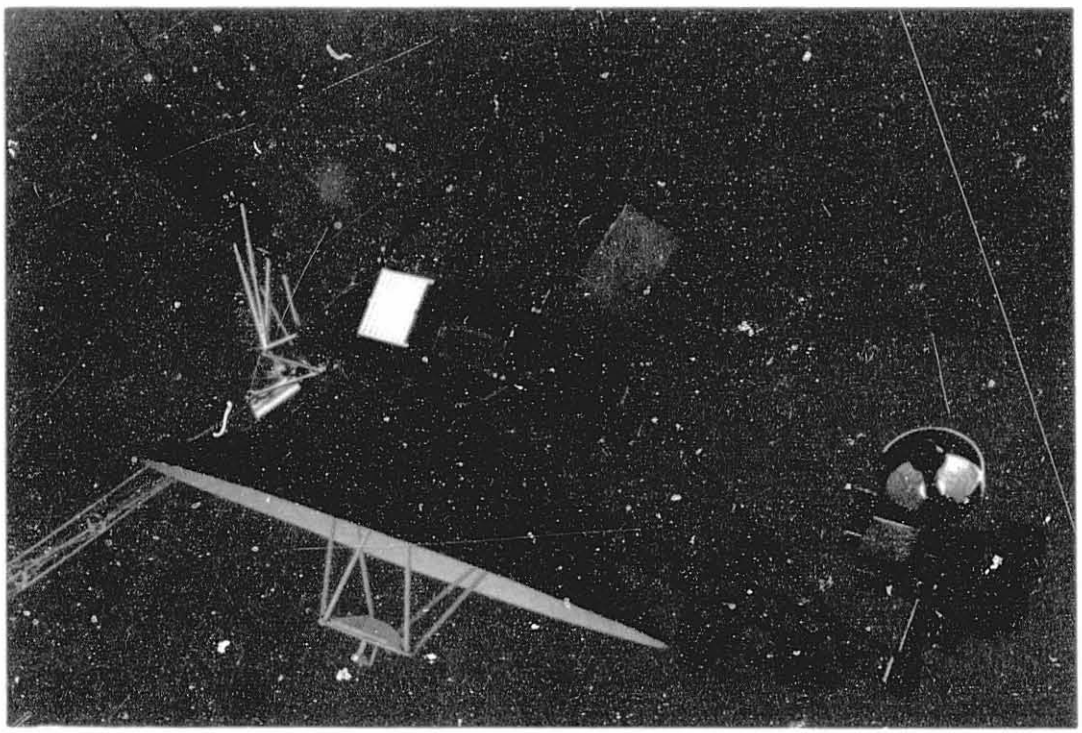

Fig. 2-9. Photograph of the Voyager 2 Spacecraft

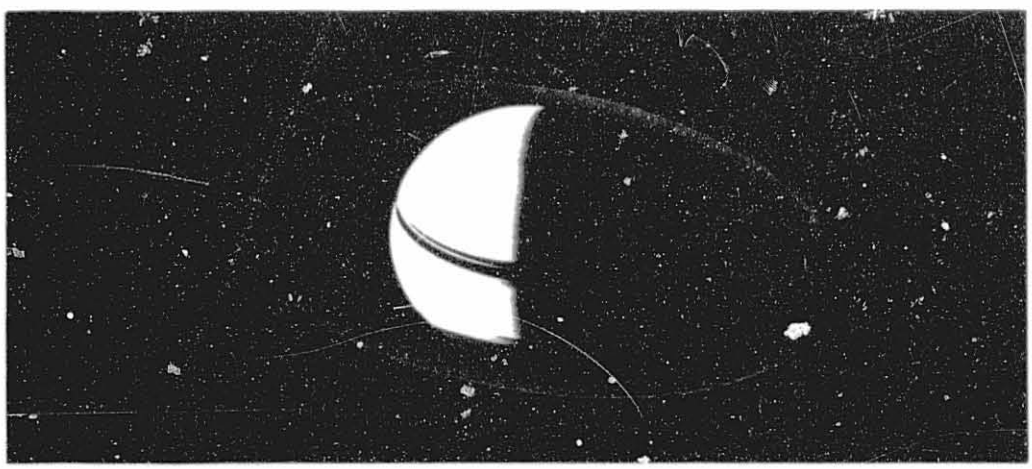

Fig. 2-10. Picture of Saturn taken 4.5 days past closest approach obtained from Voyager 2 on August 29, 1981

III. ANTENNAS

S. D. Slobin

A. INTRODUCTION

Reception of the exceedingly small signals from spacecraft typical of deep space communication requires antennas of enormous size, complexity, and precision. The two Voyager spacecraft each have 20-watt X-band transmitters; and at their Saturn-encounter distances from earth of approximately 1.5 billion kilometers, the power density received on the earth was less than 10^{-19} watts per square meter.

The thrust in deep-space communications improvement has been in the areas of ground and spacecraft antenna size and performance increases, spacecraft transmitter power increase, ground receiving system design, and telemetry information coding, to name but a few. This section of the report deals with ground antenna theory, design, and performance as related to the particular problem of receiving spacecraft signals using the Deep Space Network (DSN).

The improvement in antenna performance over the time period 1960-1990 can be seen in Table 3-1. Over this period the antenna gain will have increased a factor of 1260; and the system noise temperature will have decreased a factor of 60, resulting in a signal-to-noise improvement of 75,600, or 48.8 dB. In 1960 the Network consisted of six 26-m-diameter antennas operating at L-band (960 MHz). Since then, numerous larger antennas operating at higher frequencies have been added to the system so that spacecraft can be tracked continuously even beyond the edge of the solar system.

B. ANTENNA FUNDAMENTALS AND HISTORY

Reflector antennas (Fig. 3-1) such as used in the DSN intercept or capture a small portion of the electromagnetic wave transmitted by a spacecraft. Through a series of one or more reflections, the signal is directed into a receiving horn (feedhorn) and then into the waveguide portion of the microwave receiving system. At the distances involved in deep space communications the

spherical constant-phase surfaces of the transmitted signal are nearly planar. The antenna collects as much of the incident power as possible and concentrates it into the low noise amplifier. The concentration process involves transforming the incident plane wave into a converging spherical wave. The techniques for carrying out this process are well known in optical telescope systems; microwave reflector antennas use primarily the same methods and geometries.

Several basic equations must be presented in order for the reader to understand the relationships involved among the numerous parameters of a telecommunications system. The ability of a receiving system to distinguish a spacecraft signal from the obscuring system noise is a function of its signal-to-noise ratio (SNR). The SNR (for a 1 Hz bandwidth) may be defined by (Section II)

$$SNR = S/N_0 = \frac{P_T A_T A_R f^2}{c^2 D^2 L k T_{op}} \qquad (3\text{-}1)$$

where

S = received power level, W
N_0 = thermal noise power density, w/Hz
P_T = transmitted power, W
A_T = effective area of transmitting antenna, m^2
A_R = effective area of receiving antenna, m^2
f = frequency, Hz
c = velocity of light, 2.9979×10^8 m/s
D = distance to spacecraft from receiving antenna, m
L = loss of atmosphere and waveguide (ratio ≥ 1.0, typically ≈ 1.1)
k = Boltzmann's constant, 1.3806×10^{-23} J/K
T_{op} = receiving system noise temperature, K

From this equation it can be seen that the elements of a ground system that can be controlled to increase the SNR are A_r, f, T_{op}, and L. Hidden in Eq. (3-1) are expressions for antenna gain (G_T or G_R in terms of A_T or A_R)

$$G = 4\pi A/\lambda^2 \qquad (3\text{-}2)$$

which also depend on area and frequency. The 3-dB beamwidth (θ_{3dB}) of an axisymmetric paraboloidal reflector antenna is given by (approximately)

$$\theta_{3dB} \simeq 0.70\lambda/D, \text{ deg} \qquad (3\text{-}3)$$

where

λ = wavelength, cm (=c/f)

D = antenna diameter, m

Thus, a 64-m-diameter antenna operating at X-band (f=8.5 GHz, λ = 3.53 cm) has a 3-dB beamwidth of about 0.039 degrees. The simplest form of receiving antenna is shown schematically in Fig. 3-2.

The first large antennas operated by the Network in 1958 were 26-m-diameter reflector antennas operating at L-band (f= 960 MHz, λ = 31.2 cm) with a focal point feed that operated exactly as shown in Fig. 3-2. Figure 3-3 shows the Echo Station at Goldstone in its original 960-MHz focal-point feed configuration. The antenna operated with an HA-DEC (hour angle-declination) mount similar to that used on large optical telescopes. The polar (hour-angle) axis is aligned parallel to the earth's axis and tracking is accomplished almost entirely by the antenna's hour angle rotation about this axis. The position of any spacecraft at a large distance from earth is almost fixed with relation to the stars and planets over the period of one day, although the small variation from sidereal rate is accounted for in the tracking scheme. All microwave receiving elements in the focal point antenna can be located at the apex or conjunction point of the trusswork (or tubular) structure (quadripod) projecting from the front of the antenna. The feed horn and maser amplifier package can be located at the apex; or the maser can be located behind the surface of the dish and connected to the feedhorn by a long length of waveguide.

The nature of microwave horns and reflectors is such that they receive some amount of energy from directions other than the principal direction toward which they are pointed. Because of this, apex-mounted feed horns see beyond the edge of the large reflector and receive a small amount of energy (spillover) from the ground which adds unwanted microwave power (or noise) into the receiving system. A partial solution to the ground noise problem lies in the use of an antenna design known as Cassegrain, derived from early optical telescope design. The Cassegrain antenna system (Fig. 3-4) consists of the large paraboloid as before, and an additional reflector of hyperboloidal shape (the subreflector or hyperboloid). The receiving horn is then located near, or even behind, the surface of the paraboloid. Figure 3-5 shows an 85-foot (26-m) diameter antenna (with S-band feed) in the Cassegrain configuration.

From 1976 to 1981, three existing 26-m antennas were enlarged to 34-m diameter (cf. Table 3-2). One of these, Station 12 at Goldstone, is shown in Fig. 3-6 in its S/X-band reflex-feed configuration (described later). The new dish surface consists of a solid-panel center section and a perforated-panel outer ring to reduce wind loading. A detailed description of the 26-m antenna conversion is presented in Ref. 3-1. The 1985-era Network will also contain two new 34-m antennas, to be located at Goldstone and Canberra.

In the Cassegrain system, feedhorn, maser amplifier and other associated microwave and electronic equipment can be located in a small structure (known as the "cone") attached to the dish surface. The cone in Fig. 3-5 is about 5 meters high. The quadripod structure then supports only the subreflector and can be made thin and light to reduce interference with incoming radio signals. A large amount of microwave equipment can be located in the cone and is thus more easily maintained than if it were located at the apex. It can be seen then that at typical tracking angles (about 45° elevation) the spillover from the feedhorn receives signals from the cold sky (3-5 K) instead of the ground (about 290 K). In addition, modifications of the feedhorn pattern (tapering) and subreflector shape reduce the amount of spillover seeing the ground. The 64-m antenna in Australia is shown in Fig. 3-7 with its original single S-band feed and cone. The 64-m antennas have AZ-EL (azimuth-elevation) mountings in which significant motion about two axes is needed to track a spacecraft.

To improve the usefulness of the 64-m antenna, a tricone system was developed (Ref. 3-2) which allowed operation of the antenna at three frequencies (identical or dissimilar) without the need to remove one cone and replace it with another. Figure 3-8 shows the 64-m antenna at Goldstone in its original tricone configuration. The phase centers of the three feed horns are no longer on the axis of symmetry of the paraboloid; and if the antenna were operated in this manner with the original subreflector, three separate antenna beams would be produced, each pointing in a different direction. To solve this problem, the subreflector is tilted so that its phase center remains concident with the phase center of the paraboloid, but its vertex points in turn to each of the three feed horns as the subreflector is rotated about the paraboloid axis of symmetry. The subreflector must still reflect rays from the edge of the paraboloid, and in order to do this, the tilted hyperboloid shape is made asymmetric. This unusual geometry is shown in Fig. 3-9. Because of the asymmetries of the antenna geometry, the feed horns are each tipped inward so that the horns do not point at the hyperboloid vertex. This tends to equalize the fields at the edges of the hyperboloid and thus to equalize the illumination at the edges of the paraboloid.

A further improvement in 64-m antenna performance was made in order to make use of the simultaneous spacecraft downlink transmission at both S- and X-band frequencies, in addition to being able to transmit S-band uplink and receive X-band downlink simultaneously. This new development, installed on the 64-m antennas in 1973, was the reflex feed. Figures 3-1, -10 and -11 show the reflex feed in place on the 64-m antenna at Goldstone. Figure 3-12 shows a schematic view of the reflex feed in the tricone geometry. The reflex feed utilizes the geometrical principle that all rays emanating from one focus of an ellipse will, after reflection, converge at the other focus. An ellipsoidal reflector is placed over the S-band horn and a perforated reflective plate is placed over the X-band horn so that the S-band wave appears to emanate from the phase center position of the X-band horn. The reflective plate does not have a solid surface but contains numerous closely packed 2-1/2 cm (1-inch) diameter holes. The plate itself is about 4 cm (1-1/2 inches) thick and 1.5-m (5 feet) in diameter. The holes are too small to allow the S-band (longer wavelength) signal to pass through, and it is completely

reflected. The holes do allow the X-band signal (shorter wavelength) to pass through, and it thus appears that waves of both frequencies are reflected from the hyperboloid and paraboloid along exactly the same paths. The S- and X-band beams are thus coincident. The reflective plate in the reflex feed system is known as the dichroic (two-color) plate.

C. ANTENNA OPERATIONS AND CHARACTERISTICS

The complete operational Deep Space Network consists of 9 large antennas located around the world in the United States (Goldstone, California), Spain (Madrid), and Australia (Canberra). This global spacing allows continuous 24-hour-a-day spacecraft telecommunications; in fact, for small portions of the day, a spacecraft can be seen by two antennas at once, the spacecraft setting at one location and rising at the next westerly location. This is known as the "handover" or "overlap" period and is usually characterized by reduced signal-to-noise ratios due to atmospheric effects (long radiowave path length through the atmosphere).

Table 3-2 lists the 1985-era Network antennas and pertinent data concerning each one. Several new 34-m-diameter antennas will be constructed during the period 1983-1985. Table 3-2 indicates which antennas presently exist (early 1983) and which will be constructed in the future.

Figure 3-13 shows typical S- and X-band system noise temperature measurements made during the Voyager 2 Saturn encounter period (Ref. 3-3). The upward curved shape of both the S- and X-band curves is indicative of atmosphere and ground noise temperature increases as the antenna is pointed toward the east and west horizons at spacecraft rise and set, respectively. A typical X-band zenith atmospheric noise temperature is 2.5 K, increasing to 15 K at 10 degrees elevation. A typical X-band ground contribution due to spillover is 4 K at zenith and 7 K at 10 degrees elevation.

For S-band, the atmosphere increases from about 2.2 K at zenith to 13 K at 10 degrees elevation. Corresponding ground noise temperatures are 3 K and 6 K (Ref. 3-4). Thus, for example, at X-band, the ground, atmosphere and cosmic background contribute 9.2 K (4+2.5+2.7) to the baseline zenith system

noise temperature of about 25 K. For S-band, these elements contribute 7.9 K (3+2.2+2.7) of the baseline noise temperature of about 20 K. Additional system noise temperature contributions are due to the maser noise temperature, and waveguide and horn losses.

Additional descriptions of the antennas, microwave receiving systems, and mission support activities are given in Refs. 3-5, 6, and 7.

D. FUTURE DEVELOPMENT

As can be seen in the preceding sections there has been a long history of development and improvement of Deep Space Network antennas. Future work in the Network will involve both improvements in the ground antenna systems, and eventually the addition of orbiting antennas.

One type of antenna system that is undergoing testing at the Jet Propulsion Laboratory is a 32-GHz (K_A-band) clear aperture antenna (Figs. 3-14 and 3-15). In this system, there is no blockage of the main beam as in the conventional symmetric Cassegrain antenna system. The reflectors in the clear aperture system are portions of a paraboloid and hyperboloid so that the classical ray optics geometry still applies (in fact, the reflectors are "shaped" for purposes of illumination and beam efficiency, but closely resemble the classical shapes).

Another method of increasing receiving system performance is to use larger antennas. This usually has an upper limit of about 100-m diameter because of wind loading, gravity deformations, material strength, surface tolerances, etc. A third method is to array or link together a number of smaller antennas (64-m, 34-m, 26-m) and combine their signals in phase to achieve the effect of a much larger antenna. This technique is being tested at Goldstone and will be operational for the Voyager 1986 Uranus and 1989 Neptune Encounters.

A 100-m-diameter X- and S-band antenna design has been studied (Ref. 3-8). Although this antenna is basically a Cassegrain design, it uses

shaped reflectors and a common aperture S/X-band feedhorn (described later), thus eliminating the present reflex feed system and asymmetric rotating hyperboloid. Large antennas such as the 100-m design will probably not be constructed in the foreseeable future; instead, the arraying technique will be used because of the expense and difficulty of constructing and maintaining large antennas.

Higher frequencies can be used to increase the gain of existing antennas; or conversely, smaller antennas operating at higher frequencies will have the same gain as existing large antennas. The 1.5-m (5 ft) diameter clear-aperture antenna is being tested at 32 GHz and, because of its superior efficiency (85%), it will have the same gain (53 dB) as a 26-m antenna operating at S-band. An analysis of system performance operation at K_A-band (32 GHz) is presented in Refs. 3-9, 10, and 11.

For future missions such as Voyager at Uranus and Neptune, the antennas will be arrayed to increase receiving area as required. Figure 10-5 shows a schematic of the 11 antennas available for arraying at three sites for space-craft support in the post-1985 era. Combinations of 64-m, 34-m, and 26-m antennas will be used to increase the total receiving area at each site.

The newest improvement in the antenna system is the installation of common-aperture S/X-band feed horns (Fig. 3-16) on the 34-m antennas. This type of feed system will allow reversion to the original single-cone, sym-metric hyperboloid system that was used nearly 20 years ago. The improvement, though, is that simultaneous dual-frequency operation is possible without the need for the reflex feed system and its attendant losses. Truly coaxial beams are now achieved in this system. A recent study (Ref. 3-12) has measured the S-band performance of the 26-m research antenna at Goldstone using the new S/X-band common aperture feedhorn. Although the antenna efficiency appears to have dropped from 60.6% to 59.4%, this is more than compensated for by the greatly increased versatility of the dual-frequency system.

The existing individual elements of the antennas are continually being upgraded. Recent work to upgrade the 64-m antenna at Goldstone structure and subreflector is described in Ref. 3-13.

Development programs for new high-performance antenna systems are probably not feasible at the present time for a variety of reasons, primarily financial. With this consideration, some serious thought has gone into development programs that can upgrade performance on existing antennas. These programs would involve increasing the collecting area of some of the larger antennas, and replacing the parabolic surface of the dish with shaped, precision panels. To control gravitational surface contour deformations, the rib backing structure for both the main dish and the subreflector can be restructured and braced. Contour-deforming the subreflectors ("Y" axis deformation) to electrically compensate for distortions is another method for increasing the efficiency of the large reflector antennas. Other studies have indicated that some deformation problems can be solved by using an "adaptive array" of feedhorns that electronically compensate for contour deformation by controlling the phase front illuminating the subreflector. Any or all of these programs could conceivably increase the gain of the large antennas by as much as 2 dB.

As higher frequency bands come into use, a multiplicity of feed horns necessary to cover ever wider frequency bands will have to be included on each antenna. Single- or dual-frequency feedhorns would be selected by multiple movable subreflectors. These multiple feed systems, coupled with newly developed upconverter masers that operate over extended bands, will give the DSN unparalled diversity in science, research, and development and will keep it an international science resource.

REFERENCES

3-1. Burnell, E., et al, "26-Meter Antenna S-X Conversion Project," Publication 82-26, Jet Propulsion Laboratory, Pasadena, Calif., Mar. 15, 1982.

3-2. Stelzried C.T., et al., "Multi-Feed Cone Cassegrain Antenna," US Patent No. 3,534,375, Oct. 13, 1970.

3-3. Bartok, C.D., "Analysis of DSN PPM Support During Voyager 2 Saturn Encounter", TDA Progress Report 42-68, Jet Propulsion Laboratory, Pasadena, Calif., Apr. 15, 1982.

3-4. Potter, P.D., Efficient Antenna Systems: Calibration of the Mars Deep Space Station 64-m Antenna System Noise Temperature Degradation Due to Quadripod Scatter, Technical Report 32-1526, Vol XVI, Jet Propulsion Laboratory, Pasadena, Calif., pp. 22-29, Aug. 15, 1973.

3-5. Edelson, R.E, Madsen, B.D., Davis, E.K., and Garrison, G.W., "Voyager Telecommunications: The Broadcast from Jupiter", Science, Vol. 204, pp. 913-921 June 1, 1979.

3-6. Reid, M.S., Clauss, R.C., Bathker, D.A., and Stelzried, C.T., "Low-Noise Microwave Receiving Systems in a Worldwide Network of Large Antennas", Proc. IEEE, Vol. 61, No. 9, pp.1330-1335, Sep. 1973.

3-7. Larkin, W.E., Telecommunication and Data Acquisition System Support for the Viking 1975 Mission to Mars, JPL Publication 82-18, Jet Propulsion Laboratory, Pasadena, Calif., Apr. 15, 1982.

3-8. Williams, W.F., DSN 100-Meter X- and S-Band Microwave Antenna Design and Performance, JPL Publication 78-65, Jet Propulsion Laboratory, Pasadena, Calif., Aug. 1, 1978.

3-9. Potter, P.D., "64-Meter Antenna Operation at K_A-Band", TDA Progress Report 42-57, Jet Propulsion Laboratory, Pasadena, Calif., June 15, 1980.

3-10. Potter, P.D., "Use of K_A-Band for Radio Metric Determinations", TDA Progress Report 42-58, Jet Propulsion Laboratory, Pasadena, CA, (Aug. 15, 1980).

3-11. Clauss, R., Franco, M., and Slobin, S., "K_A-Band Weather-Dependent System Performance Estimates for Goldstone," TDA Progress Report 42-71, Jet Propulsion Laboratory, Pasadena, Calif., Nov. 15, 1982.

3-12. Klein, M. J., "S-Band Aperture Efficiency of the DSS 13 26-Meter Antenna with the S-X Common Aperture Feed," TDA Progress Report 42-72, Jet Propulsion Laboratory, Pasadena, Calif., Feb. 15, 1982.

3-13. Freiley, A. J., "Radio Frequency Performance of DSS 14 64-Meter Antenna at X-Band Using An Improved Subreflector," TDA Progress Report 42-60, Jet Propulsion Laboratory, Pasadena, Calif., Dec. 15, 1980.

Table 3-1. Tabulation of the Deep Space Network antenna measured and predicted gain performance from 1960 to 1990

Parameter	Calendar year										
	Measured								Predicted		
	1960	1962	1963	1965	1967	1971	1975	1980	1986	1987	Post 1990
Frequency f, Ghz	0.96	0.96	0.96	2.30	2.30	2.30	8.42	8.42	8.42	8.42	32
Diameter D_R, m	26	26	26	26	64	64	64	64	64	70	70
Antenna gain G_R, dB	43	45	45	53	61	61	72	72	72[a]	74[b]	84[a]

[a] assume 50% efficiency.

[b] assume 60% efficiency.

System noise temperature: 1960 .... 1500 K (960 MHz)
1990 .... 25 K (32 GHz)

Table 3-2. Deep Space Ne

Station No.	Diameter m	Description	3-dB beamwidth S-band deg	3-dB beamwidth X-band deg	Height above sea level m
Goldstone, Calif.					
11 *	26	Decommissioned	0.33	--	1036
12 *	34	T/R, DS, HEO	0.26	0.075	1001
13 *	26	R&D	0.33	0.10	1094
14 *	64	T/R, DS	0.140	0.036	1032
15	34	VLBI, DS, HEO, HE	0.26	0.070	1005
Canberra, Australia					
42 *	34	T/R, DS, HEO	0.26	0.075	664
43 *	64	T/R, DS	0.140	0.036	670
44 *	26	Decommissioned	0.33	--	1130
45	34	VLBI, DS, HEO, HE	0.26	0.070	670
Madrid, Spain					
61 *	34	T/R, DS, HEO	0.26	0.075	796
62 *	26	Decommissioned	0.33	--	789
63 *	64	T/R, DS	0.140	0.036	812

T/R = transmit/receive
DS = deep space support
HEO = High Earth Orbiter support
* = Existing as of mid-1982
R&D = Research and development station
VLBI = Very Long Baseline Interferometry
HE = high efficiency

FOLDOUT FRAME

Network antennas in the 1985 era

e	Gain		System noise temp.		Uplink	Downlink	Feed System
	S-band	X-band	S-band	X-band			
	dB		K				
	53.3	--	41	--	--	S	One-cone, S-band feed
	56.1	66.9	21.5	21.5	S	S, X	One-cone, reflex
	53.7	63.7	27	23	S, X	S, X	S/X common aperture feed
	61.7	72.1	14.5	20.0	S	S, X	Tricone, reflex
	55.8	67.3	150	18.5	--	S, X	S/X common aperture feed
	56.1	66.9	21.5	21.5	S	S, X	One-cone, reflex
	61.7	72.1	14.5	20.0	S	S, X	Tricone, reflex
	53.3	--	41	--	--	S	One-cone, S-band feed
	55.8	67.3	150	18.5	--	S, X	S/X common aperture feed
	56.1	66.9	21.5	21.5	S	S, X	One-cone, reflex
	53.3	--	41	--	--	S	One-cone, S-band feed
	61.7	72.1	14.5	20.0	S	S, X	Tricone, reflex

2 FOLDOUT FRAME

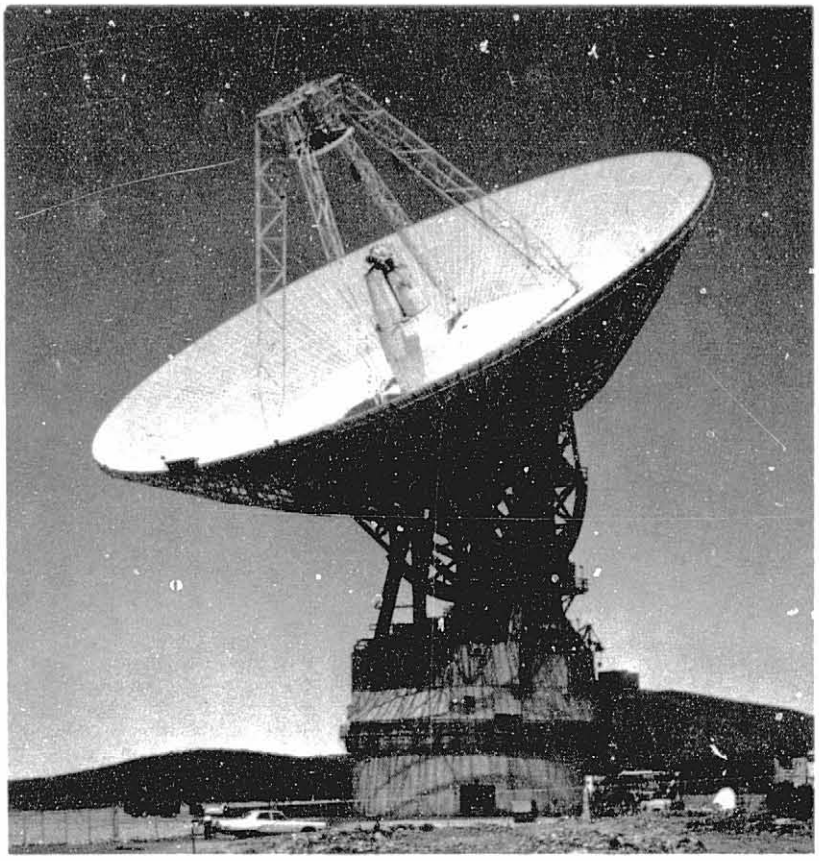

Fig. 3-1. Goldstone Station 14 64-m-diameter antenna with tricone and reflex feed, 1983 era S/X-band

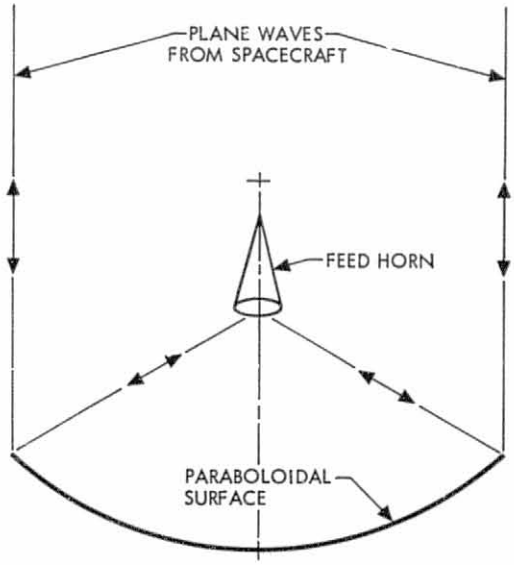

Fig. 3-2. Schematic view of paraboloidal antenna with a focal-point feed

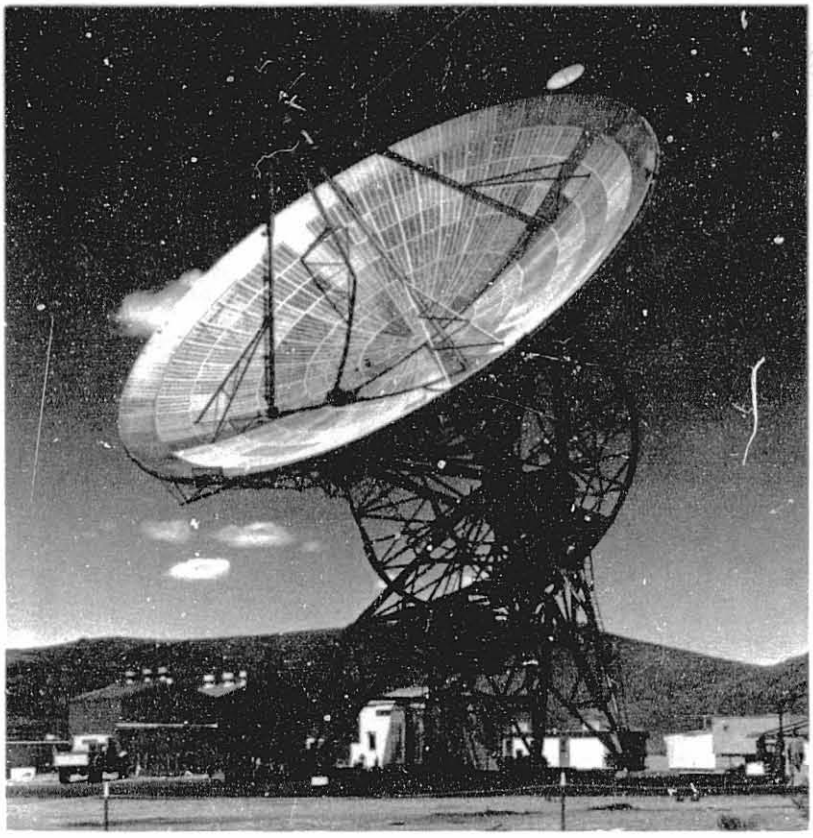

Fig. 3-3 One of the first 26-m-diameter antennas at Goldstone in 1961, Echo Station 12

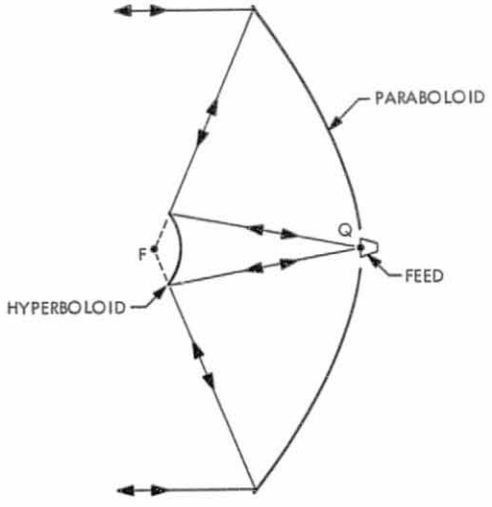

Fig. 3-4. Geometry of a two-reflector Cassegrain antenna system with a symmetrically positioned hyperboloidal subreflector (F and Q are foci of hyperboloid)

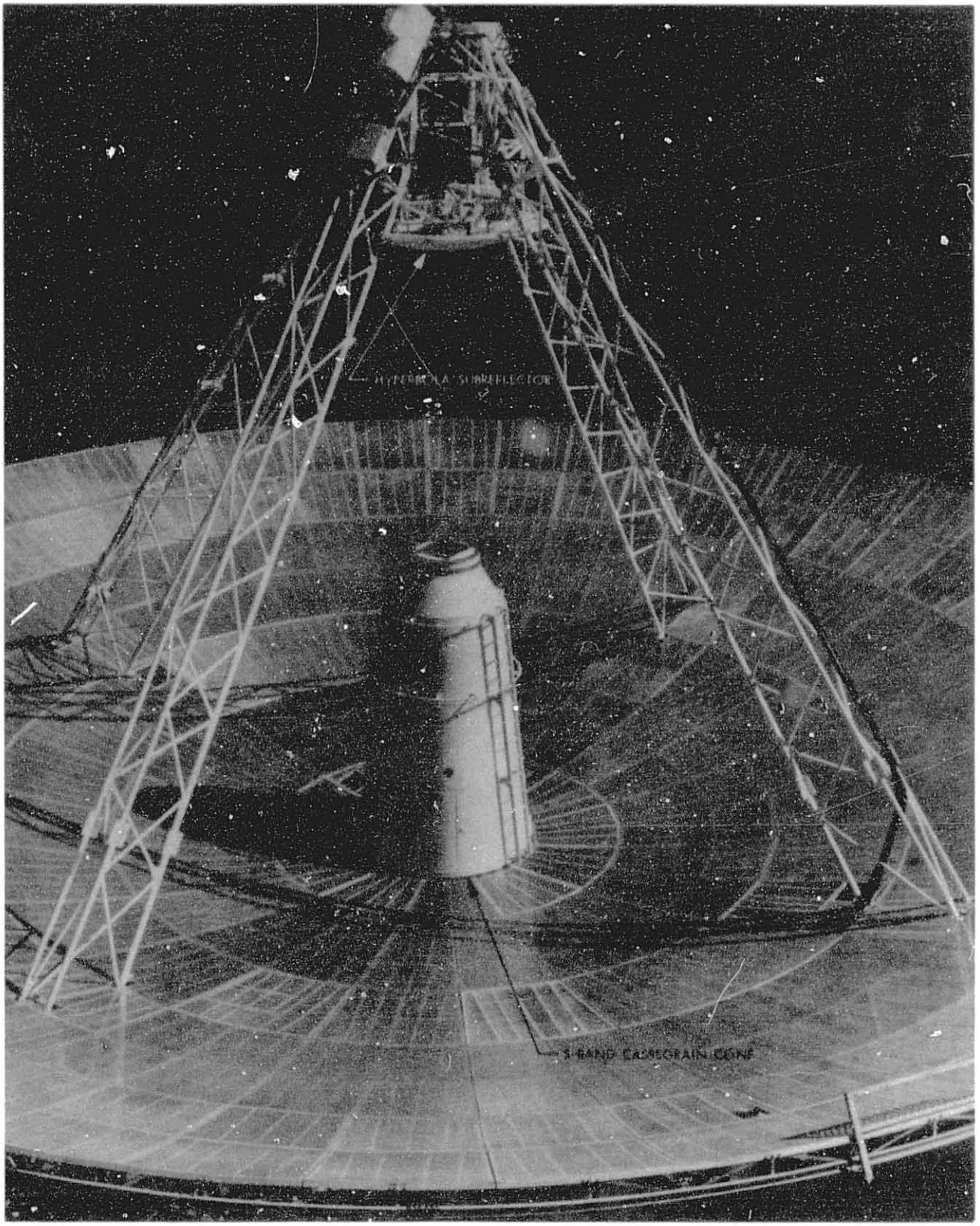

Fig. 3-5. 26-m S-band Cassegrain antenna system, showing subreflector, feedhorn, and cone

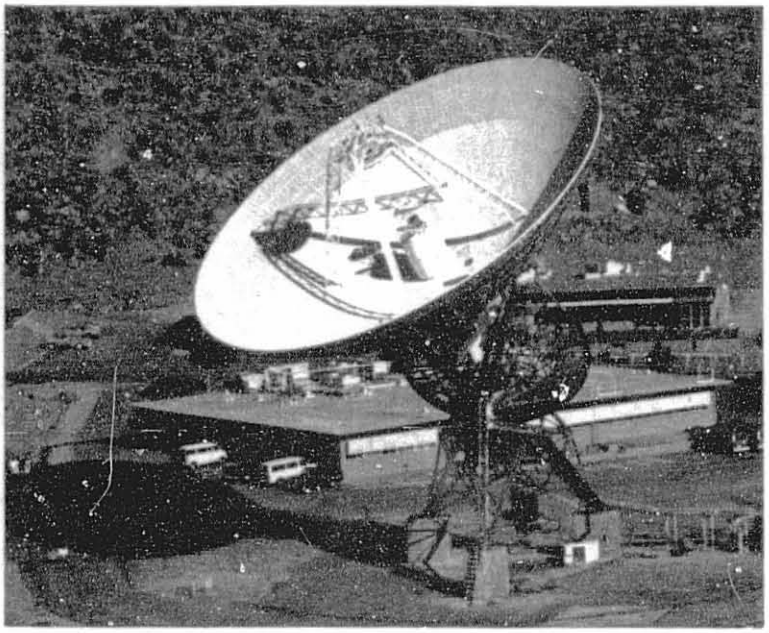

Fig. 3-6. 34-m antenna at Goldstone, Station 12, with S/X-band reflex feed system

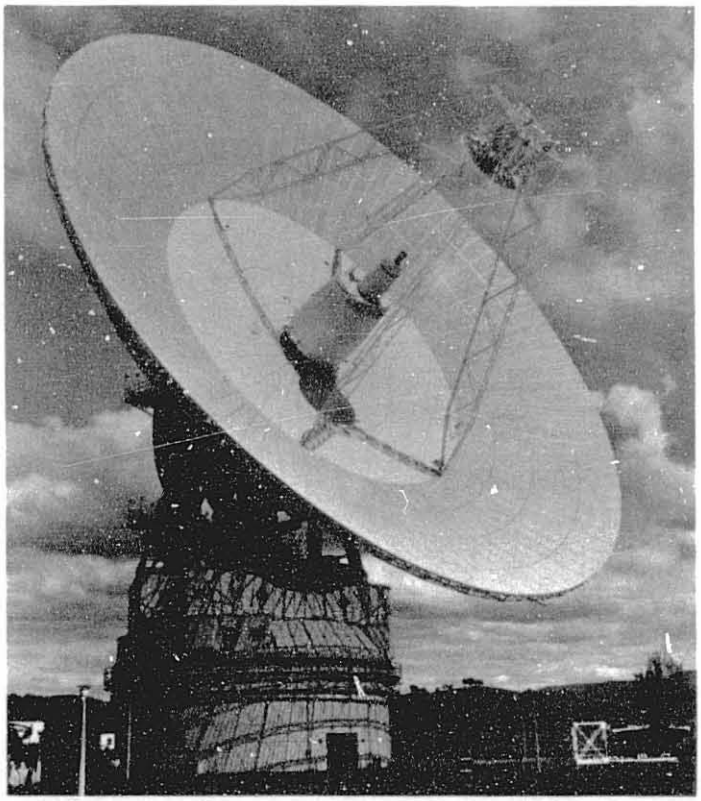

Fig. 3-7. Canberra Station 43 64-m antenna showing subreflector and single S-band feedhorn

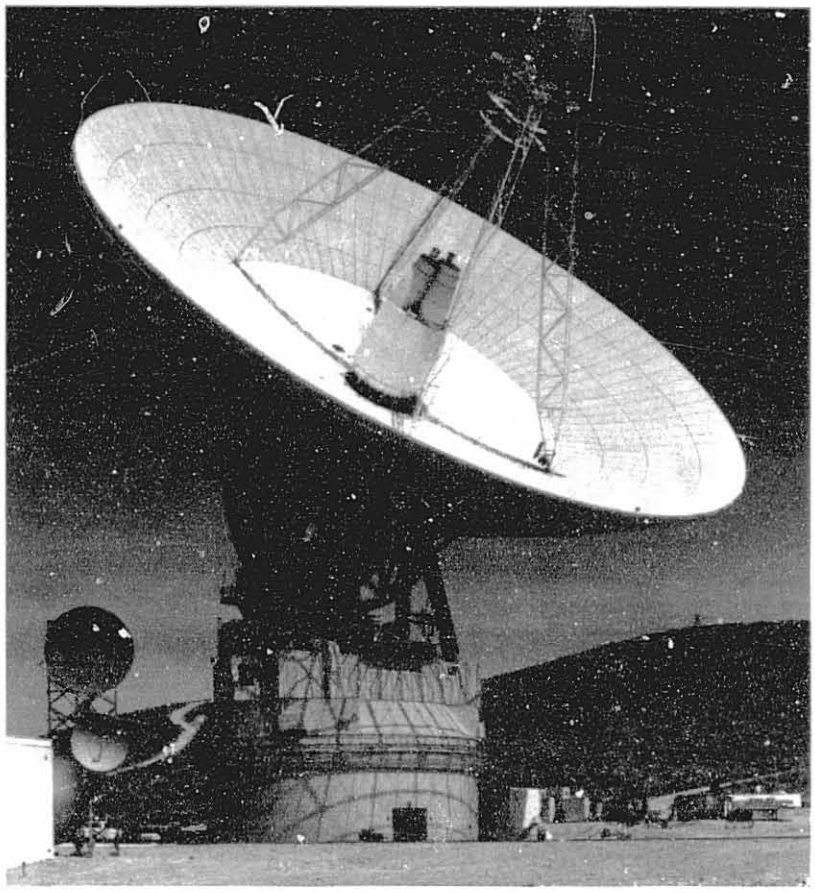

Fig. 3-8. Goldstone Station 14 64-m antenna showing tricone and asymmetric hyperboloidal subreflector

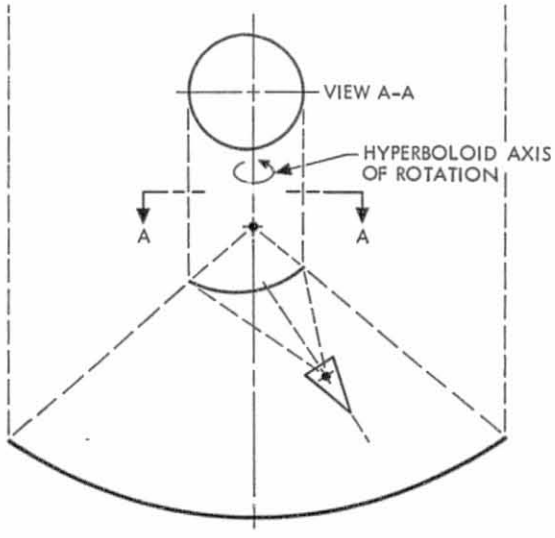

Fig. 3-9. Geometry of asymmetric subreflector and feedhorn in tricone feed assembly

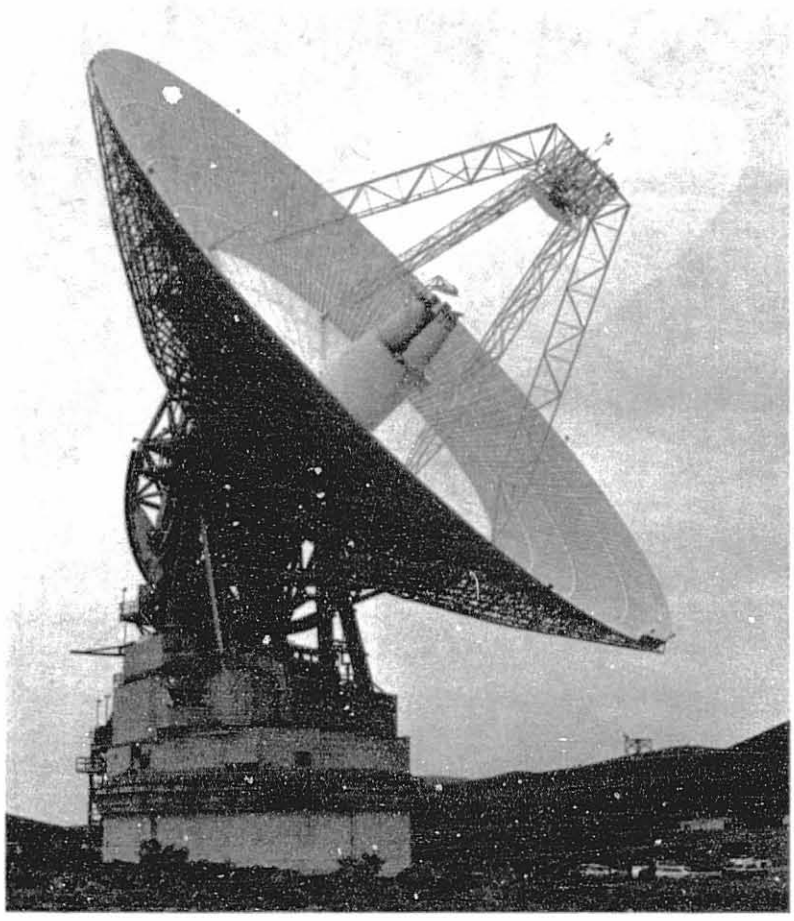

Fig. 3-10. Goldstone Station 14 64-m antenna with tricone, reflex feed, and asymmetric subreflector

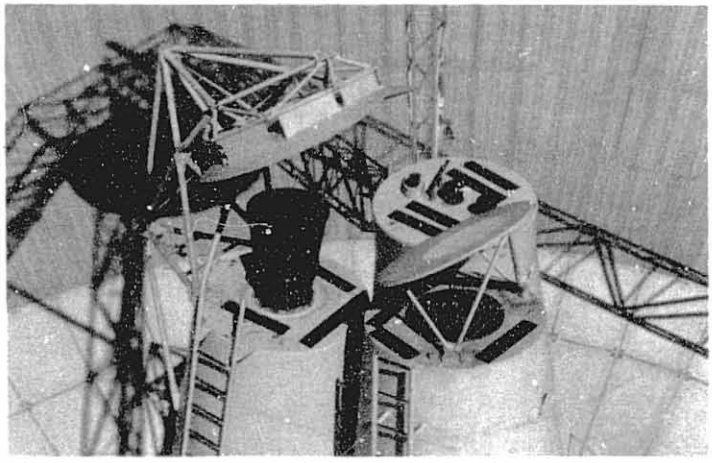

Fig. 3-11. Close-up view S- and X-band feedhorns, elliptical reflector, and dichroic plate in reflex feed assembly

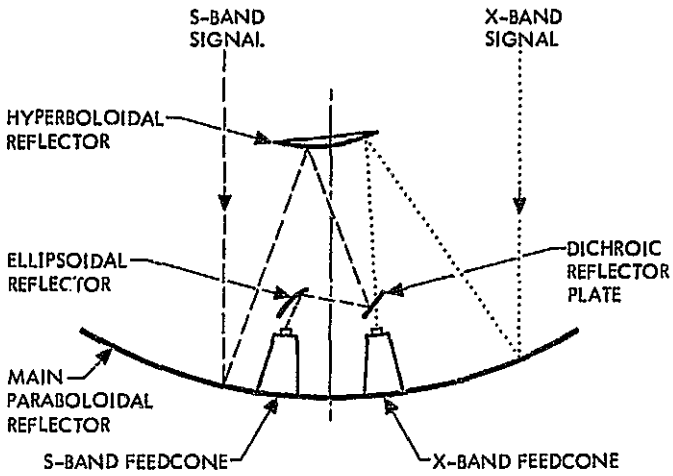

Fig. 3-12. Geometry of S/X-band reflex feed system

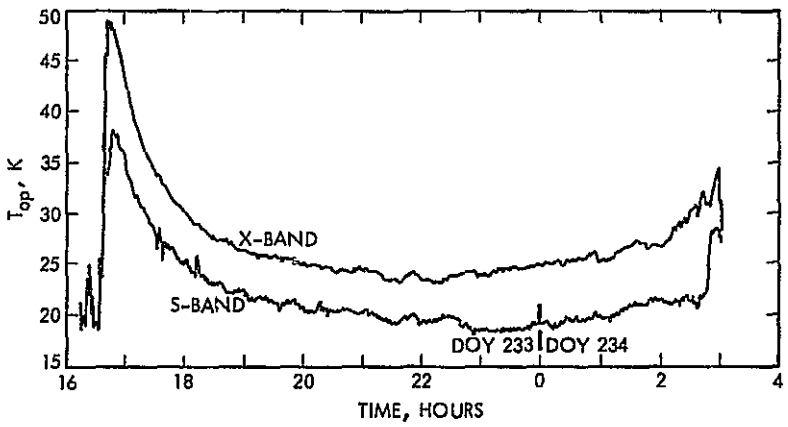

Fig. 3-13. S- and X-band 64-m system noise temperatures measured at Goldstone DSS 14 during Voyager Saturn encounter

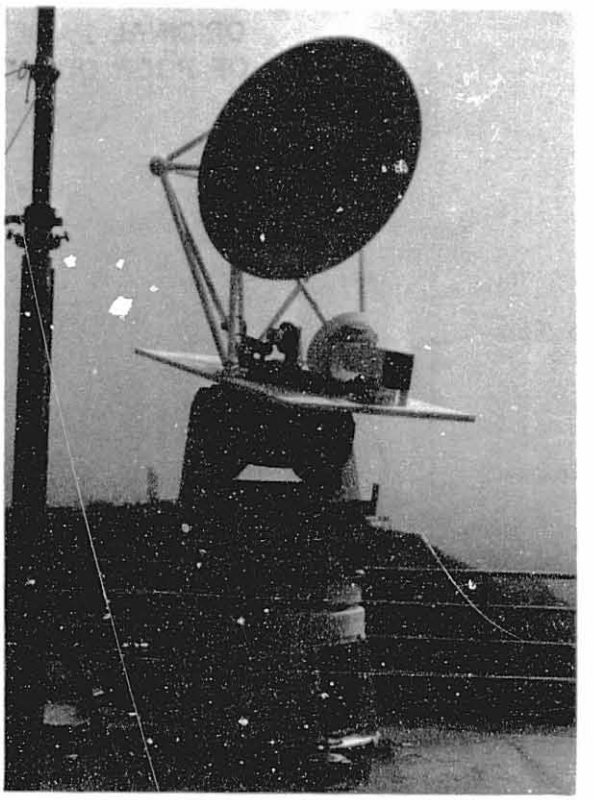

Fig. 3-14. 32-GHz clear aperture antenna (1.5-m diameter) undergoing testing at the Jet Propulsion Laboratory

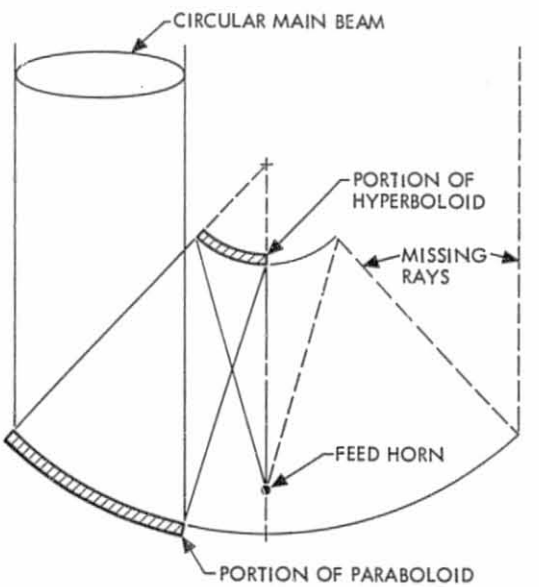

Fig. 3-15. Geometry of clear aperture antenna system

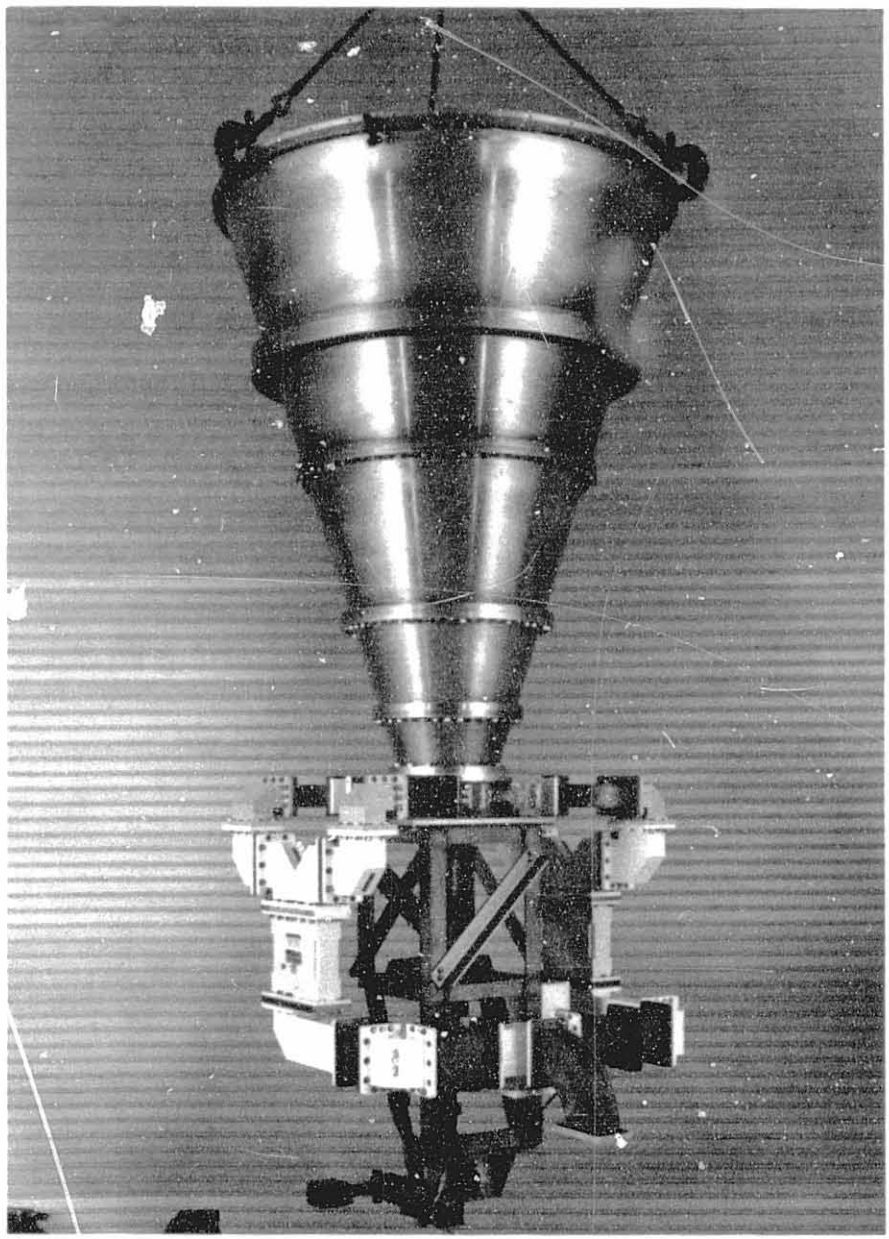

Fig. 3-16. Common aperture S/X-band feedhorn and waveguide, 2.6-m overall length

IV. LOW NOISE AMPLIFIERS

S. M. Petty and D. L. Trowbridge

A. INTRODUCTION

During its history, one of the great technical challenges facing the Deep Space Network has been to receive signals from a severely weight-limited spacecraft that is hundreds of thousands to billions of kilometers from earth. This weight limitation has always imposed strict limitations on the size of the spacecraft antenna and the amount of transmitter power radiated. The communication burden is therefore placed upon the ground systems of the Deep Space Network which must recover an extremely weak signal in the presence of nearly overwhelming amounts of noise.

Two key parameters that determine the signal-to-noise ratio of a received signal using a deep space station are 1) the collecting area and efficiency of the antenna, and 2) the amount of noise which is generated in, as well as allowed to enter in, the antenna-mounted receiver. These parameters can be used to describe the relative ability of a deep space station to receive weak signals. The communications link receiving system figure of merit M is given by (Sections I and II):

$$M = G_R/T_{op} \qquad (4\text{-}1)$$

where G_R is the receiving antenna effective gain, and T_{op} is the operating system noise temperature. As spacecraft-to-earth communication distances have increased over the years, the Deep Space Network has been engaged in a relentless effort to increase the figure of merit through larger and more efficient antennas, higher frequencies, and lower system noise temperature.

Reduction in system noise temperature has been brought about primarily by improvements in the low noise amplifier. In this section, the evolution of low noise amplifiers will be described from their beginnings to the maser amplifiers used today. A short discussion of maser design techniques will then be presented, and finally, the high performance systems being planned for the late 1980s will be described. Table 4-1 summarizes the performance of low-noise amplifiers from 1960 to 1982, and gives the expected additional

performance of future Network maser systems during the time period 1983-1989. In Tables 4-1, 4-2, and 4-3, two values are often given for gain, bandwidth, and noise temperature. The first value is the best measured performance among all units of that type at a selected frequency within the bandwidth and/or tuning range. The second value (in parentheses) is the worst measured performance among all units at the outside edge of the bandwidth or tuning range.

B. HISTORY

1. Vacuum Tubes and Parametric Amplifiers

In 1958, when JPL was designi . the world-wide network which would become the future Deep Space Network, a new 26-m antenna had just been constructed in the Mojave Desert at Goldstone, California, and two similar antenna were about to be built overseas. The space race was in full swing and the Goldstone station was equipped with mixers operating at 960 MHz with a nominal system operating noise temperature of about 1500 K. This antenna was tracking Pioneer 4, the first U.S. spacecraft to leave the Earth's gravitational field, and it was already obvious that lower noise parametric amplifiers would be needed for future missions. In fact, General Electric's Schenectady facility, equipped with a tiny 6-m dish and a parametric amplifier, claimed to have tracked Pioneer 4 from a greater distance than JPL. By 1960, JPL had added a second antenna at Goldstone in preparation for the Echo satellite experiment. Parametric amplifiers had been under development at JPL for several years, and the Echo experiment saw their first operational use on both Goldstone antennas. These early units reduced the system noise temperature by an order of magnitude--from 1500 to about 220 K --and plans were made to upgrade the entire network (Ref. 4-1).

2. The First Maser Amplifiers

Another type of amplifier device was appearing on the scene that had the potential of reducing system noise temperature another order of magnitude. In 1953, Professor J. Weber of the University of Maryland published a brief article describing a process that might result in amplification in a

manner different from any previously known principle of amplification. In 1954 and 1955, U.S. and Russian groups, using these ideas independently, succeeded in obtaining amplification and oscillation at 23.870 GHz, using a beam of ammonia molecules operating on a natural resonance of the ammonia molecule. They called their device a maser, for Microwave Amplification by Stimulated Emission of Radiation. The ammonia maser found application as an ultrastable frequency standard, but was not suitable as a tuneable amplifier with reasonable bandwidth. Then, Professor Bloembergen of Harvard published his proposal for a solid state microwave maser amplifier which could provide tuneability, reasonable bandwidths, and noise temperatures lower than any other known device. Soon after, in 1957, the first successful solid state maser amplifiers were developed by groups at Bell Telephone Labs and Massachusetts Institute of Technology (Ref. 4-2).

The potential for this new maser amplifier in the Deep Space Network was not lost on Dr. Walt Higa and his group at JPL. They stopped work on the ammonia maser frequency standard, and began development of a maser amplifier for the Goldstone antennas. The result of this effort was a single-cavity reflection-type ruby maser which operated at 960 MHz with 20 dB net gain, 750 kHz bandwidth, and an input effective noise temperature of 30 K (later units measured 22 K, Ref. 4-3). The necessary 4.2 K cryogenic environment was provided by an open-cycle liquid-helium dewar which could function on a moving antenna without spilling refrigerant. In 1960, the first of these masers was installed at the prime focus of the Pioneer 26-m antenna at Goldstone. Later, a similar unit proved its worth by receiving satisfactory signals from Ranger 3 when the paramp-equipped Echo antenna could not because of unfavorable spacecraft orientation.

3. Goals of the JPL Maser Program

These early events marked the beginning of an ultra-low-noise maser development program that has continued at JPL to the present day. Then and now, major goals in the development and implementation of maser amplifiers have been:

(1) Provide state-of-the-art performance to continually increase the capacity to acquire data at greater distances.

(2) Introduce new technology on an experimental, non-interference basis, and then implement as an operational capability on a later mission.

(3) Respond "beyond the call of duty" to flight programs with needed new technology, especially in emergency situations.

(4) Steadily improve overall reliability in spite of increased performance and complexity.

(5) Provide for operation and maintainability by field personnel.

4. Planetary Radar At Goldstone

JPL's planetary radar program at Goldstone was proving to be an astronomical tool that could provide astronomers and mission planners alike with valuable information. It was also an excellent proving ground for new antenna, low noise amplifier, and transmitter equipment that would eventually become operational in the Network. Very soon after the 960 MHz maser was developed, a similar maser was built for 2388 MHz operation on the Pioneer antenna at Goldstone. The first major JPL success at interplanetary radar was achieved from the planet Venus with the use of this maser (Ref. 4-4). In 1962, a 2388 MHz dual-cavity maser was developed with 34 dB net gain, 2.5 MHz bandwidth, and 18 K noise temperature (Ref. 4-5). A Cassegrainian antenna feed configuration made it possible to achieve a total system temperature of 40 K. Radar echoes from Mars were obtained with this system in 1963.

5. Closed-Cycle Refrigerators

It was painfully obvious to everyone concerned that the open-cycle liquid helium dewar required by the maser amplifier would have to be replaced with a reliable closed-cycle refrigerator (CCR) if masers were to become an

operational reality. There was a commercially manufactured CCR available in 1962 from Arthur D. Little, Inc. JPL procured one of these units, installed a 960 MHz cavity maser inside, and operated it at Goldstone for a short time.

Meanwhile, the maser group started development work on a traveling-wave maser (TWM) structure for the planetary radar project that would provide much larger gain bandwidth products than were available with cavity masers. In September 1963, the first JPL traveling-wave maser/closed cycle refrigerator (TWM/CCR) system was installed in the Venus antenna. Performance at 2388 MHz exceeded previous cavity masers by a wide margin: 40 dB net gain, 12 MHz bandwidth, and 8 K noise temperature. Half the known planets of our solar system were probed with earth based radar using this maser system.

As far as spacecraft tracking operations were concerned during this time period (1962-63), the Echo and Venus stations were both equipped with 960 MHz liquid helium-cooled cavity masers in a Cassegrain feedcone, providing a nominal system noise temperature of 50 K. Overseas stations were still equipped with 300 K parametric amplifiers.

6. Move to S-Band

In 1962, the recommendation was made that the entire Network switch over from 960 MHz to 2295 MHz (S-band). The resulting increase in figure of merit would be required for future missions to Mars and beyond. While the Network was engaged in tracking the Mariner Venus Flyby in late 1962, plans were made to develop and test the S-band TWM/CCR discussed previously on the DSS 13 research antenna at Goldstone. The decision was made to implement all Network stations with similar S-band units and a contract was placed with Airborne Instruments Laboratories to provide traveling wave masers (TWM's) mounted on Arthur D. Little, Inc. CCR's (Ref. 4-6). These TWM/CCR systems were more complex than any amplifiers used previously in the Network and consisted of a 1) CCR mounted in the cassegrain feedcone, 2) TWM contained within the CCR, 3) large helium compressor mounted in a lower portion of the antenna or on the ground, 4) control and RF instrumentation racks located in a control room, 5) gas lines connecting the compressor and CCR, and 6) an array of vacuum and cryogenic support equipment. The first system was installed at Goldstone in March 1964 and all antennas were so equipped by the 1965 Mariner

flyby of Mars. These masers provided 35 dB net gain, 17 MHz bandwidth, and 2270-2300 MHz tuning range. Maser input noise temperature was 9 K, and nominal system noise temperature was 55 K, a factor of 4 improvement over parametric amplifier-equipped systems.

The Network was now committed to maser amplifiers and CCR's for full-time field use on all antennas. This first experience with full-scale maser implementation was not without problems. Both the refrigeration and maser pump systems proved to have reliability problems, and the new and sophisticated nature of the equipment made field repairs by Network personnel very difficult. Parallel efforts were begun at JPL to develop a more efficient and reliable CCR, and a more rugged, stable maser amplifier assembly.

7. Field-Operational Masers Come of Age

A very ambitious Mariner mission to Venus was being planned for 1967 encounter. The first of the 64-m antennas had been built at Goldstone, and would be equipped with a very low noise receive-only feedcone (Ref. 4-7) for this mission. The backup for the 64-m station would be the DSS 13 research 26-m antenna equipped with a similar feedcone. The two masers developed for these "ultra-cones" represented a successful milestone in the program to make the TWM/CCR system a dependable high-performance component (Ref. 4-8). The maser tuned from 2270-2400 MHz , covering both Network and planetary radar frequencies with net gains of 50-35 dB. An input noise temperature of 5.5-7 K was achieved with the help of a cooled coaxial input line center conductor. The rugged one-piece slow-wave structure proved very reliable and stable under thermal cycling, and the construction is still used in many Network TWM's today. The CCR likewise included innovations which improved reliability (MTBF was increased from ≈ 500 hours to ≈ 3000 hours), simplified assembly, and reduced cooldown time (Ref. 4-9).

New milestones for noise temperature and reliability were established by these TWM/CCR's and the receive-only feedcone. The system noise temperature measured 16 K and these two systems accumulated over 10,000 hours run time by January 1967 without incident. During 1970-71, all Network stations received JPL-built TWM/CCR systems similar to the above research units. These systems, denoted Block III S-band TWM/CCR (Ref. 4-10), are still operating on

Network antennas at the present time (1982). Radar capability was not needed, so they were designed for maximum gain (45 dB) and bandwidth (40-50 MHz) at a fixed frequency of 2285 MHz. Input noise temperature ranges from 5 to 8 K.

8. Lowest Noise Maser Amplifier

A crash research and development program was initiated in 1973 to develop an S-band maser with a lower noise temperature than existing units. Two significant JPL technological developments contributed to the success of this effort: 1) use of a superconducting magnet inside the CCR, replacing the massive external magnet used on the Block III masers, and 2) development of an evacuated coaxial input transmission line with the entire center conductor cooled to 4.5 K. This TWM/CCR measured the lowest input noise temperature achieved to date for a microwave maser amplifier - 2.0 K (Ref. 4-11). The 64-m antennas at Canbarra and Goldstone achieved a system noise temperature of 13 K $\pm$ 1 K for Mariner 10 Encounter with Venus and Mercury using this maser (this is the lowest system noise temperature ever achieved on a Network antenna). Today, a production version of this maser is in the S-band Polarization Diversity (SPD) feedcone of each 64-m antenna in the Network.

9. Deep Space Network Moves to X-Band

The Network was aware of the need to operate at even higher frequencies than S-band for future space missions. Preparation for this eventuality began in 1964 when a multiple-cavity maser operating in a liquid helium dewar was purchased from Hughes Research Laboratories (Ref. 4-12). This unit was installed and evaluated in a 9-m R&D antenna at Goldstone. It operated at 8448 MHz, providing 18 K maser noise temperature and 15 MHz bandwidth.

The first X-band TWM/CCR system was designed and built at JPL using the considerable expertise that had been gained during the S-band maser development. This unit (Ref. 4-13) was tuneable from 8370-8520 MHz, with 45-30 dB net gain, 17 MHz bandwidth, and 18-22 K noise temperature. It was installed on the 64-m antenna at Goldstone in 1966, and removed in 1968 to await an improved, more reliable replacement. This improved TWM/CCR (Ref.

4-14) arrived at the 64-m station in early 1970. In addition to providing 7-13 K noise temperature, about half that of the previous design, this system also demonstrated the short- and long-term gain stability necessary for a successful field-operable maser.

The first use of an X-band spacecraft downlink in the Network occurred in 1973, when the Mariner 10 Venus-Mercury probe transmitted simultaneous S- and X-band signals for a transmission media charged-particle calibration experiment. A tuneable X-band TWM/CCR (Ref. 4-15) was installed at the 64-m Goldstone antenna in January 1973 for this occasion, and represented a further improvement over previous designs. Noise temperature was lowered to 6.5 - 10.5 K over a 7750-8750 MHz tuning range. This was the first JPL X-band maser to use a superconducting magnet.

The 1975 Viking Orbiter/Lander missions to Mars and future Voyager missions to Jupiter and Saturn depended on X-band downlink communications. The 9 years of orderly X-band maser development (1964-1973) had virtually assured the Network that a well-engineered reliable system would be available for implementation at all stations when needed. The implementation process began by converting the tuneable maser design used for Mariner 10 to a fixed-tuned design so that maximum gain bandwidth product could be achieved at the Network frequencies. Most other features of the research maser were incorporated with the addition of some innovations. The design effort was very successful: noise temperature ranged between 5-9.5 K with over 50 MHz of bandwidth and 45 dB nominal gain at 8420 MHz. These systems, termed Block I X-band TWM/CCR (Ref. 4-16), were manufactured and installed on all antennas during 1975-76. At present all 34-m antennas are still equipped with these systems.

10. New X-Band Maser for Jupiter and Saturn

After the Voyager Jupiter-Saturn spacecraft were launched, mission planners found that the science value from Saturn would be greatly enhanced if the X-band data rate could be increased 63%. To accomplish this, three major candidates for increasing downlink figure of merit were identified - one of these was to design and build an X-band TWM/CCR with one-half the noise

temperature of the existing Block I systems. The maser group at JPL found this task to be a very challenging one, and the version that was developed represented a major departure from then-current technology in the areas of 1) amplifier slow-wave structure, 2) signal input transmission line, and 3) superconducting magnet.

This maser provided the reduction in noise temperature (over existing Block I units) requested: 3-4.5 K at the input flange. The 60-110 MHz bandwidth (center frequency 8450 MHz) also represents a milestone for masers in this frequency range. Six of these systems, termed Block II X-band TWM/CCR's (Ref. 4-17), were hurriedly installed during 1980-81 in the 64-m antenna Subnet as the Voyager spacecraft were nearing encounter.

11. Ku-Band Maser

The rugged, one-piece, copper, slow-wave structure developed by JPL in the mid-1960's, and which has served so successfully in all Network masers (except for the new Voyager X-band maser development), reached its highest practical operating frequency with the development of a tuneable Ku-band maser system tuning 14.3 to 16.3 GHz (Ref. 4-18). 8.5-13 K noise temperatures were demonstrated over the tuning range with 17 MHz bandwidth and 48-30 dB gain. This maser, the first to incorporate a superconducting magnet, was installed on the 64-m antenna at Goldstone from 1971 to 1982 and used for antenna calibrations and radio science.

12. K-Band Reflected-Wave Maser

The highest frequency maser amplifier system that has been supplied to a Network antenna is a K-band maser that has attracted a large amount of interest among radio astronomers nationwide and worldwide.

The concept for this design was developed under a California Institute of Technology President's Fund grant with the University of California at San Diego and JPL (Ref. 4-19). The first field-worthy reflected-wave maser and associated superconducting magnet were designed and developed at JPL in a cooperative venture by personnel from JPL and the National Radio Astronomy

Observatory (NRAO) in West Virginia (Ref. 4-20). This maser is unique among maser designs in that it can provide a very large instantaneous bandwidth (up to 500 MHz) and a large tuning range (19-25 GHz) over frequencies of particular interest to radio astronomers. The interest generated by this development led to a number of additional cooperative ventures between JPL and various radio astronomy centers whereby these centers have been able to develop and operate similar K-band maser systems for their own use.[1]

Two of these K-band masers are presently operating on the 64-meter antennas in support of antenna calibration and radio astronomy applications. Both units have dual feedhorns for antenna beam switching and a cryogenically cooled electronic Dicke switch. The maser at DSS 43 provides approximately 150 MHz bandwidth and 30 dB gain over a 18-25 GHz tuning range. The maser at DSS 14 provides 110 MHz bandwidth and 30 dB gain at a frequency of 22.2 GHz (tuning range limited by maser pump source). Input noise temperature for these maser systems is in the range 10-16 K.

Table 4-2 summaries all maser amplifier systems built for the Network from the first cavity maser in 1960 to the present.

C. PRESENT (1982) MASERS

The Network at the present time (1982) consists of three Deep Space Communication Complexes. Each complex has one 64-m-diameter steerable antenna and one 34-m-diameter steerable antenna. Each antenna contains maser amplifiers operating continuously at S-band and X-band. In addition to the above the complex at Goldstone, California, has a 26-m antenna which is

---

[1]These centers include the Massachusetts Institute of Technology (maser installed on Haystack antenna), Princeton University (maser flown on high altitude balloon), National Radio Astronomy Observatory, Commonwealth Scientific Industrial Research Organization (CSIRO) (maser with cryogenically cooled Dicke switch installed on the Network 64-m antenna in Australia), Max Planck Institute in Bonn, Germany (maser with cryogenically cooled feedhorns and Dicke switch installed on the Effelsberg, Germany, 100-meter antenna), and California Institute of Technology (maser installed on the Owens Valley Radio Observatory).

committed to supporting research and development activities, and two of the 64-m antennas (Goldstone and Australia) have masers operating at K-band. All TWM/CCR systems are located in Cassegrainian feedcones on the antennas. Each system's associated helium compressor is located either at a lower elevation on the antenna structure or on the ground.

A tabulation of the maser amplifiers operating on each antenna in the Network is summarized in Table 4-4. The typical operating parameters of each maser type presently in use in the DSN are listed in Table 4-3.

D. MASER DESIGN PRINCIPLES

The maser is a Microwave Amplifier by Stimulated Emission of Radiation. Masers (and lasers) are quantum electronic devices which operate according to the principles of quantum mechanics, which include the concepts that (1) atoms (or atomic-sized systems) can exist only in certain discrete allowed energy states or energy levels, and (2) interaction between applied electromagnetic radiation and the atoms can occur only in discrete amounts of energy corresponding to specific frequencies.

All masers share a common requirement for one or more pump oscillators, which provide energy for the amplification of the desired microwave signal. The power delivered by the pump oscillator rearranges the populations of the various quantum states of electrons in the maser material such that the material will emit radiation at the signal frequency, and therefore provide amplification, when it is stimulated by a small amount of input signal radiation.

A simple practical form of maser amplifier using a solid maser material is shown in Fig. 4-1. The maser crystal is placed in a microwave resonator which is designed to provide efficient interaction between the crystal and both signal and pump microwave frequencies. The signal to be amplified is fed into the cavity via a coaxial transmission line. Regenerative amplification then occurs in the cavity, and the amplified signal returns out the same transmission line and is externally separated from the input signal by a non-reciprocal device called a circulator. Microwave power at the pump frequency is also sent to the cavity via the same signal transmission line (in

most maser designs, a separate waveguide pump transmission line is used). In order to place the active electrons in the maser crystal into suitable quantum states, a dc magnetic field is applied to the crystal and a refrigeration system is provided to cool the crystal to cryogenic temperatures (typically 1.8-4.5 K.

In the Deep Space Network, the form of maser amplifier in general use today is the traveling-wave maser. Typically, this type of maser construction has a much greater gain bandwidth product than is available from a single or dual cavity maser. A recent design of this type of maser is shown schematically in Fig. 4-2. The signal circuit consists of coaxial input and output lines connected to a slow-wave structure having a long row of conducting metal strips. This slow-wave structure is sandwiched on one side by a slab of ruby crystal maser material and on the other side by a ferrite isolator strip. The slow-wave structure lengthens the interaction time of the input microwave signal with the maser material, and the isolator strip prevents regenerative amplification or oscillation by absorbing undesired signal frequency waves traveling in the backward direction.

The sandwiched slow-wave structure is enclosed in a rectangular channel which acts as a waveguide transmission line at the pump frequency. Pump energy is fed into one end of this channel and illuminates the entire length of ruby maser material.

A number of these maser amplifier channels are cascaded to provide the desired signal gain and bandwidth. They are installed inside a superconducting electromagnet, the magnetic field of which adjusts the quantum states in the ruby material to desired values, and biases the ferrite isolator strip to provide reverse isolation at the signal frequency.

The maser amplifier-superconducting magnet assembly is cooled to 4.5 kelvins operating temperature inside a vacuum insulated closed-cycle helium refrigerator. The system is completed with the addition of 1) signal input, signal output, and pump transmission lines which connect the cooled maser amplifier with the outside room temperature environment, 2) external Gunn diode pump oscillator(s), 3) remotely located helium compressor which provides

purified high pressure helium gas to the refrigerator, 4) electronic controls for the pump oscillator(s), magnet, refrigerator, compressor, etc., and 5) a monitor receiver with which to calibrate maser gain.

Photographs of a recent Network traveling-wave maser, the Block II X-band maser, are shown in Figs. 4-3 through 4-8 with labels pointing out many of the components discussed above. The low noise temperatures, wide bandwidth, high stability and reliability of present Network masers are the result of over 20 years development of these components, which include:

(1) Slow-wave structures with improved uniformity and low signal frequency insertion loss.
(2) Long-life solid-state pump oscillators.
(3) Compact persistent-mode superconducting electromagnets in place of massive external permanent magnets.
(4) Extremely low noise input signal transmission lines using cryogenically cooled segments.
(5) Sophisticated ferrite isolator designs having lower forward insertion loss than simple strips.
(6) High quality single crystals of ruby maser material.
(7) Highly stable closed-cycle helium refrigeration systems capable of round-the-clock operation on steerable antennas.

Figure 4-9 shows a typical S-band maser installation in a Network antenna.

E. FUTURE LOW NOISE AMPLIFIERS

Future plans for low noise amplifiers in the Network include providing additional high-performance S- and X-band maser/CCR systems, and developing new systems with more versatile performance characteristics to support a wide variety of users. Specifically:

1. Additional Block II-A X-Band Masers

The Network is implementing two new 34-meter antennas. These antennas will be equipped with Block II-A X-band TWM/CCR's similar to the Block II units presently installed on the 64-m antennas. Other large non-NASA radio telescopes are expected to obtain Block II-A X-band TWM/CCR's in support of Voyager Uranus and Neptune encounters.

2. Additional Block IV S-Band Masers

Certain Block III S-band TWM/CCR's will be converted to lower noise Block IV S-band systems on 64-m antennas.

3. New Wide Bandwidth S-Band Masers

Future S-band mission downlink frequency requirements include 2217 MHz for the Giacobini-Zinner Comet Mission, various frequencies in the 2270-2300 MHz band, and 2320 MHz for planetary radar. The existing Block III and Block IV S-band masers will not operate over all those frequencies. Development is now underway on a new maser which uses the concept of the half-wave printed circuit slow-wave structure used so successfully in the Block II X-band maser program. This new maser is expected to have a noise temperature similar to that of the Block IV S-band maser, but will provide a bandwidth of over 60 MHz and a center frequency tuning range sufficient to permit operation over the range 2217-2320 MHz. Two of these units will be built and installed on the DSS 14 and DSS 63 64-m antennas.

4. Multifrequency Upconverter-Maser System

Recent advances in many areas of technology have made possible the development of a low-noise receiving system that can exhibit noise temperatures similar to those of present maser amplifiers, while providing instantaneous bandwidths and tuning ranges many times greater than those of present

maser amplifiers in the 1-18 GHz range. This system comprises a cryogenically cooled, upper-sideband parametric upconverter followed by a maser amplifier (Ref. 4-21). Two recent developments in particular have made these performance levels possible: the first is the availability of very-high-quality gallium arsenide varactor diodes with low package parasitic reactances, and the second is the development of wideband microwave maser techniques suitable for frequencies above 18 GHz.

A demonstration model multifrequency upconverter-maser system, shown in Fig. 4-10, is being designed and built at JPL for evaluation in the Network. The cryogenic refrigerator package will contain inputs at 2, 8, and 32 GHz, thus having the potential to replace three separate maser/refrigerator systems. Multiple frequency bands in one refrigerator package are possible because of the small size and weight of the parametric upconverter needed for each frequency.

Present plans call for two modes of operation. In the first mode, the 2 GHz and 8 GHz inputs will be upconverted to adjacent bands in the 32 GHz region, then amplified simultaneously by a 32 GHz wideband maser amplifier now being developed at JPL. Instantaneous bandwidths at S- and X-band would be approximately 100 and 400 MHz, respectively. In the second mode of operation, the maser amplifier would be switched directly to the 32 GHz input line to provide 500 MHz instantaneous bandwidth for the new 31.8-32.3 GHz space-to-Earth downlink allocation. In addition, single band operation at either S-band or X-band with full 500 MHz instantaneous bandwidth is possible. This system will also be the first low-noise amplifier in the Network to have a microprocessor-based remote data acquisition and control system.

5. FET Amplifiers

An S-band field-effect transistor (FET) amplifier will be provided to the 34-m listen-only antennas at Goldstone and Canberra to support missions that do not require the noise performance of a maser amplifier. These units will provide a nominal 70 K noise temperature over the frequency range of 2200-2300 MHz.

F. CONCLUSION

As seen in previous sections, the long history of development and improvement of the Network has been accompanied by a corresponding improvement in performance and reliability of maser amplifiers and associated cryogenic refrigerators. Much of this past development has been aimed at the reduction of maser noise temperature. With the achievement of 2 K noise temperature with the Block IV S-band maser, and 4 K with the Block II X-band maser, effort to further reduce these very low noise temperatures is of little present value. Rather, development is now directed toward providing additional versatility to economically support a wide variety of users with various low-noise amplifier requirements by providing wider bandwidths, wider tuning ranges, increased RFI protection, and eventually multiple frequency bands (including 32 GHz) in one CCR. The Figure of Merit requirements for Network receiving systems in coming years are not abating, but are becoming more stringent. Therefore, maser amplifiers and associated cryogenic refrigerators are expected to remain a necessary part of the Deep Space Network for a long time.

REFERENCES

4-1. Corliss, W. A., A History of the Deep Space Network, NASA CR-151915, National Aeronautics and Space Administration, Nov. 1976.

4-2. Siegman, A. E., Microwave Solid State Maser, New York, McGraw Hill, 1964.

4-3. Sato, T., and Stelzried, C. T., "An Operational 960-MC Maser System for Deep-Space Tracking Missions," IRE Trans Space Electron. Telem., Vol. SET-8, June 1962.

4-4. Victor, W. K., and Stevens, R., "The 1961 JPL Venus radar experiment," IRE Trans. Space Electron. Telem., Vol. SET-8, June 1962.

4-5. Clauss, R. C., "A 2388-Mc two-cavity maser for planetary radar," Microwave J., Vol. 8, May 1965

4-6. Clauss, R. C., Higa, W., Stelzried, C., and Weibe, E., "Total system noise temperature: 15°K," IEEE Trans. Microwave Theory Tech. (Corresp.), Vol. MTT-12, Nov. 1964

4-7. Levy, G. S., Bathker, D. A., Higa, A., and Stelzried, C. T., "The ultra cone: An ultra-low-noise space communications ground radio-frequency system," IEEE Trans. Microwave Theory Tech., Vol. MTT-16, Sep. 1968

4-8. Clauss, R. C., A Traveling Wave Maser for Deep Space Communication at 2295 and 2388 MHz, Technical Report 32-1072, Jet Propulsion Laboratory, Pasadena, Calif., Feb. 15, 1967

4-9. Higa, W. H., and Weibe, E., "A simplified approach to heat exchanger construction for cryogenic refrigerators," Cryogenic Technol., Vol. 3, Mar./Apr. 1967

4-10. Trowbridge, D. L., Block III Maser Implementation Program, Technical Report 32-1526, Vol. XVIII, p. 130-135, Jet Propulsion Laboratory, Pasadena, Calif., December 15, 1973

4-11. Clauss, R. C., and Weibe, E., Low Noise Receivers: Microwave Maser Development, Technical Report 32-1526, Vol. XIX, pp. 93-99, Jet Propulsion Laboratory, Pasadena, Calif., Feb. 15, 1974

4-12. Stelzried, C. T., "Operational performance of an H-band coupled cavity transmission maser," Microwave J., Vol. 10, pp. 103-106, Mar. 1967

4-13. Petty, S. M., and Clauss, R. C., "X -band traveling wave maser," IEEE Trans. Microwave Theory Tech (Corresp.), Vol. MMT-16, pp. 47-48 Jan. 1968

4-14. Clauss, R., and Quinn, R., Tracking and Data Acquisition Elements Research: Low Noise Receivers: Microwave Maser Development, Tech. Rep. 32-1526, Vol. V, pp. 102-108 Jet Propulsion Laboratory, Pasadena, Calif. Oct. 15, 1971

4-15. Clauss, R. C., Weibe, E., and Quinn, R. R., Low Noise Receivers: Microwave Development, Technical Report 32-1526, Vol. XI, pp. 71-80 Jet Propulsion Laboratory, Pasadena, Calif., October 15, 1972

4-16. Trowbridge, D. L., X-Band Traveling Wave Maser Amplifier, Technical Report 32-1526, Vol. XVII, pp. 123-130, Jet Propulsion Laboratory, Pasadena, Calif., Oct. 15, 1973

4-17 Trowbridge, D. L., "X-Band Low Noise Traveling-Wave Maser," TDA Progress Report 42-60, pp. 126-131, Jet Propulsion Laboratory, Pasadena, Calif., Dec. 15, 1980

4-18. Clauss, R. C. and Quinn, R., Low Noise Receivers-Microwave Maser Development, Technical Report 32-1526, Vol. V, pp. 102-108, Jet Propulsion Laboratory, Pasadena, Calif., October 15, 1971.

4-19. Flesner, L., Schultz, S., and Clauss, R., "Simple waveguide reflection maser with broad tunability," Review of Scientific Instruments, Vol. 48, No. 8, pp. 1104-1105, August 1977.

4-20. Craig R. Moore and Clauss, R. C., "A reflected-wave ruby maser with K-band tuning range and large instantaneous bandwidth," IEEE Trans. Microwave Theory and Tech., Vol. MTT-27, No. 3, Mar. 1979

4-21. Petty, S., Neff, D., and Norris, D., "Low Noise Receivers: S-Band Parametric Upconverter Development," DSN Progress Report 42-48, pp. 31-47, Jet Propulsion Laboratory, Pasadena, Calif., Dec. 15, 1978

Table 4-1. Noise temperature performance of the Deep Space Network Operational Low Noise Amplifiers

Parameter	Calender year								
	Measured								Predicted
	1960	1962	1963	1965	1971	1975	1980	1981	1988
Frequency f, GHz	0.96	0.96	0.96	2.3	2.3	8.4	2.3	8.4	32
Input amplifier effective noise Temperature T_e, K	1400	200	22	9	5(8)	5(10)	2(3.5)	3(4.5)	10

Table 4-2. Antenna mounted performance summary of Deep Space Network maser amplifiers

Frequency MHz	Maser type refrigerator, magnet type[a]	Net gain dB	Half-power bandwidth MHz	Noise temperature K	Installation month, year (first system)	Removal month, year (last system)
960	cavity, OCR, PM	20	0.75	22.30[e]	Sep. 1960	June 1965
960	cavity, CCR PM	20	0.75	17	Mar. 1962	May 1962
2295	TWM, CCR, PM	35	17	9	Nov. 1965	Mar. 1966
2270-2300	TWM, CCR, PM[b,c]	35	17	9(13)	Mar. 1964	Sep. 1971
2285	TWM, CCR, PM	45	50(40)	5(8)	Oct. 1970	Currently in use
2388	cavity, OCR, PM	20	2.5	25	Feb. 1961	May 1961
2388	dual cavity, OCR, PM	34	2.5	18	Aug. 1962	June 1963
2388	TWM, CCR, PM	40	12	8	Sep. 1963	Feb. 1966
2270-2400	TWM, CCR, PM	50(35)	14	5.5(7)	Mar. 1966	f
2240-2420	TWM, CCR, PM	45(30)	16	5.2(6)	Sep. 1967	f
2240-2420	TWM, CCR, SCM	45(27)	16	4.2(6)	Jan. 1972	f
2270-2400	TWM, CCR, SCM	40	40(10)	2(5)	Sep. 1973	Currently in use
2285	TWM, CCR, SCM	45	40	2(3.5)	Apr. 1979	Currently in use
8450	multiple cavity OCR, PM[d]	33	15	18	Oct. 1964	July 1966
8370-8520	TWM, CCR, PM	45(30)	17	18(23)	Nov. 1966	Nov. 1968
7600-8900	TWM, CCR, PM	42(30)	17	7(13)	Feb. 1970	Nov. 1972
7750-8750	TWM, CCR, SCM	45	20(17)	6.5(10.5)	Jan. 1973	Currently in use
8420	TWM, CCR, SCM	45	40	5(10)	Apr. 1975	Currently in use
8450	TWM, CCR, SCM	42	108(65)	3(4.5)	May 1980	Currently in use
14,300-16,300	TWM, CCR, SCM	48(30)	17	8.5(13)	Sep. 1971	Sep. 1982
22,200	RWM, CCR, SCM	30	110	≈16	Sep. 1982	Currently in use
18,000-25,000	RWM, CCR, SCM[g]	30	≈150	≈12	Feb. 1981	Currently in use

[a]OCR--open cycle liquid-helium dewar refrigeration. PM--permanent magnet. SCM--superconducting magnet.
[b]TWM's purchased from Airborne Instruments.
[c]CCR's purchased from Arthur D. Little, Inc.
[d]System purchased from Hughes Research Laboratories.
[e]First system was 30 K; later systems were 22 K.
[f]Removal date unknown, no longer in use.
[g]Maser on loan from National Radio Astronomy Observatory.

Table 4-3. Typical operating parameters of present (1982) Deep Space Network maser amplifiers

	Center frequency range	Net gain dB	Half power bandwidth MHz	Noise temperature K
S-Band masers				
Block III	2285 MHz	45	50(40)	5(8)
Block IV	2285 MHz	45	50(40)	2(3.5)
Research Block IV type at Station 14	2285-2388 MHz	40	40(10)	2(5)
Research at Station 13	2200-2388 MHz	[a]	[a]	[a]
X-Band masers				
Block I	8420 MHz	45	70(40)	5(10)
Block II	8450 MHz	42	108(65)	3(4.5)
Research at Station 13	8410-8425 MHz	40	15[b]	5(10)
K-Band masers				
Research at Station 43[c]	18-25[d] GHz	30	150[d]	12[d]
Research at Station 14	22.2[e] GHz	30	110	16

[a] Data not available

[b] Bandwidth can be increased to 30 MHz at 30 dB net gain

[c] Maser/CCR on loan from National Radio Astronomy Observatory

[d] Estimate

[e] Operation at other frequencies in 19-25 GHz range is possible with implementation of different pump source.

Table 4-4. Maser amplifiers in the present Deep Space Network (1982)

DSN Complex	Station	Maser amplifier/closed-cycle refrigeration systems
Goldstone, Calif.	DSS 12 34-m operational station	One X-band Block I Two S-band Block III
	DSS 13 26-m research station	One research X-band One research S-band
	DSS 14 64-m operational station	Two X-band Block II One S-band Block IV One S-band R&D Block IV-type One research X-band One research K-band
Tidbinbilla, Australia	DSS 42 34-m operational station	One X-band Block I Two S-band Block III
	DSS 43 64-m operational station	Two X-band Block II One S-band Block IV One S-band Block III One research K-band
Madrid (Robledo), Spain	DSS 61 34-m operational station	Two X-band Block I Two S-band Block III
	DSS 63 64-m operational station	Two X-band Block I Two S-band Block III

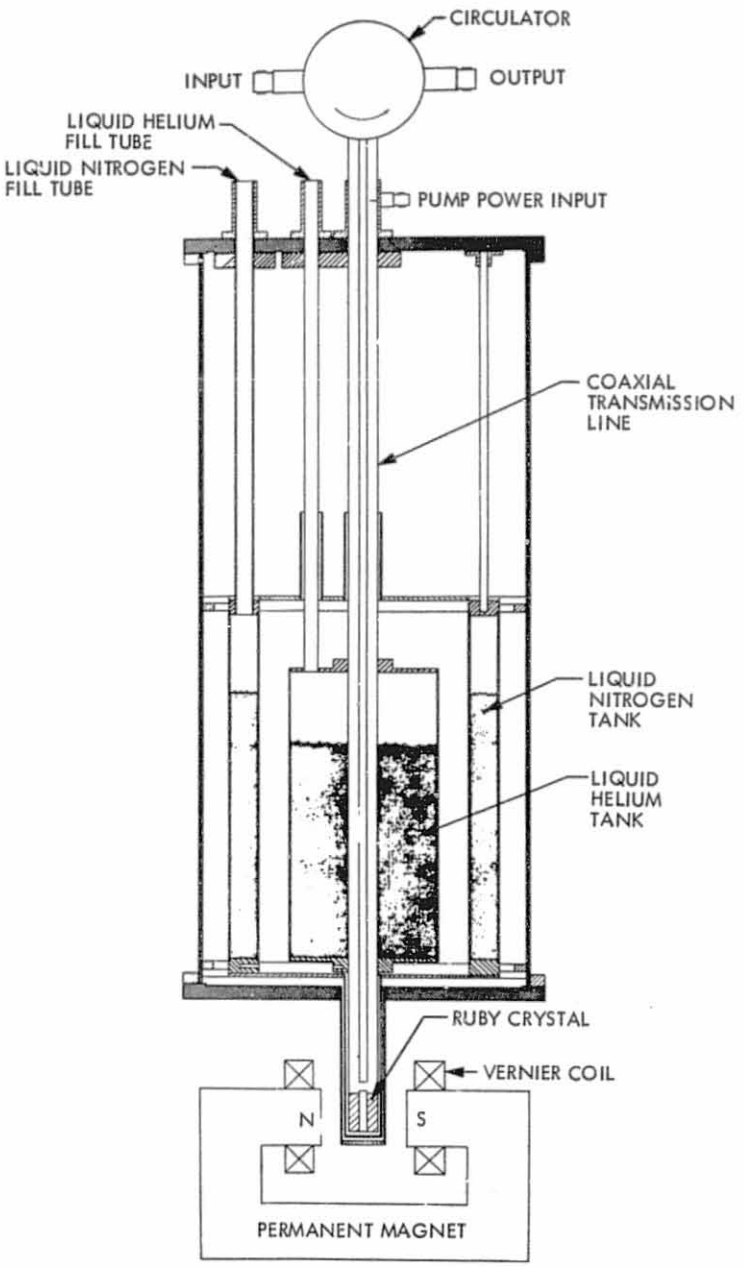

Fig. 4-1. Cavity maser amplifier

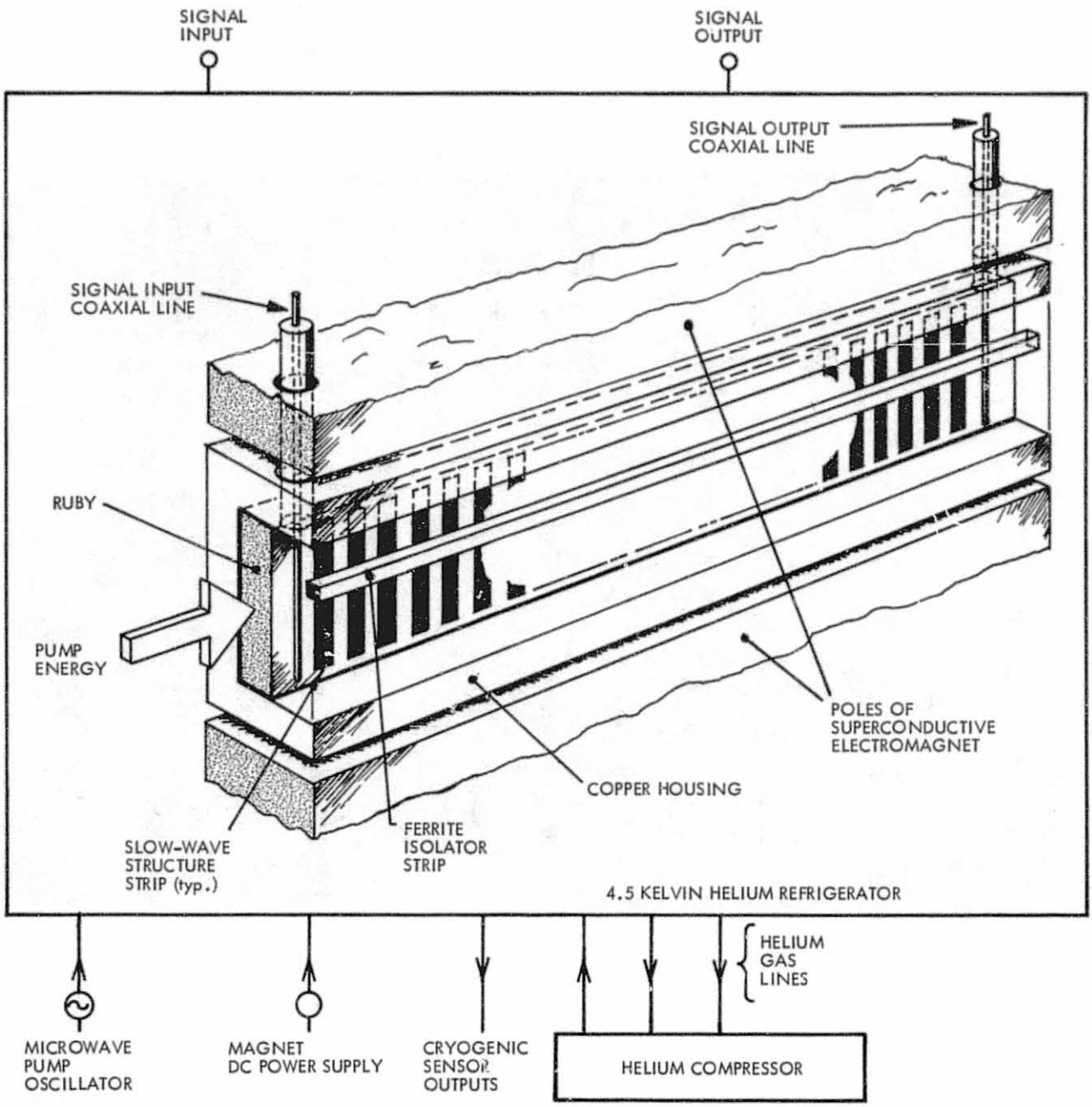

Fig. 4-2. Schematic representation of modern traveling-wave maser amplifier

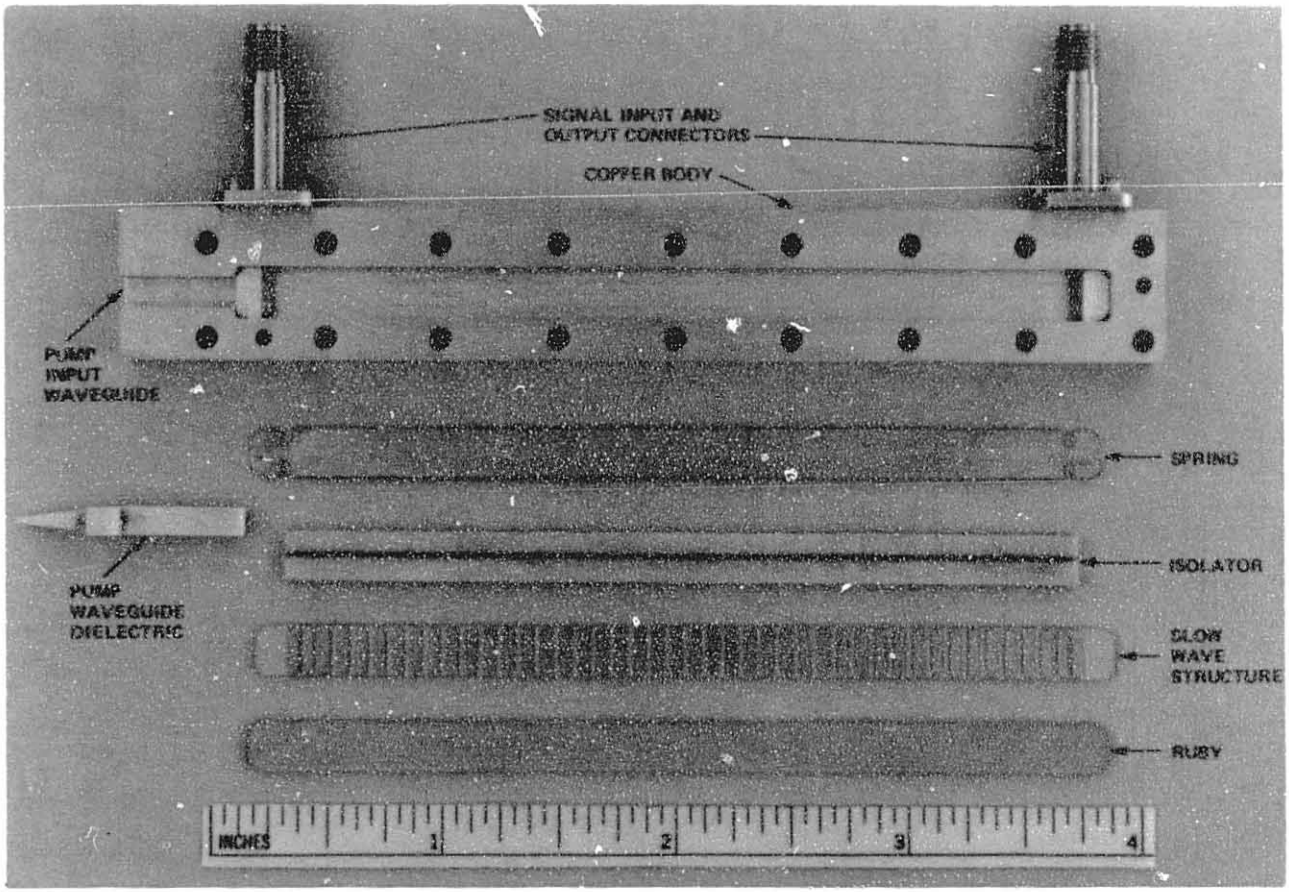

Fig. 4-3. X-band Block II-A traveling-wave maser channel

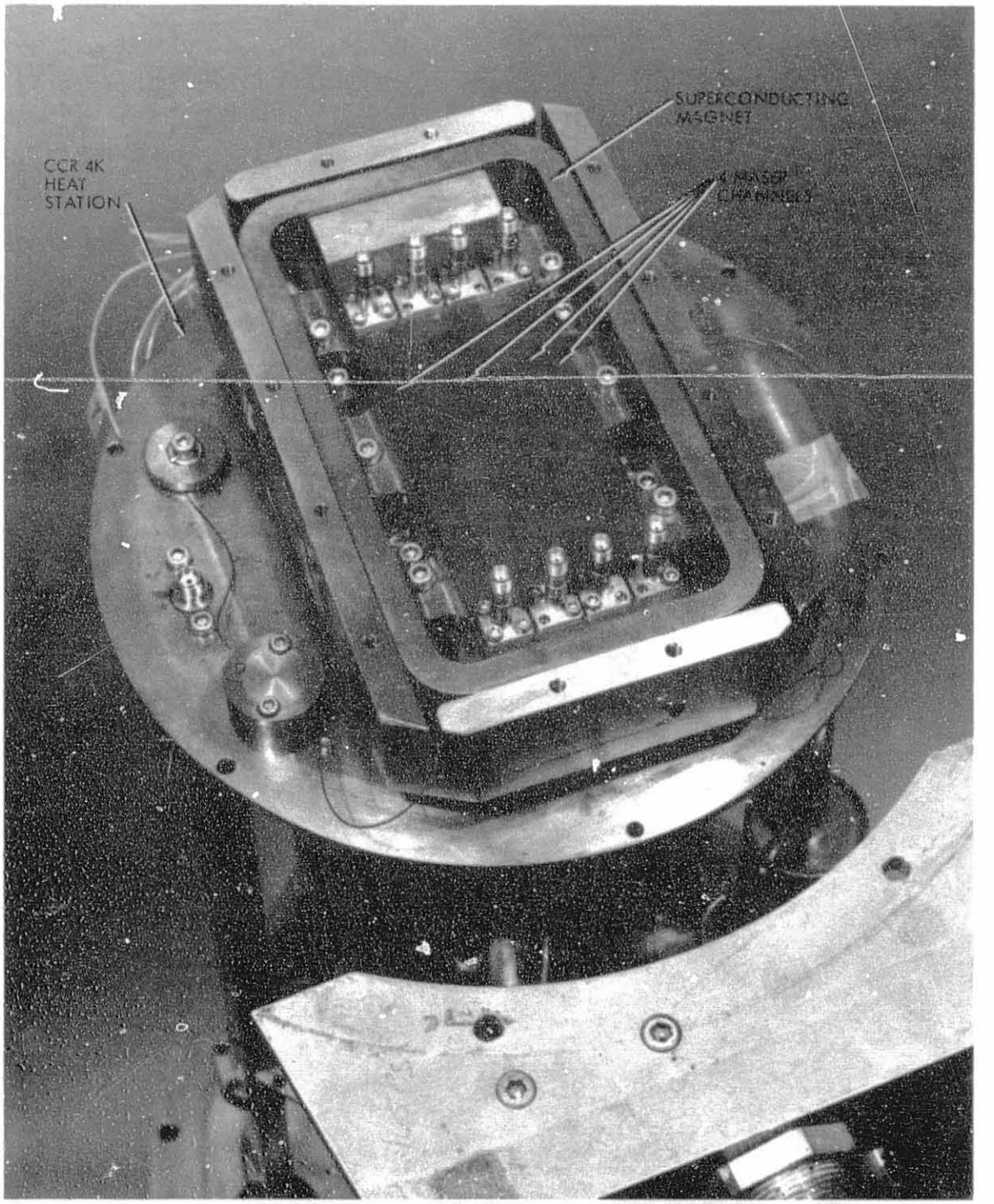

Fig. 4-4. X-band Block II-A maser assembly mounted inside superconducting magnet

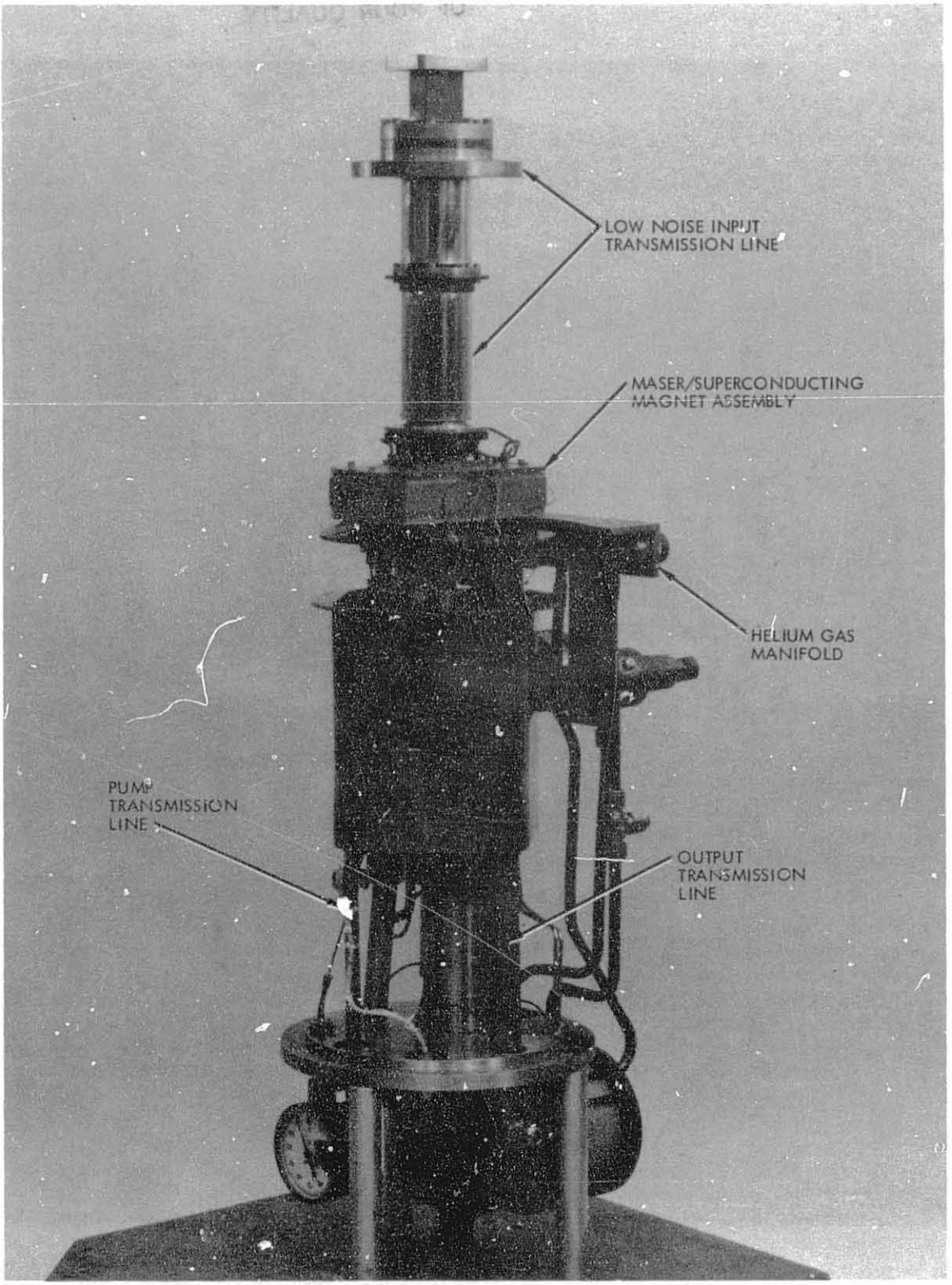

Fig. 4-5. X-band Block II-A maser/CCR assembly with radiation shields, vacuum housing and mounting frame removed

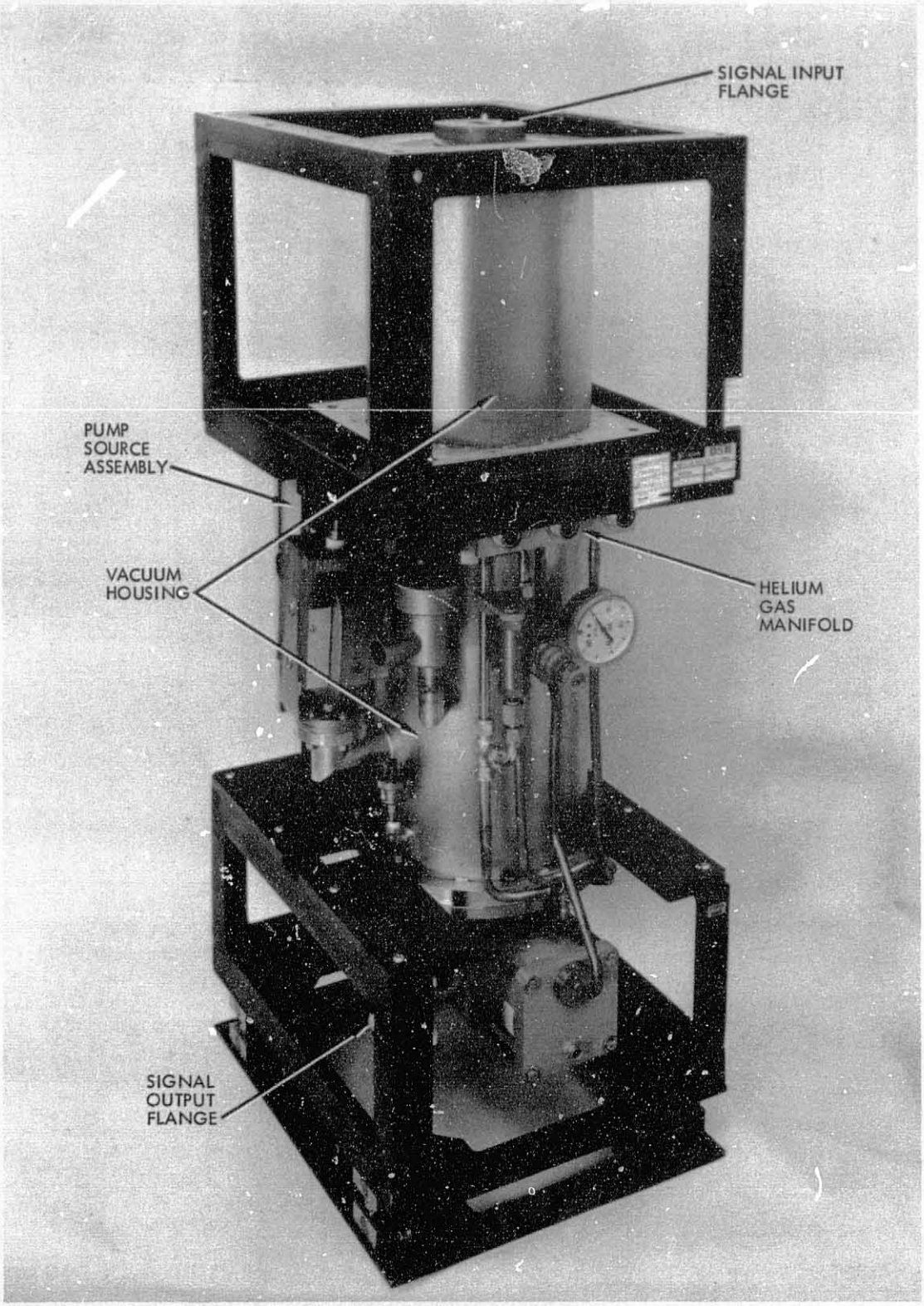

Fig. 4-6. X-band Block II-A TWM/CCR package

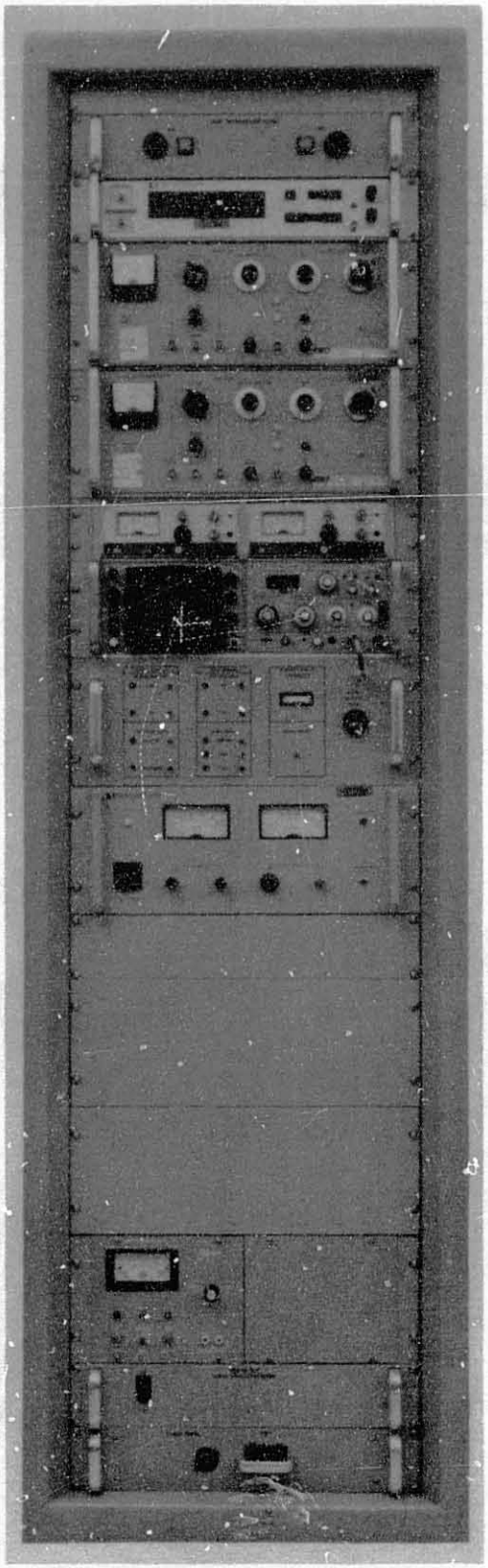

Fig. 4-7. Control room instrumentation for X-band masers

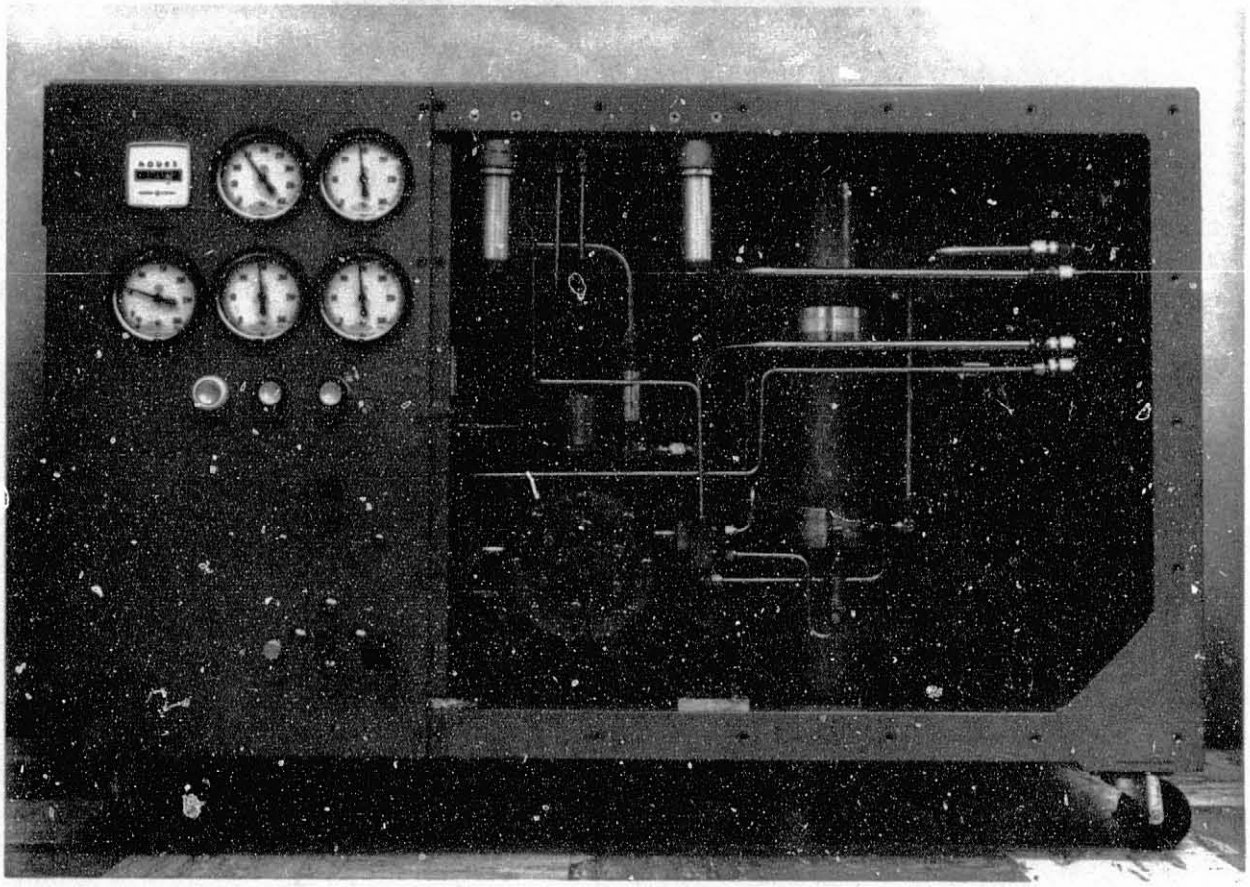

Fig. 4-8. Helium compressor for DSN closed cycle refrigerators

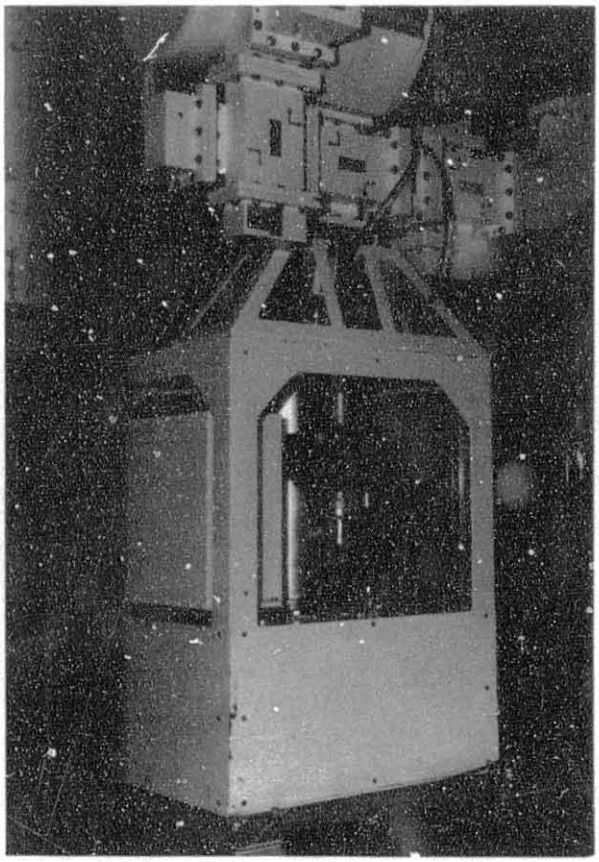

Fig. 4-9. S-band TWM/CCR installed in Cassegrain antenna assembly

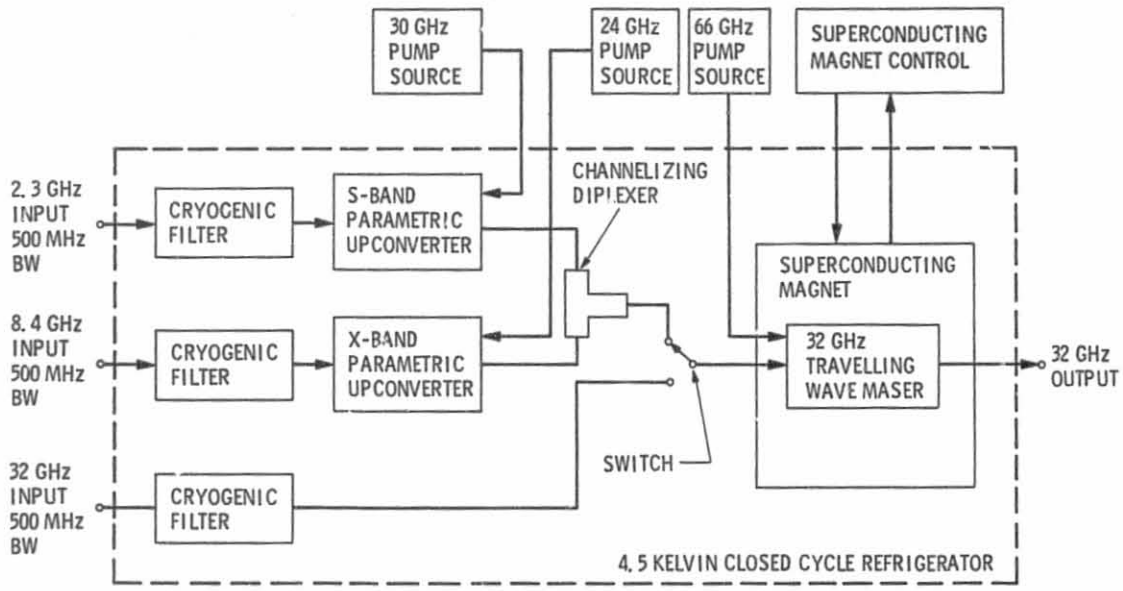

Fig. 4-10. Multifrequency upconverter-maser block diagram

C-2

V. RECEIVERS

H. Donnelly

A. INTRODUCTION

Before discussing Deep Space Network receivers, a brief description of the functions of receivers and how they interface with other elements of the Network will be presented. Not all the present capability described has been functional in the receivers since the formation of the Deep Space Network. Some of this capability has been gradually introduced over the years, as covered later in the history of receivers. Future receiver capability is also described later.

Different types of receivers are used in the Network for various purposes. The principal receiver type is used for telemetry and tracking. This receiver provides the capability, with other elements of the Network, to track the space probe utilizing doppler and range measurements, and to receive telemetry, including both scientific data from the on-board experiments and engineering data pertaining to the health of the probe.

Another type of receiver is used for radio science applications. This receiver measures phase perturbations on the carrier signal to obtain information on the composition of solar and planetary atmospheres and interplanetary space.

A third type of receiver utilizes very long baseline interferometry (VLBI) techniques for both radio science and spacecraft navigation data. Only the telemetry receiver is described in detail in this document.

The integration of the Receiver-Exciter subsystem with other portions of the Deep Space Network is shown in Fig. 5-1. A description of the major assemblies of the Receiver-Exciter Subsystem follows. Here again, all functions of the Receiver-Exciter are discussed briefly in the following. Later, the focus is on the communications function, principally the reception of telemetry data.

1. Exciter. The exciter generates a carrier, modulated with command and ranging signals, of sufficient power to drive the transmitter amplifier. This signal is used to communicate with the spacecraft over the ground-to-spacecraft uplink.

2. Phase Tracking Receiver. The phase tracking receiver maintains phase lock with the spacecraft-to-ground downlink carrier and thereby generates a reference signal used to coherently detect telemetry and ranging modulation signals for real-time data processing or to record the data for processing some time later.

3. Doppler Extractor. From an exciter reference signal and a receiver signal, the doppler extractor generates the doppler signal.

4. Subcarrier Demodulator Assembly. The subcarrier demodulator coherently detects telemetry subcarrier signals in order to extract data for processing.

5. Precision Power Monitor. This equipment provides a measurement of received carrier level using the Precision Signal Power Monitor assembly and a measurement of the system noise temperature using a Noise Adding Radiometer assembly.

6. Spectral Signal Indicator. This equipment provides a display of the received signal spectrum and a measurement of the carrier frequency to aid the receiver operator in the acquisition of the received signal. The display also provides a gross indication of telemetry modulation anomalies.

7. Real-Time Combiner. During some critical mission periods (such as a planetary flyby) when the signal levels are near threshold, it becomes necessary to combine signals from two or more antennas to obtain an adequate telemetry signal-to-noise ratio. The Real-Time Combiner combines baseband telemetry signals from more than one antenna.

8. Open-Loop Receiver. The open-loop receiver is used primarily for the support of radio science. The receiver is used to record the carrier (translated to a low frequency) for later data processing of occultation measurements. With the open loop receiver, data can be obtained during the critical period of occultation when the closed-loop receiver fails to maintain lock.

9. Very Long Baseline Interferometry Receivers. Another open-loop receiver is used for very long baseline interferometry (VLBI) measurements. This receiver utilizes VLBI techniques for radio science application to catalog radio sources and for Deep Space Network application to determine relative station locations and UT1 polar variations, to obtain intercomplex time synchronization, and to provide navigation support for space probes.

The open-loop receivers, which are used for both radio science and VLBI measurements, are part of the Multi-Mission Receiver. It is planned at some future date to use the front end of the Multi-Mission Receiver for part of the phase tracking and telemetry receiving function as well.

B. HISTORY

The present Deep Space Network, which provides communications to lunar and planetary probes, started with the tracking of Pioneer II and IV lunar probes launched in December 1958 and March 1959 respectively. These Pioneer probes used only one-way communications, downlink at L-band (960 MHz). Prior to that time a worldwide network of four tracking stations was used to support early Explorer earth satellites operating in the VHF band (108 MHz downlink).

Several lunar missions followed the Pioneer probes. These also operated at L-band, using two-way communications, an uplink at 890 MHz being added to the Network. L-band was selected as an interim frequency, used primarily

because the capability of devices that existed for the early Pioneer probes extended only to this frequency range.

During those early days of L-band tracking, the planning of lunar unmanned missions to obtain information on the lunar surface for the Apollo program and the planning of planetary exploration brought to light the need for multiple channel assignments. As a result, S-band was chosen, both because of the availability of the spectrum and because of the application of this frequency band to future deep space communication. For example, galactic background noise is high at L-band, while at the higher S-band frequency the noise level decreases. The higher frequency also provides additional advantages, including increased gain of spacecraft antennas (which are limited in area) and increased bandwidth to accommodate higher telemetry data rates. The first application of S-band was in support of Mariner IV during 1964.

S-band was used for command, tracking and telemetry in the two-way coherent configuration and for occultation measurements in the open-loop configuration.

The equipment used was designated the Block IIIC Receiver-Exciter. It was also used in the Manned Space Flight Network and referred to as the Unified S-Band System. The Block IIIC receiver-exciter, both in the phase tracking mode and open loop configuration, supported all of the S-band missions during the decade of the 1960's.

By the end of the 1960's, three Deep Space Network complexes existed. These three complexes (located in Spain, Australia and Goldstone, California) provided continuous tracking capability for the net. At each of these complexes, one 64-m and two 26-m antennas with associated electronics were operating. These antennas were grouped into one 64-m subnet and two 26-m subnets.

The Deep Space Network capability and performance during the decade of the 1960's is described in detail in Ref. 5-1, published in 1971. Since then, the Network communication link has further increased in capability and improved in performance. The changes that have occurred during the 70's are described in the following text. Each of these changes is identified with the mission for which it was first implemented. These newly added capabilities then became standard features of the Network.

1. Mariner 10 - X-Band Downlink

The addition of the X-band channels provided the capability to communicate on the downlink at higher data rates due to the increased gains of the ground and space probe antennas and the greater channel bandwidth available. X-band capability was obtained with the implementation of the Block IV receiver-exciter subsystem. The initial X-band downlink of Mariner 10 was used on an experimental basis as a radio science experiment to gain experience in operating at these frequencies. The higher data rate capability of an X-band downlink was not utilized until the Voyager program.

2. Pioneer 10 - Telemetry Data During Planetary Encounter

Pioneer 10 presented a new challenge, tracking a spacecraft through high doppler rates and a large doppler range during a single pass over a long communications link. This occurred during the flyby of the planet Jupiter in 1973. Due to the extreme range, a narrowband receiver loop was required, which is inherently unable to track large doppler rates. A tracking aid was needed during this period to maintain receiver lock. This was accomplished by the addition of a controllable oscillator in the receiver local oscillator chain, the first application of programmed frequency control in the Deep Space Network. The controllable oscillator consisted of a synthesizer and a control unit that generated precisely timed frequency ramp control inputs to the synthesizer. Using the controllable oscillator, the signal doppler was simulated in the receiver local oscillator by a sequence of linear ramps. The synthesizer control unit was designated a Programmed Oscillator Control Assembly and was installed in the Block III receivers to aid tracking during the Jupiter encounter phase of the mission (Refs. 5-2, 3).

Programmed frequency control of the receiver local oscillator provides two advantages for the telemetry channel:

(a) The receiver loop phase error is kept small and consequently the signal-to-noise degradation in the telemetry channel is minimized.

(b) Operating in narrower receiver loop bandwidths reduces the signal-to-noise degradation in the telemetry channel caused by receiver oscillator noise.

3. Pioneer Venus - Multiprobe Mission

The primary objective of the Pioneer Venus multiprobe mission was to obtain information about the planet's atmosphere. To accomplish this, four probes were released from a bus spacecraft and directed to four selected sites on the surface of the planet. During the descent, data on such physical characteristics of the atmosphere as temperature, pressure, etc. were obtained.

Supporting tracking and data acquisition for the multiprobe mission presented a significant challenge for the Receiver-Exciter Subsystem. The probes entered the atmosphere sequentially, which did somewhat simplify the acquisition and tracking at the ground station. However, there was only one opportunity to obtain tracking and telemetry data from each probe during the descent through the atmosphere. The challenge was to obtain all of the data, not to lose any during acquisition periods or from loss of lock in any of the data channels.

To assure no probe data was lost, a primary and a backup receiver channel were provided for each of the probes. The primary channel, using closed-loop tracking receivers, supported real-time data handling. However, in closed-loop tracking, some data is lost during the acquisition period. Therefore, a backup open-loop channel was used to recover the data during this period as well as provide the capability to recover any data if the primary channel, for any reason, failed to function properly. The data output of the open-loop channel, in the form of the probe signal spectrum translated to a low frequency band, was recorded and processed at a later time (Ref. 5-4).

Three of the probes, called small probes, provided downlink channels only. The fourth probe, called the large probe, had two-way communication capability. To minimize the loss of real-time data during the acquisition phase, two closed-loop receivers were used to track the large probe. One receiver covered the period of time that one-way downlink only existed (during uplink acquisition) and the other receiver covered the period of time that two-way communications was available.

The probe signals were turned on just weeks prior to entry, and consequently no history of power level or frequency of these probe signals was available. To assure the signal frequency and level of the probes were close to nominal, a digital spectrum analyzer was developed and implemented to support this phase of the mission. Although no anomalies occurred, the existence of the Spectral Signal Indicator provided assurance during the tracking that the local oscillator frequency of the receiver was set properly and the probe signals were within the passband of the receiver. The Spectral Signal Indicator is now part of the Network serving as a tracking aid.

The entry phase of the probe mission was visible over both the Goldstone, California and Australian complexes. The configuration of each of these complexes used during the entry phase is shown in Fig. 5-2. As can be seen, a total of nine receivers at each 64-m station was required.

To effectively handle the tracking during the initial entry phase, operating personnel had to be trained over a period of several months. To assist in the training, a signal simulator was provided (Refs. 5-5, 6). This Multiprobe Simulator provided four simultaneous dynamic signals which duplicated the four probe signals in power level variations, doppler frequency variations and relative transmission time periods.

For the Pioneer Multiprobe Mission it was not practical to implement permanent multimission equipment in the Deep Space Network. Much of the equipment used was of a special purpose nature and was not retained as part of the Network after the completion of tracking. The special purpose equipment is identified in Fig. 5-2.

4. Voyager - Antenna Array

Up to this time all X-band tracking was done at the 64-m subnet. The 64-m subnet, however, did not have the capacity to handle all existing X-band tracking plus Voyager as well. To provide additional X-band tracking capability to handle this increased tracking load, one 26-m subnet was upgraded. This upgrade included the modification of the Block III receiver-exciter closed-loop receivers to provide X-band capability. The antennas of this 26-m subnet were extended to 34-m at this time.

For the first time the combining of telemetry baseband signals from two antennas, to obtain an improvement in signal-to-noise over a single antenna, was imposed as a mission requirement. The device used to combine these telemetry baseband signals is called a Real-Time Combiner (RTC). The first use of the Real-Time Combiner for telemetry data occurred during the Voyager 1 Jupiter encounter. An improvement of 0.62 to 1.0 dB was attained and a significant improvement in picture quality was noticeable (Refs. 5-7, 8).

Another new capability being implemented in the Deep Space Network and first used during the Voyager Saturn encounter was the Precision Power Monitor assembly. Two measurements are obtained with this device: the system noise temperature and the received carrier signal level. The received carrier signal level can be determined to an accuracy of 0.5 dB. Knowing received carrier levels to this accuracy, the communications link can be optimized for division of power between carrier and data.

C. PRESENT STATUS

As mentioned previously, three Deep Space Network complexes were operational at the end of the 1960's (Spain, Australia and Goldstone, California). At each of these complexes, one 64-m antenna and two 26-m antennas with associated electronic equipment were in operation. The telemetry receiver equipment that existed at that time at each of the antennas in these complexes is listed in Table 5-1.

Since the end of the 1960's many changes have taken place in the network. One of the 26-m tracking antenna subnets has been decommissioned, the other has been converted to a 34-m tracking antenna subnet. The capability and performance of the network has also been increased and improved as previously discussed. The telemetry receiver equipment that now exists in the network after these changes have occurred is listed in Table 5-2. Changes in the network are continuing as discussed in Section F.

D. THEORY AND DESIGN

The first telemetry and tracking receiver used in the Deep Space Network was an outgrowth of the development and implementation of missile telemetry and guidance systems by the Laboratory (Ref. 5-1). These systems utilized second-order phase tracking receiver designs (Ref. 5-9). This first Network system actually used surplus hardware from these telemetry and guidance systems modified to operate at L-band. The systems were replaced in a few years with the new S-band solid state receiver-exciter called the Block I. Improvements in performance to provide the capability to track both deep space probes and the Apollo lunar craft were implemented and the receiver-exciter was designated Block IIIC.

After the Block IIIC had been in use for about a decade operating at S-band with both uplink and downlink, additional capability was provided in the network by adding X-band downlink. A new receiver subsystem, called the Block IV (Ref. 5-10), was implemented at the 64-m subnet to provide both the S- and X-band downlink. The Block IV included several other improvements in performance over the Block IIIC, such as:

(1) More accurate tracking.

(2) Increased receiver signal bandwidths to handle higher telemetry data rates.

(3) Narrower loop noise bandwidths for greater carrier signal sensitivity and consequent reduction of oscillator noise degradation of telemetry data.

(4) Automatic acquisition of carrier signal (Ref. 5-11).

(5) Programmable frequency control for both the uplink and downlink to provide the ability to operate in narrow loop noise bandwidths during periods of large spacecraft dynamics (Refs. 5-12, 13).

(6) Capability of computer control (Ref. 5-14).

X-band downlink tracking became available with the implementation of the Block IV receiver-exciter at the 64-m subnet. Supporting all the X-band missions soon overloaded the 64-m subnet. To share this tracking load, the 34-m subnet was upgraded for X-band reception. This was accomplished with modifications to the Block IIIC receiver-exciter (Refs. 5-15, 16, 17). The objective was to accomplish this task with little or no change to the existing S-band equipment. This was done by downconverting the X-band signal to S-band (Fig. 5-3) using a coherent reference signal derived from the exciter. The doppler frequency range capability was also increased to that of the Block IV to handle expected X-band doppler ranges.

Two other devices enhance the tracking function of the receiver. The first device is a Spectral Signal Indicator, using digital Fourier transform techniques (Ref. 5-18), which displays the receiver output spectrum. For the closed-loop receiver, this device is used during acquisition to determine the frequency offset of the local oscillator signal. A frequency correction is then applied to the local oscillator signal to assist in carrier acquisition. For the open-loop receiver, the display of the receiver output spectrum will verify whether or not the signal is within the passband of the receiver. This provides a quick look to assure that data is being delivered to the recorders.

The second device, which supports tracking, measures system noise temperature and carrier signal level. This device, called a Precision Power Monitor, contains two assemblies, a Noise Adding Radiometer and a Precision Signal Power Monitor unit. The Noise Adding Radiometer adds a controlled amount of wideband noise to the receiving system at the input of the Traveling

Wave Maser. The increase in noise at the receiver output measured by a square law detector, using the Y-factor technique, provides the system operating noise temperature (T_{op}). Knowing the system noise temperature, the received signal power level can be determined using the Precision Signal Power Monitor. The Precision Signal Power Monitor performs a Fourier transform of a 100 Hz region. The ratio of the power in a segment of this region containing the carrier to an equal size segment not containing the carrier provides a measurement of the ratio of noise + carrier signal to noise. Knowing the system noise temperature, the noise power can be calculated, and from the measured ratio value, the signal power level is obtained. The Noise Adding Radiometer is capable of measuring a system noise temperature over the range of 10 K to 400 K with an accuracy of 0.5 K. This results in a signal power measurement accuracy of 0.5 dB over the range of -120 dBm to -165 dBm.

During the early days of the Network, the deep space stations received telemetry from spacecraft at a wide range of subcarrier frequencies, data rates and types of modulation. Each flight project selected its own parameters for its telemetry requirements, and because each project was different, the ground demodulation equipment differed. The interface from the receiver to the demodulators was the telemetry signal containing the subcarriers modulated with data. This telemetry signal, called baseband, was obtained by using a telemetry detector in the receiver to extract the carrier (Fig. 5-4).

It became apparent that future flight projects had to standardize their modulation mode. The modulation mode selected was a square wave subcarrier bi-phase modulated with digital data. On this basis, it was decided to begin developing a multiple mission telemetry system consisting of general purpose, mission-independent equipment capable of meeting the requirements of all projects at any Deep Space Network station.

The receiver portion of this multiple-mission telemetry system consisted of a flexible and efficient subcarrier demodulator, tuneable from 2ʊ kHz to 1.5 MHz. Since the subcarrier signal is completely suppressed with data modulation, the subcarrier demodulator design chosen was a Costas type second

order phase tracking loop that accepted the 10 MHz IF signal from the receiver containing the modulation spectrum. It is desirable that the bandwidth of the 10 MHz receiver IF signal input to the subcarrier demodulator pass the seventh subcarrier harmonic so that no more than 5% of the modulation power is lost in the demodulation process. The output of the Subcarrier Demodulation Assembly, the telemetry data stream, is then delivered to the data processing equipment.

The maximum data rate that can be handled by the receiver is a compromise between data signal-to-noise ratio and efficiency. With a poor data signal-to-noise ratio, efficiency is important. A receiver with a bandwidth that will accept the seventh-order sidebands of the subcarrier is required.

If the data signal-to-noise ratio is good, some of the higher order subcarrier sideboards can be deleted. This permits the use of a higher subcarrier frequency and, consequently, higher data rates. In addition, the required receiver bandwidth is also a function of the type of telemetry coding that is used. Consequently, data rates that can be handled by the receiver cover the range of:

$$\text{Data Bit Rate (b/s)} = \frac{\text{Receiver Channel Bandwidth (Hz)}}{30 \text{ to } 150}$$

At the time the Block IV receiver, which provided the capability to program the local oscillator in order to track the high doppler rates of planetary flyby at low signal levels, was implemented, the Block IV Subcarrier Demodulator Assembly was also added to the Network. This problem of high doppler rates was resolved in the Block IV Subcarrier Demodulator Assembly with the use of a third-order tracking loop (Refs. 5-19 through 23).

Another capability added to the telemetry system is the combining of telemetry signals from more than one antenna. The baseband signal output from the telemetry detector, comprised of subcarrier and data, is used in this configuration. The combining is performed in the Real-Time Combiner Assembly (Refs. 5-24, 25, 26). Telemetry combining is becoming a mission requirement to handle high data rates over long space communication distances. The Real-Time Combiner automatically adjusts for the different propagation time of the

signal from the two antennas. The decision whether or not to combine two telemetry streams is made by the operator based on signal-to-noise ratios as measured in the data processing equipment. The combined baseband signal can then be processed through the Subcarrier Demodulator Assembly, which will accept either the IF signal from the receiver or the baseband telemetry signal.

E. PERFORMANCE

The principal receiver parameters affecting the performance of telemetry are listed in Table 5-3. Reference 5-27 describes the performance of the Deep Space Network systems in more detail.

F. FUTURE

Advancement of Deep Space Network capabilities and performance is a continuing process. During the 1980's advances will be implemented in radio metric data accuracy, improved telemetry performance, added radio science capability and improved operation efficiency. To contribute to these advances, improvements in the receiver subsystem are planned in the following areas.

1. Network Consolidation

Improved performance on the communications link from a space probe can be obtained by combining received signals from more than one antenna at a Deep Space Network complex. This, in effect, increases the aperture of the ground antenna. Studies have been made to determine the most effective way to handle this. The plan, at the present time, is to construct a new 34-m High Efficiency antenna at the Deep Space Network complexes in Goldstone, California and Australia (Fig. 5-5). These will be equipped with the Block III receiver-exciters that had been installed in the decommissioned 26-m antenna subnet.

At each of the three complexes all antennas will be colocated at the 64-m sites except for the 34-m tracking antenna in Goldstone, California. This antenna will remain at the Station 12 location and transmit baseband telemetry over a data link to the 64-m site.

The next generation of the real-time combiner, which was first used to combine telemetry signals from two antennas for Voyager Jupiter encounter, will have the capability to analyze the telemetry signals from each antenna, measure the ratio of data power to noise spectral density, automatically determine what improvement in performance will be obtained by combining the telemetry signals, make a decision whether or not to switch to the array configuration, and if the array configuration is selected, to automatically adjust time delays in the data streams for optimum combining. The combiner will continuously monitor the effectiveness of the array and remove any data stream that is no longer contributing to an improvement in the data quality (Ref. 5-26).

Real-time combining together with refinements in the design of the Network antenna groups will produce a signal-to-noise ratio improvement of 1.5 dB or more in the spacecraft telemetry signal.

Also under consideration is the use of existing radio science antennas with the Deep Space Network antennas to provide increased aperture by combining telemetry from all these antennas.

Computer control is another feature that is continually being advanced. Presently, some operational functions such as exciter frequency are under computer control. It is planned to provide more computer control for operations, monitoring and maintenance functions. The planned controller for the receiver-exciter is covered in Ref. 5-28.

2. Telemetry

Telemetry capability is being increased in two areas. The first is the combining of signals from two or more antennas discussed previously. The second is an increase in the data rate that can be handled, which translates into increased bandwidth of receiver data channels. The plan is to increase the Block IV receiver telemetry channel at the baseband output to 8 MHz bandwidth (-3 dB). This represents an increase in receiver data rate capability to approximately 100 to 500 kbps. The Block III receiver telemetry channel baseband output bandwidth (-3 dB) will remain at 1.3 MHz (15 to 80 kbps).

3. Digital Receiver

A plan for converting the existing analog receivers to partially (or fully) digital units is currently under study. Digital receivers, under microcomputer control, will be able to automatically acquire signals via a parallel frequency search using fast Fourier transform techniques. After acquisition, the receiver will be able to automatically optimize tracking loop parameters based on observed signal and noise statistics in order to obtain the maximum performance attainable. Digital receivers are expected to be more flexible; for example, digital IF filters can be realized that are stable and insensitive to environmental variations (in particular, temperature). These filters can be quickly and easily modified should requirements change. It is also expected that the digital approach will result in a simplification of the hardware (e.g., multiple filters will not be required, since the desired filter can be programmed) and in lower life-cycle maintenance costs.

REFERENCES

5-1. Renzetti, N. A., A History of the Deep Space Network, Technical Report 32-1533, Vol. I, Jet Propulsion Laboratory, Pasadena, Calif., Sep. 1, 1971.

5-2. Donnelly, H., and Wick, M. R., Programmed Oscillator Development, Technical Report 32-1526, pp. 180-185, Jet Propulsion Laboratory, Pasadena, Calif., Aug. 15, 1972.

5-3. Wick, M. R., "DSN Programmed Oscillator", DSN Progress Report 42-20, pp. 167-177, Jet Propulsion Laboratory, Pasadena, Calif., Apr. 15, 1974.

5-4. Kent, S. S., "Predetection Telemetry Analog Recording and Playback for Pioneer Venus 1978," DSN Progress Report 42-43, pp. 197-203, Jet Propulsion Laboratory, Pasadena, Calif., Feb. 15, 1978.

5-5. Johns, C. E., "Pioneer Venus Entry Simulator," DSN Progress Report 42-33, pp. 155-158, Jet Propulsion Laboratory, Pasadena, Calif., June 15, 1976.

5-6. Friedenberg, S. E., "Pioneer Venus 1978 Multiprobe Spacecraft Simulator," DSN Progress Report 42-38, pp. 148-151, Jet Propulsion Laboratory, Pasadena, Calif., Apr. 15, 1977.

5-7. Simon, N. K., and Hoynes, C., "Preliminary Telemetry Operations Experience with the Real Time Combiner," DSN Progress Report 42-55, pp. 90-95, Jet Propulsion Laboratory, Pasadena, Calif., Feb. 15, 1980.

5-8. Bartok, C. D., "Performance of the Real-Time Array Signal Combiner During the Voyager Mission," TDA Progress Report 42-63, pp. 191-202, Jet Propulsion Laboratory, Pasadena, Calif., June 15, 1981.

5-9. "Phase-Locked Loops," IEEE Trans. Comm., Vol. COM-30, Number 10, Oct. 1982.

5-10. Donnelly, H, Shallbetter, A. C., and Weller, R. E., "Block IV Receiver-Exciter Development", Space Programs Summary 37-66, Vol. II, pp. 115-124, Jet Propulsion Laboratory, Pasadena, Calif., Nov. 30, 1970.

5-11. Bunce, R. C., "Block IV Receiver Automatic Carrier Acquisition," Space Programs Summary 37-65, Vol. II, pp. 107-116, Jet Propulsion Laboratory, Pasadena, Calif., Sep. 30, 1970.

5-12. Wick, M. R., "Programmed Oscillator Development," Space Programs Summary 37-66, Vol. II, pp. 127-132, Jet Propulsion Laboratory, Pasadena, Calif., Nov. 30, 1970.

5-13. Wick, M. R., DSN Programmed Oscillator Development, Technical Report 32-1526, Vol. VIII, pp. 111-124, Jet Propulsion Laboratory, Pasadena, Calif., Apr. 15, 1972.

5-14. Johns, C. E., Block IV Receiver-Exciter Control and Monitoring, Technical Report 32-1526, Vol. XVI, pp. 159-162, Jet Propulsion Laboratory, Pasadena, Calif., Aug. 15, 1973.

5-15. Lobb, V. B., "26-Meter S-X Conversion Project", DSN Progress Report 42-39, pp. 157-167, Jet Propulsion Laboratory, Pasadena, Calif., June 15, 1977.

5-16. Weller, R. E., "S-X Conversion for the Block III Receiver-Exciter," DSN Progress Report 42-42, pp. 141-148, Jet Propulsion Laboratory, Pasadena, Calif., Dec. 15, 1977.

5-17. Buchanan, H. R., "S-X 34-Meter Conversion Receiver and Microwave Performance," DSN Progress Report 42-50, pp. 219-225, Jet Propulsion Laboratory, Pasadena, Calif., Apr. 15, 1979.

5-18. Chaney, B., Cooper, H., and Crow, B., "Spectral Signal Indicator Progress Report", DSN Progress Report 42-50, pp. 216-218, Jet Propulsion Laboratory, Pasadena, Calif., Apr. 15, 1979.

5-19. Tausworthe, R. C., A Second/Third-Order Hybrid Phase-Locked Receiver for Tracking Doppler Rates," Technical Report 32-1526, Vol. I, pp. 42-45, Jet Propulsion Laboratory, Pasadena, Calif., Jan. 15, 1971.

5-20. Crow, R. B., Holmes, J. K., and Tausworthe, R. C., Block IV Subcarrier Demodulator Assembly Acquisition Problem, Technical Report 32-1526, Vol. XIII, pp. 42-47, Jet Propulsion Laboratory, Pasadena, Calif., Feb. 15, 1973.

5-21. Dunn, G. L., Effects of Doppler Rate on Subcarrier Demodulator Performance, Technical Report 32-1526, Vol. XIV, pp. 200-204, Jet Propulsion Laboratory, Pasadena, Calif., Apr. 15, 1973.

5-22. Crow, R. B., Block IV Subcarrier Demodulator Assembly Design, Technical Report 32-1526, Vol. XVI, pp. 140-158, Jet Propulsion Laboratory, Pasadena, Calif., Aug. 15, 1973.

5-23. Crow, R. B., Bandwidth Selection for SDA, Technical Report 32-1526, Vol. XIX, pp. 122-125, Jet Propulsion Laboratory, Pasadena, Calif., Feb. 15, 1974.

5-24. Wilck, H., "A Signal Combiner for Antenna Arraying," DSN Progress Report 42-25, pp 111-117, Jet Propulsion Laboratory, Pasadena, Calif., Feb. 15, 1975.

5-25. Winkelstein, R. A., "Analysis of the Signal Combiner for Multiple Antenna Arraying," DSN Progress Report 42-26, pp. 102-118, Jet Propulsion Laboratory, Pasadena, Calif., Apr. 15, 1975.

5-26. Howard, L.D., "Prototype Real-Time Baseband Signal Combiner," TDA Progress Report 42-60, pp. 145-151, Jet Propulsion Laboratory, Pasadena, Calif., Dec. 15, 1980.

5-27. "Deep Space Network/Flight Project Interface Design Handbook," Document 810-5, Rev, D, Vol. 1, Jet Propulsion Laboratory, Pasadena, Calif., Oct. 15, 1981 (an internal document).

5-28. Jansma, P. A., "Receiver-Exciter Controller Design," TDA Progress Report 42-69, pp. 117-125, Jet Propulsion Laboratory, Pasadena, Calif., June 15, 1982.

Table 5-1. 1970 status of telemetry receiver equipment in the Deep Space Network

	Network complex								
	Goldstone, California			Canberra, Australia			Madrid, Spain		
	Station			Station			Station		
	11 26-m	12 26-m	14 64-m	44 26-m	42 26-m	43 64-m	62 26-m	61 26-m	63 64-m
Receiver (Block III)[a]	1	1	1	1	1	1	1	1	1
Subcarrier Demodulator Assembly (Block III)	2	2	4[b]	2	2	2	2	2	2

[a] Contains 1 exciter (S-band)
2 receivers (S-band)

[b] Two of the four Subcarrier Demodulator Assemblies available for assignment in the Network, where required to support a critical mission phase

Table 5-2. Present status of telemetry receiver equipment in the Deep Space Network

	Network Complex					
	Goldstone, California		Canberra, Australia		Madrid, Spain	
	Station		Station		Station	
	12 34-m	14 64-m	42 34-m	43 64-m	61 34-m	63 64-m
Receover						
Block III	1[a]	1[b]	1[a]	1[b]	1[a]	1[b]
Block IV[a]		1		1		1
Subcarrier Demodulator						
Block III	2	2	2	2	2	4
Block IV		1		1		
Real-Time Combiner		1		1		1
Spectral signal indicator		1		1		1
Precision power monitor noise adding radiometer		1		1		1

[a] Contains 1 exciter (S-band)
2 receivers (S- or X-band)

[b] Contains 1 exciter (S-band)
2 receivers (S-band)

Table 5-3. Receiver-Exciter Subsystem Performance

	Block III 34-m antenna	Block IV 64-m antenna
Exciter		
Frequency band	S	S
Frequency programming	MSC[a]	MSC[a]
Command		
Subcarrier frequency, Hz	100 to 16,000	100 to 16,000
Modulation bandwidth (-3 dB), kHz	100	1000
Data rate, b/s	1 to 128	1 to 128
Receiver		
Quantity	2	2
Frequency band	S & X	S & X
Loop noise bandwidth, Hz	12 to 152	1 to 300
Frequency programming	CS[b]	POCA[c]
Telemetry channels		
10 Hz IF output		
Bandwidth (-3 dB), MHz	±1.7	±5.0
Baseband output		
Bandwidth (-3 dB), MHz	1.3	8.0
Combiner		
Channels	NA	2
Symbol rate, s/s	NA	10 to 2000
S/N degradation, dB	NA	0.2
Subcarrier Demodulator		
Subcarrier frequency, kHz	200 to 1000	0.4 to 1250
Max. S/N Degradation, dB	0.5	0.5

[a] MSC microprocessor synthesizer controller

[b] CS commercial synthesizer (no programming capability)

[c] POCA programmed oscillator synthesizer controller

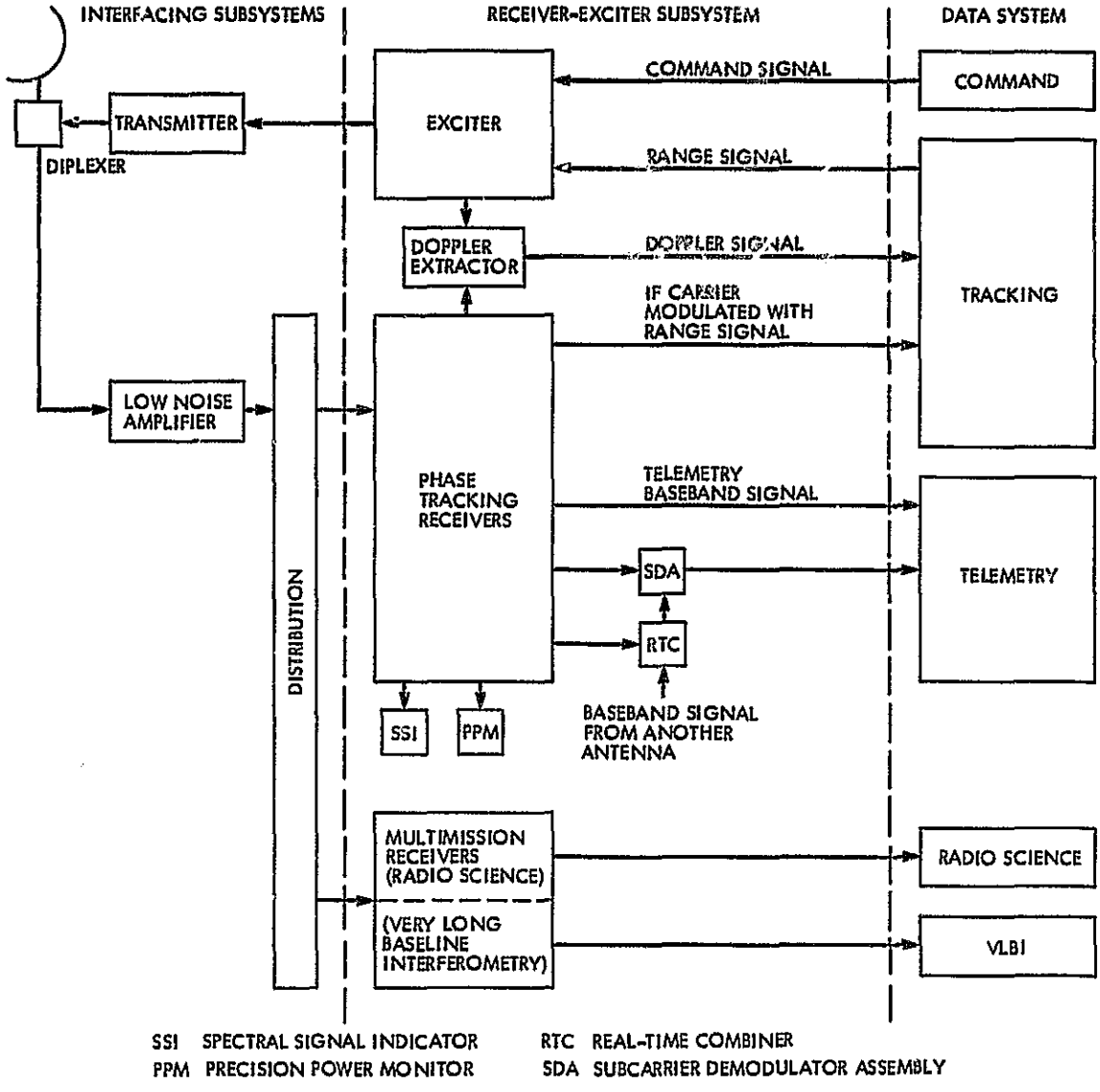

Fig. 5-1. Receiver-exciter subsystem

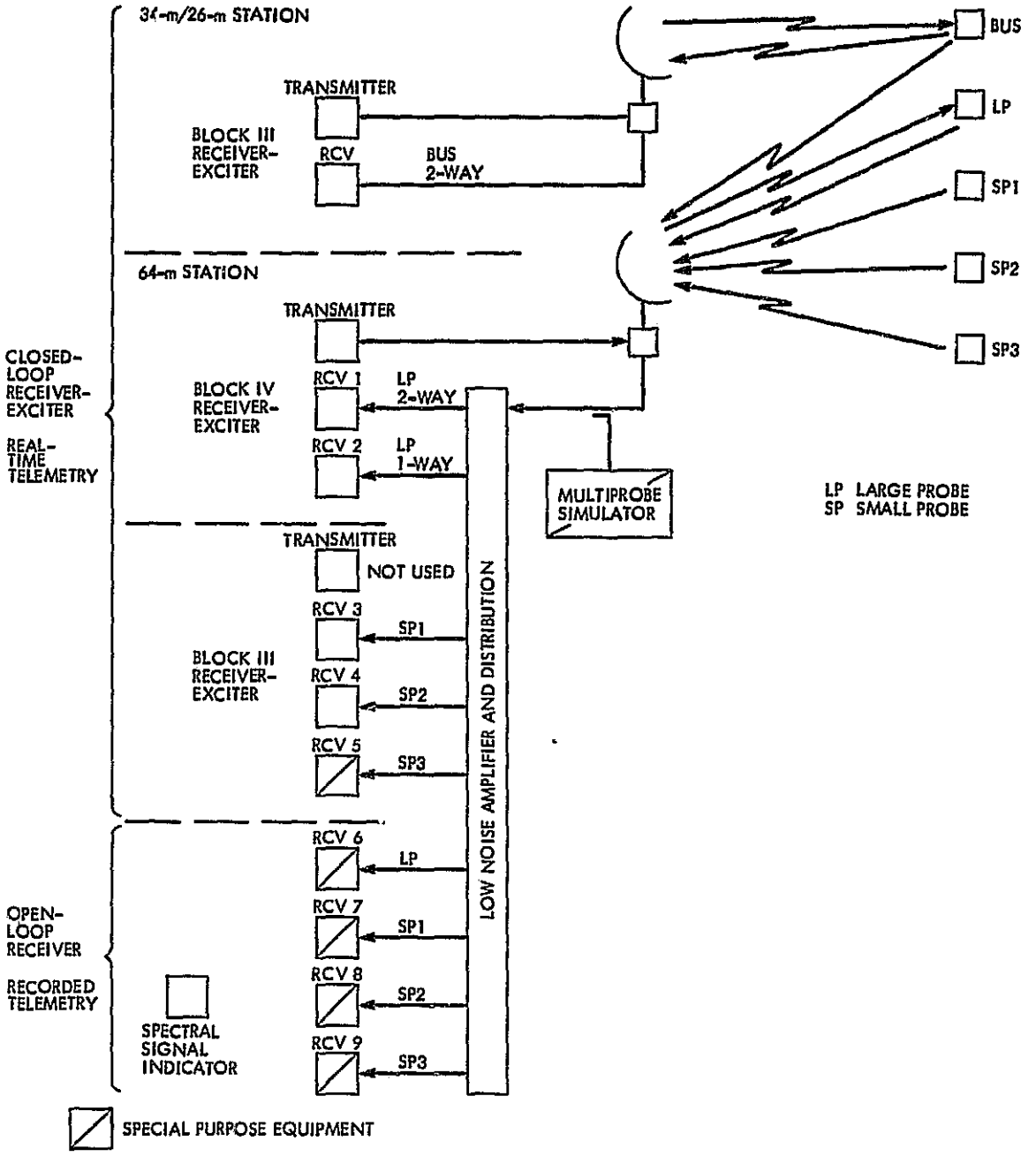

Fig. 5-2. Deep Space Network complex configuration: Pioneer Venus multiprobe mission

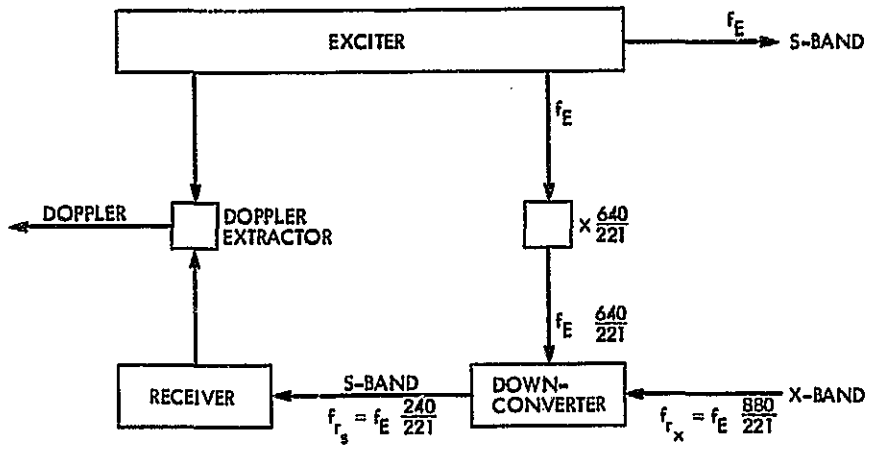

Fig. 5-3. Block IIIC receiver X-band conversion

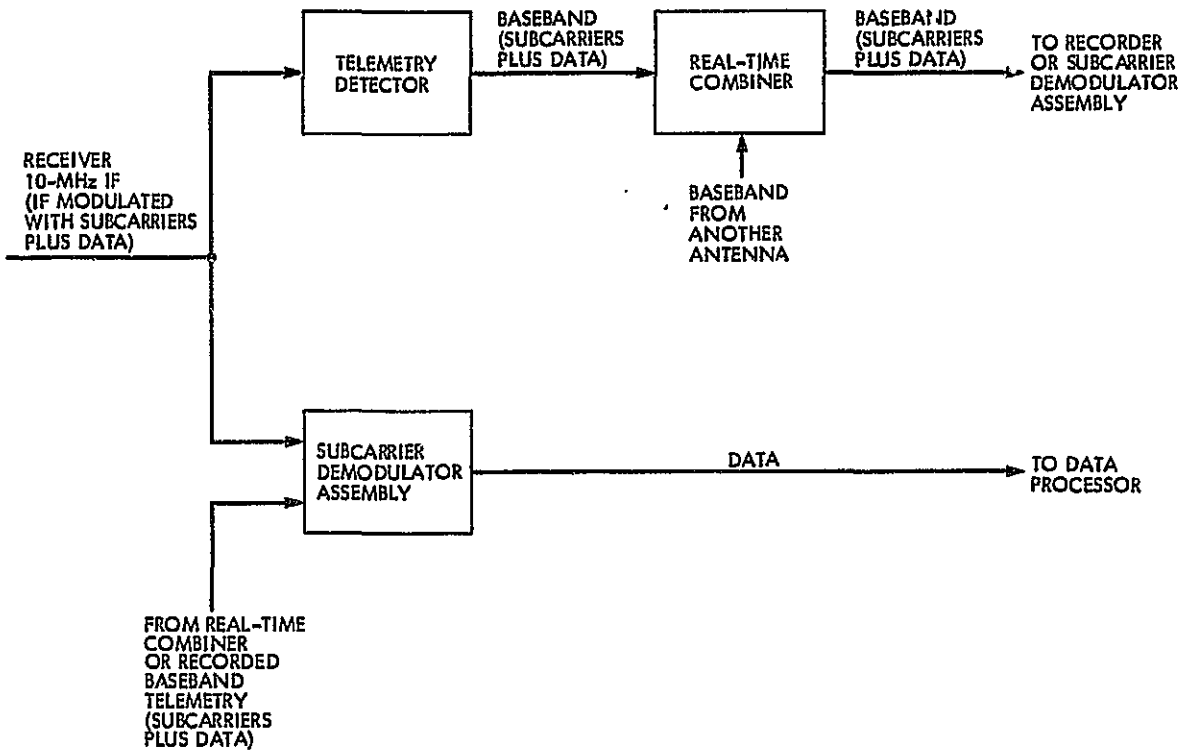

Fig. 5-4. Telemetry channel

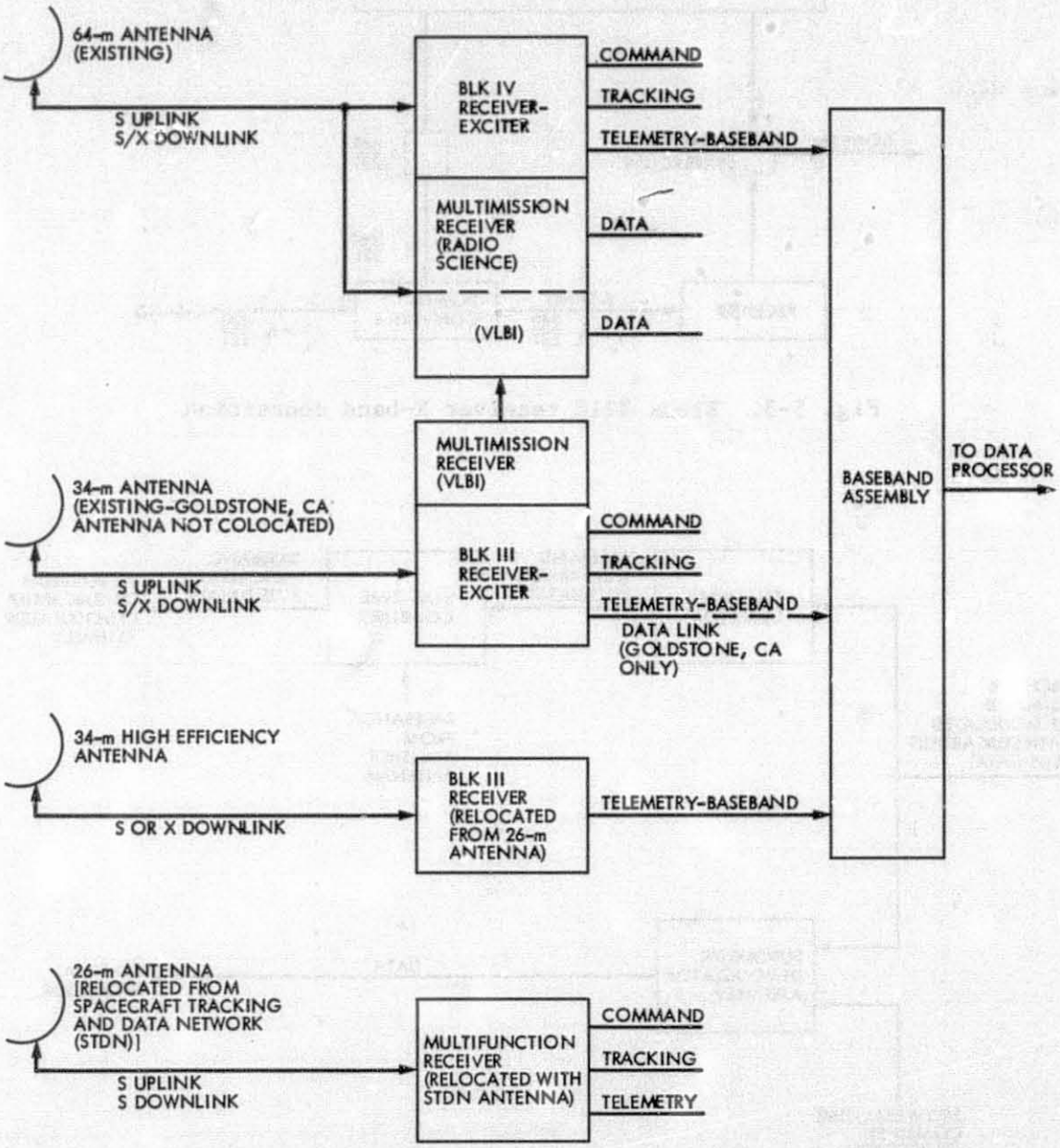

Fig. 5-5. Network consolidation complex

VI. TELEMETRY MODULATION AND CODING

P. W. Kinman

A. INTRODUCTION

Digital telemetry has supplanted analog telemetry for deep space communications. Not since the Rangers and the Lunar Orbiters of the 1960s has analog telemetry been designed into a deep space mission. Accordingly, only digital telemetry is discussed here.

With digital telemetry, the telecommunications systems design engineer may use error-correcting codes. This allows increased error protection at the cost of increased bandwidth. All science telemetry returned from the Voyager and Galileo spacecraft are protected by error-correcting codes.

Both the modulation and coding of digital telemetry for the deep space channel are considered below. The descriptions include relative performance of some competing schemes. However, the treatment given here is, of necessity, cursory. The reader should consult Deep Space Telecommunications Systems Engineering (Ref. 6-1) for a comprehensive treatment of the design of coding and modulation schemes for the deep space channel.

B. MODULATION

A small class of modulation schemes has proven to be best for the deep space channel. The digital telemetry is either phase-shift-keyed onto a squarewave subcarrier and then phase modulated onto the carrier (PCM/PSK/PM), or the digital telemetry is directly phase modulated (i.e., phase-shift-keyed) onto the carrier (PCM/PM). In the abbreviations PCM/PSK/PM and PCM/PM, the acronym PCM means "Pulse Code Modulation" and serves as a reminder that the telemetry is digital.

PCM/PSK/PM and PCM/PM are well suited to the deep space channel because:

(1) Phase-shift-keying is the most efficient binary signalling scheme (Refs. 6-2, 3).

(2) A phase modulated carrier has a constant envelope

The constant envelope property is important because the final downlink amplification stage on the typical spacecraft is a travelling-wave tube operated in a nonlinear (saturation) mode. If the modulated downlink carrier does not have a constant envelope, distortion will result.

Before proceeding to the mathematical descriptions of PCM/PSK/PM and PCM/PM, the issue of data formats needs to be addressed. Various data formats are illustrated in Fig. 6-1. With a non-return-to-zero-level (NRZ-L) data format, a logical "one" is represented by one level and a logical "zero" by the other. With NRZ-M (mark), a logical "one" is represented by a change in level and a logical "zero" by no change. NRZ-S (space) is the same as NRZ-M but with the roles of "one" and "zero" reversed. NRZ-M and NRZ-S are often referred to as differential encoding. It is important to note that differential encoding is <u>not</u> an example of error-correction encoding. With bi-phase-level (Bi-ϕ-L), a logical "one" is represented by one cycle of a squarewave and a logical "zero" by one cycle of a square wave with reversed polarity. Bi-ϕ-L is often called a Manchester code; but, again, it is <u>not</u> an error-correcting code. Bi-ϕ-L is identical to NRZ-L data phase-reversal-keying a squarewave subcarrier whose cycle period equals the bit period and such that a transition occurs at mid-bit. Thus, PCM/PM with Bi-ϕ-L data formatting is a special case of PCM/PSK/PM with NRZ-L data formatting.

A modulated carrier, in the cases of both PCM/PSK/PM and PCM/PM, may be represented mathematically by (assuming nothing else modulates the carrier)

$$\sqrt{2P_t}\sin\left(\omega_c t + \theta\, s(t)\right) \qquad (6\text{-}1)$$

where

P_t = total signal power, W

ω_c = carrier angular frequency, rad/sec

θ = modulation index, rad

and s(t) represents a normalized data sequence (in the case of PCM/PM) or a normalized modulated squarewave subcarrier (in the case of PCM/PSK/PM).

In the latter case, the telemetry is invariably phase-reversal-keyed (i.e., phase-shift-keyed with signalling levels of $\pm 90^{\circ}$) onto the subcarrier. Furthermore, phase-reversal-keying a squarewave with a data sequence is the same as multiplying the squarewave by the data sequence. So

$$s(t) = \begin{cases} d(t), & \text{PCM/PM} \\ d(t) \; \square\sin(\omega_{sc}t), & \text{PCM/PSK/PM} \end{cases} \qquad (6\text{-}2)$$

and

$$|s(t)| = 1$$

where

$d(t)$ = normalized data sequence (one of the waveforms of Fig. 6-1)

$|d(t)| = 1$

$\square\sin(\omega_{sc}t)$ = squarewave subcarrier

$|\square\sin(\omega_{sc}t)| = 1$

ω_{sc} = subcarrier angular frequency, rad/sec

Using Eq. (6-2) and trigonometric identities, Eq. (6-1) may be expanded as

$$\sqrt{2P_t}\sin(\omega_c t + \theta\, s(t)) = \sqrt{2P_t}\cos(\theta)\sin(\omega_c t) + \sqrt{2P_t}\, s(t)\sin(\theta)\cos(\omega_c t) \qquad (6\text{-}3)$$

If $0^{\circ} < \theta < 90^{\circ}$, this phase-modulated carrier comprises a pilot tone (residual carrier) and a double-sideband (DSB) modulated carrier. A system with $\theta < 90^{\circ}$ is called a residual carrier system. A system with $\theta = 90^{\circ}$ is called a suppressed carrier system. A residual carrier receiver employs a phase-locked loop to track the pilot tone and provide a coherent reference for demodulating the DSB modulated carrier (Refs. 6-1, 4). A Costas loop may be used as a suppressed carrier receiver (Refs. 6-1 and 4). Until now, all deep space probes to Network digital telemetry systems have been of the residual carrier type.

The power in the telemetry sidebands is $P_t \sin^2(\theta)$, and the energy-per-bit-to-noise-spectral-density ratio is given by

$$E_b/N_0 = (P_t/N_0)\frac{1}{R}\sin^2(\theta) \qquad (6\text{-}4)$$

where

R = data bit rate

N_0 = one-sided noise spectral density.

Equation (6-4) underlines the advantage of suppressed carrier systems: they suffer no "modulation loss." For this reason, suppressed carrier systems will play a role in the future of the Deep Space Network.

With residual carrier systems, it is important that the telemetry sidebands not interfere with carrier recovery in the phase-locked loop receiver. Figure 6-2 illustrates the spectrum of (a) PCM/PM with NRZ data format, (b) PCM/PSK/PM with NRZ data format, and (c) PCM/PM with Bi-ϕ format. These spectra make clear that a subcarrier is desirable when the data format is NRZ, and that a subcarrier might be unnecessary when the data format is Bi-ϕ-L. For the low-to-medium data rates, PCM/PSK/PM with NRZ data format provides better spectral isolation between telemetry sidebands and residual carrier than does PCM/PM with Bi-ϕ format. An advantage of Bi-ϕ-L which is not evident from Fig. 6-2 is that symbol synchronization at the receiver is easier since a transition occurs every mid-bit. PCM/PSK/PM with NRZ-L data is the most common modulation scheme in the Deep Space Network.

With respect to minimizing the bit error rate, there is an optimum modulation index for residual carrier systems. The optimum index depends on the data rate, the characteristics of the receiver, and the coding scheme (if any). Figure 6-3 serves as an example. The curve of Fig. 6-3 appears to have a minimum at a modulation index of 74°. For smaller modulation indices, E_b/N_0 decreases. For larger modulation indices, the power in the pilot tone ($P_t \cos^2 \theta$) is so small that the phase-locked loop tracks the pilot with sizable phase error, resulting in added inefficiency for the demodulation of the double-sideband modulated carrier.

For a given modulation index, the bit error rate performance of PCM/PSK/PM with NRZ-L data formatting is the same as for PCM/PM with Bi-ϕ-L data formatting. However, PCM/PSK/PM with NRZ-M (or NRZ-S) data formatting has poorer performance (Fig. 6-4). In Fig. 6-4, the curve marked "NRZ-L uncoded" represents the performance of NRZ-L formatted PCM/PSK/PM (or Bi-ϕ-L formatted PCM/PM) with no error-correcting code. Also, an assumption of perfect carrier, subcarrier, and bit synchronization at the receiver was made. More will be said about Fig. 6-4 in the paragraphs to follow.

C. CODING

Error-correcting codes improve the bit error rate performance of digital telemetry by adding redundancy to the channel digits. This improvement is readily seen by plotting the bit error rate performance of coded and uncoded systems vs the energy-per-information-bit-to-noise-spectral-density ratio, E_b/N_0. Figure 6-4 is such a plot. The left edge of the Fig. 6-4 plot is Shannon's fundamental limit, $E_b/N_0 = -1.6$ dB. It is impossible to design a code with arbitrarily good performance when the operating E_b/N_0 is -1.6 dB or less (Ref. 6-5).

The curve marked "convolutional code (k=7, r=1/2)" in Fig. 6-4 represents the following coding/modulation scheme: convolutionally coded with constraint length = 7, rate = 1/2; Viterbi decoded with eight-level quantization; and NRZ-L formatted PCM/PSK/PM. This is the most common coding/modulation system presently in use on the deep space channel.

One important advantage to convolutional codes is the simplicity with which their encoders may be implemented (see Fig. 6-5). Also, good hardware decoders exist. Short-constraint-length convolutional codes (e.g., k=7) are decoded by the Viterbi algorithm (Refs. 6-6, 7). Long-constraint-length convolutional codes (e.g., k=32) have also been used on the deep space channel; they require sequential decoders (Refs. 6-3 and 8).

The Fig. 6-4 curve marked "Reed-Solomon/Viterbi concatenated code" represents the following coding/modulation scheme: concatenated coding with a

Reed-Solomon (J=8, E=16) outer code and a convolutional (k=7, r=1/2, Viterbi decoded with eight-level quantization) inner code; and NRZ-L formatted PCM/PSK/PM. As with the other curves of Fig. 6-4, perfect carrier, subcarrier, and bit synchronization at the receiver have been assumed.

The Reed-Solomon/Viterbi concatenated coding system described above is illustrated in Fig. 6-6. Interleaving is required because Viterbi decoders tend to produce errors in bursts. The Reed-Solomon/Viterbi system will be used by Voyager 2 for its Uranus and Neptune encounters and was the design choice for Galileo's imaging telemetry. Further details of the Reed-Solomon/Viterbi system can be found in Refs. 6-9, 10, 11.

REFERENCES

6-1. Yuen, J. H., editor, Deep Space Telecommunications Systems Engineering, Publication 82-76, Jet Propulsion Laboratory, Pasadena, Calif., July 1982.

6-2. Viterbi, A. J., Principles of Coherent Communication, McGraw-Hill, New York, 1966.

6-3. Wozencraft, J. M., and Jacobs, I. M., Principles of Communication Engineering, Wiley, New York, 1965.

6-4. Lindsey, W. C., and Simon, M. K., Telecommunication Systems Engineering, Prentice-Hall, Englewood Cliffs, N.J., 1973.

6-5. Shannon, C. E., and Weaver, W., The Mathematical Theory of Communication, University of Illinois Press, Urbana, Ill., 1963.

6-6. Heller, J. A., and Jacobs, I. M., "Viterbi Decoding for Satellite and Space Communication," IEEE Trans. Commun. Tech., Vol. COM-19, pp. 835-848, Oct. 1971.

6-7. Viterbi, A. J., and Omura, J. K., Principles of Digital Communication and Coding, McGraw-Hill, New York, 1979.

6-8. Jacobs, I. M., "Sequential Decoding for Efficient Communication from Deep Space," IEEE Trans. Commun. Tech., Vol. COM-15, pp. 492-501, August 1967.

6-9. Rice, R. F., Channel Coding and Data Compression System Considerations for Efficient Communication of Planetary Imaging Data, Technical Memorandum 33-695, Jet Propulsion Laboratory, Pasadena, Calif., 1974.

6-10. Butman, S. A., Deutsch, L. J., and Miller, R. L., "Performance of Concatenated Codes for Deep Space Missions," TDA Progress Report 42-63, pp. 33-39, Jet Propulsion Laboratory, Pasadena, Calif., June 15, 1981.

6-11. Liu, K. Y., and Lee, J: J., An Experimental Study of the Concatenated Reed-Solomon/Viterbi Channel Coding System Performance and Its Impact on Space Communications, Publication 81-58, Jet Propulsion Laboratory, Pasadena, Calif., Aug. 15, 1981.

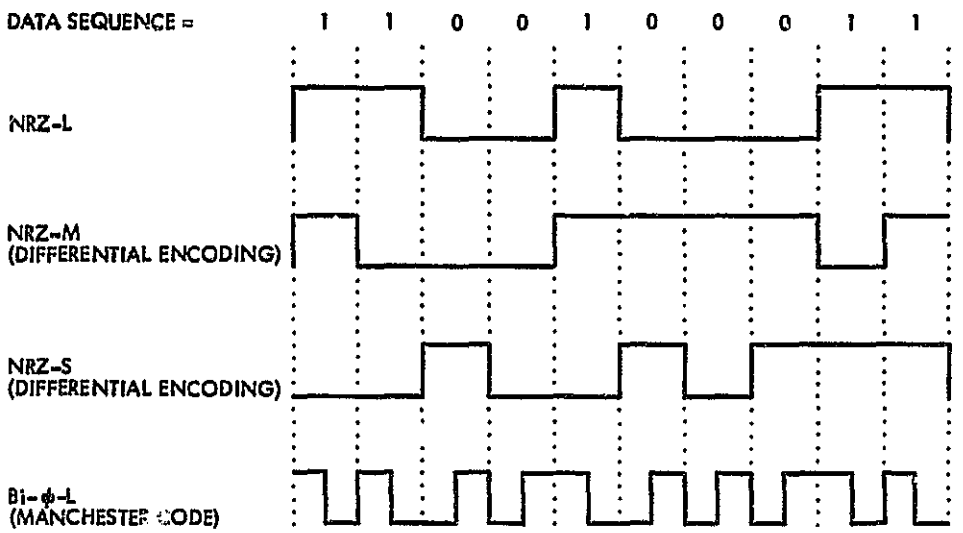

Fig. 6-1. Data formats

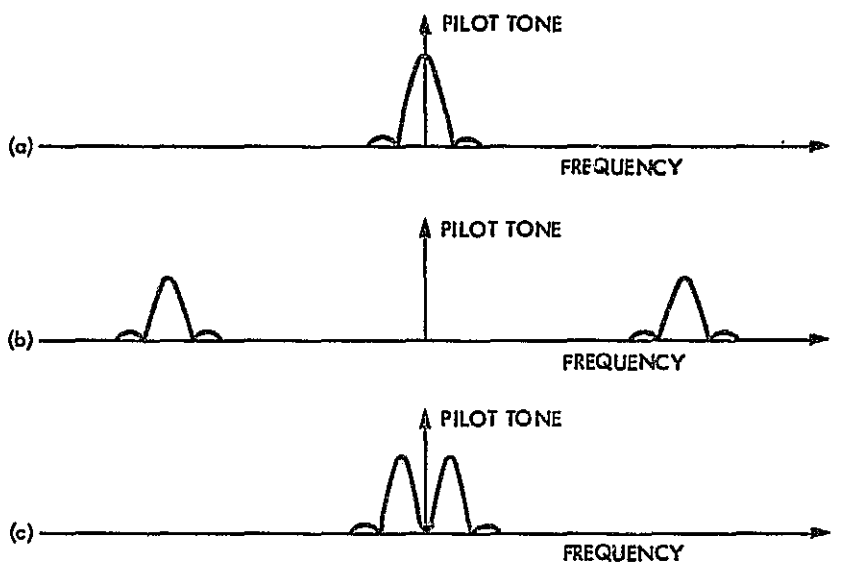

Fig. 6-2. Spectra of (a) PCM/PM with NRZ data format,
(b) PCM/PSK/PM with NRZ data format,
(c) PCM/PM with Bi-ϕ-L data format

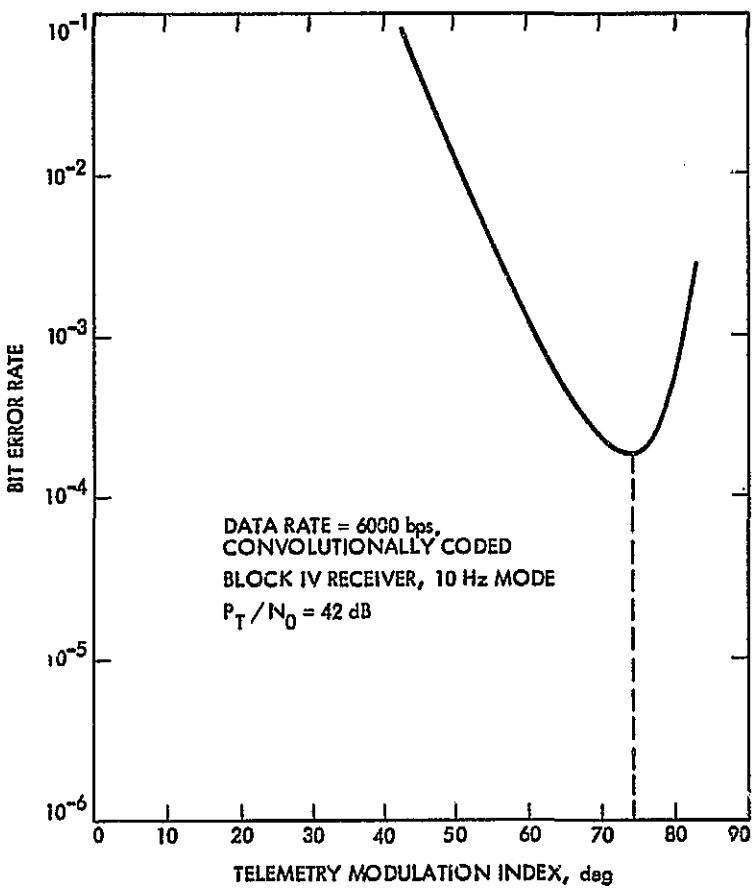

Fig. 6-3. Optimization of the modulation index for a residual carrier system

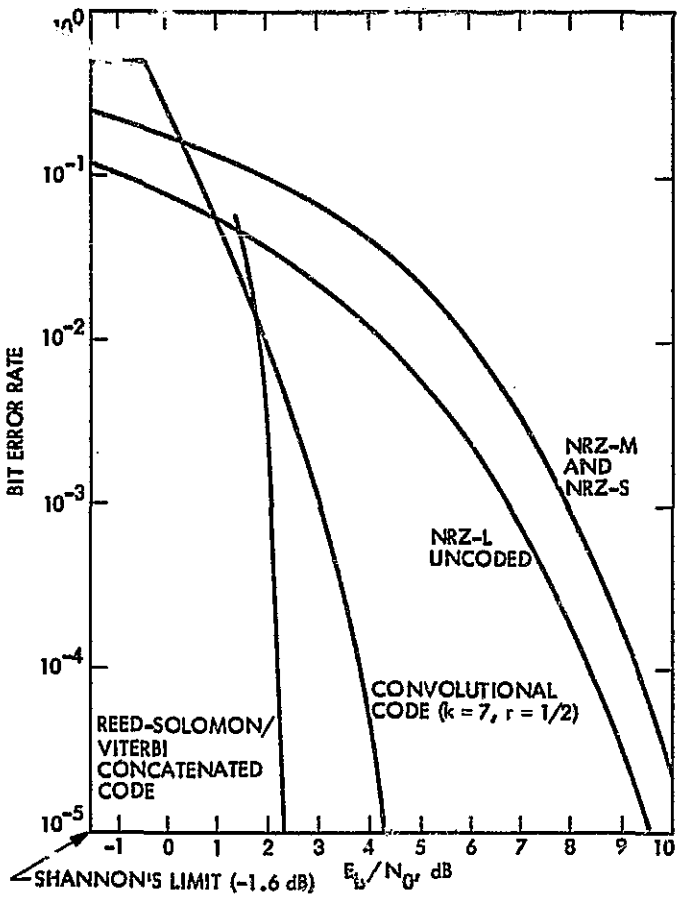

Fig. 6-4. Bit error rate performance of several coding/modulation schemes

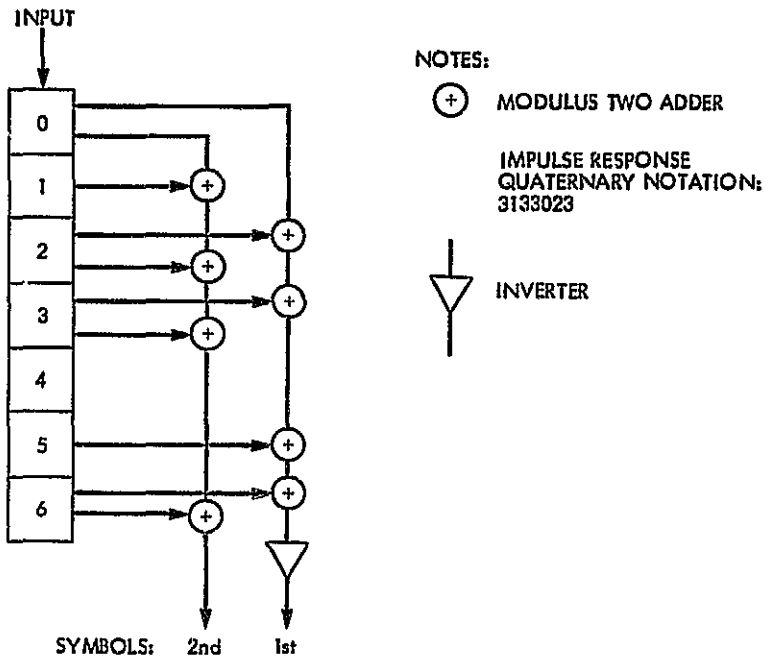

Fig. 6-5. Encoder for convolutional (k=7, r=1/2) code

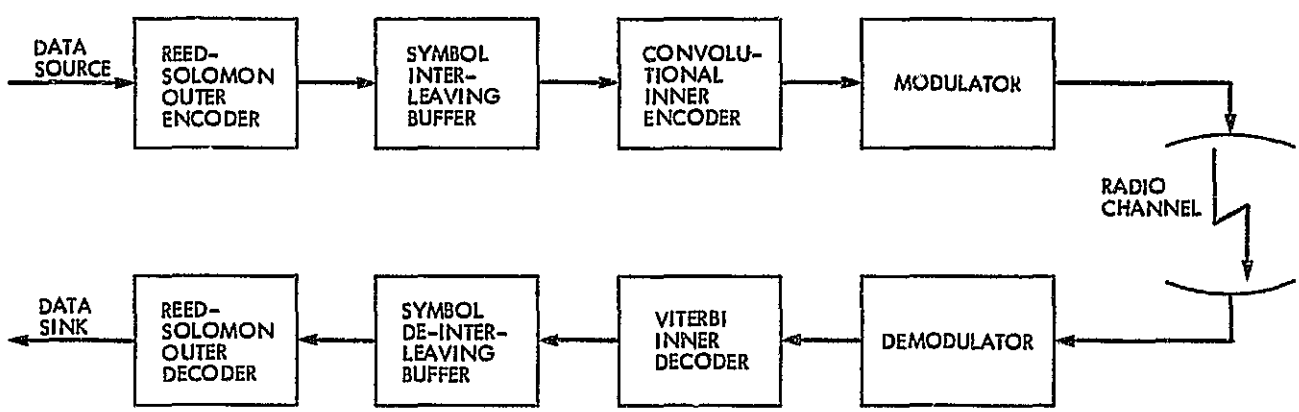

Fig. 6-6. Reed Solomon (J=8, E=16)/convolutional (k=7, r=1/2, Viterbi) coding system (Reed-Solomon/Viterbi)

VII. PLASMA EFFECTS

J. W. Armstrong

A. INTRODUCTION

Radio communication with space probes requires sending signals through the earth's ionosphere and usually the solar wind. During planetary flybys, the signal may also pass through the ionosphere of another planet. These ionized media can perturb the radio signal in a variety of ways. Examples of these perturbations are variations in the electrical length between the spacecraft and the ground station, Faraday rotation of linearly polarized signals, amplitude and phase scintillations, and spectral and angular broadening. These plasma effects can have undesirable influences on telemetry performance and thus need to be understood from a communications engineering viewpoint. The plasma effects are, however, useful from a scientific viewpoint, since the effects on the communications link can often be inverted to estimate the physical conditions in the plasma.

B. CHARGED PARTICLE INFLUENCE ON RADIO WAVE PROPAGATION

There exists an extensive literature on the interaction of radio waves with plasmas (Refs. 7-1, 2). Fortunately, most of the communications link effects observable with the Deep Space Network can be understood in terms of a relatively small subset of the full plasma theory. In particular, for cases where the magnetic field and particle collisions can be neglected and where the frequency of the radio wave is high compared with the plasma frequency, the radio waves are propagated without attenuation but with effective index of refraction, n, given by (Ref. 7-1)

$$n = c/v = \left[1-(\omega_p/\omega)^2\right]^{1/2} \qquad (7\text{-}1)$$

where

c = speed of light = 3×10^8 m/sec

$$v = \text{phase velocity} = c\left[1-\left(\omega_p/\omega\right)^2\right]^{-1/2}, \text{ m/sec}$$

$$\omega_p = \text{plasma frequency} = (Ne^2/\varepsilon_o m)^{1/2}, \text{ rad/sec}$$

N = electron density , m^{-3}
e = electron charge = -1.6×10^{-19} coul
ε_0 = permittivity of free space = 8.9×10^{-12} farads/m
m = electron mass = 9.1×10^{-31} kg
ω = angular frequency of the radio wave, rad/sec

There is also an associated group velocity v_g, such that $v_g\ v = c^2$. The situation when a substantial static magnetic field is present (for example, for the earth's ionosphere or the near-sun solar wind) is more complicated (Refs. 7-2, 3). In this latter case the phase velocities of orthogonal circularly polarized waves differ, with the result that a linearly polarized wave cannot propagate without rotation of its plane of polarization ("Faraday rotation"). In the quasilinear approximation the Faraday rotation Ω (in radians) is given by (Ref. 7-4, integrating from the source to the observer):

$$\Omega = (e^3/8\pi^2 c\ m^2\ \varepsilon_0 f^2)\int N(\ell)\ \vec{B}\ .\ d\vec{\ell} \qquad (7\text{-}2)$$

where

B = magnetic field, weber/m^2

f = radio frequency (assumed much higher than either the plasma frequency or the gyro frequency), Hz

ω_g = gyro frequency = eB_z/m, rad/sec

These plasma effects manifest themselves in a number of physical observables. Those that are relevant to the link and its analysis are ranging, Faraday rotation, amplitude and phase scintillation, and spectral and angular broadening.

1. Ranging

Ranging is the measurement of the distance between a station and a spacecraft performed by computing the time interval between transmission and reception of a coded signal (range code). Because of the presence of plasma between the station and spacecraft, the measured time-of-flight will be different from that which would have been obtained without the intervening plasma. From the equation for group velocity (above), in the high-frequency limit of interest v_g becomes $v_g \simeq c[1-\omega_p^2/\omega^2]^{1/2}$. Hence because the range code travels with the group speed $v_g < c$ the presence of charged particles causes time-of-flight to be <u>larger</u> than it would be in the absence of the plasma. Thus precision ranging for navigation or radio science is complicated by the existence of the plasma. This is particularly severe for ranging measurements close to the sun, where one would like ultraprecise ranging to do tests of relativistic theories of gravity. General relativity predicts that the round trip time-of-flight to a spacecraft far behind the sun is increased by about 250 microseconds for ray paths that come very close to the sun. This effect must be measured in the presence of a plasma-induced time increase on the order of 10's of microseconds for S-and X-band signals (Refs. 7-5, 6, 7, 8). The experimental situation is complicated further by the fact that the radial gradient in the coronal electron density causes the ray paths to be bent inward toward the sun in a frequency-dependent way (Ref. 7-9).

2. Faraday Rotation

As noted above, a magnetized plasma causes orthogonal circularly polarized waves to propagate with different speeds. If a linearly polarized wave is synthesized from two circularly polarized waves, the effect will be to rotate the plane of polarization as the wave propagates through the plasma. The magnitude of the effect depends both on the electron density and the projection of the (assumed static) external magnetic field onto the axis of propagation. Figure 7-1 shows an example of a transient solar wind Faraday rotation effect observed using Pioneer 6 in November 1968. Faraday rotation "events" have also been widely observed in the transionospheric radio channel,

including some anomalous situations where there is a loss of correlation between two circularly polarized signals (Ref. 7-10). (That is, the usual concept of Faraday rotation which relates to linearly polarized waves, is not valid.) Although apparently rare, such events have implications for frequency reuse schemes based on polarization diversity.

3. Phase and Amplitude Scintillations

Variations in the received amplitude or phase of the radio wave can be caused by irregularities in the intervening plasma. There is a fundamental difference between phase and amplitude fluctuations: amplitude scintillations are essentially a diffraction phenomenon while phase scintillations are principally a refraction effect (Ref. 7-11). Amplitude fluctuations are caused mainly by irregularities that are smaller than or approximately equal to the effective Fresnel zone size at the plasma irregularity:

$$FZS = (\lambda z_e)^{1/2} \tag{7-3}$$

where

FZS = Fresnel zone radius, m
λ = radio wavelength, m
z_e = effective distance to the plasma irregularity, m
$= z_1 z_2 / (z_1 + z_2)$
z_1 = source to plasma distance, m
z_2 = plasma to earth distance, m

Amplitude scintillations can be caused by the solar wind (Refs. 7-12 and 13), the earth's ionosphere (Ref. 7-14), or planetary ionospheres (Ref. 7-15). If the scintillations are weak (rms intensity fluctuation $\lesssim$ mean intensity), then the typical time scale for amplitude fluctuations is FZS/v, where v is the speed with which the irregularities cross the line of sight connecting the spacecraft and the ground station. If the scintillations are strong (rms intensity = mean intensity) the time scale can be much shorter. Figure 7-2 (a-c) shows a set of intensity time series due to solar wind

scintillations as the ray path offset between the spacecraft and earth approaches the sun. In Fig. 7-2, the top panel shows S-band data taken at a sun-earth-probe (SEP) angle of 35 solar radii, while the middle and bottom panels show S-band time series taken at 20 and 10 solar radii, respectively. Figure 7-3 shows a plot of the scintillation index (≡ rms intensity fluctuation /mean intensity) as a function of SEP angle for S-band observations.

Phase scintillations differ fundamentally from amplitude scintillations in that they respond to large as well as small scale plasma irregularities (Ref. 7-16). If, as is the typical case for astrophysical plasmas, the spatial power spectrum of the density fluctuations is approximately power law (spectrum = constant wavenumber^{-p}), then the observed phase power spectrum is also power law, except near the Fresnel wavenumber. Thus, unlike amplitude scintillations, there is no characteristic scale to the phase fluctuations. Fig. 7-4 shows a time series of phase, while Figure 7-5 shows power spectra of phase in the solar wind (Ref. 7-17). Phase scintillations due to plasma fluctuations in the earth's ionosphere (Ref. 7-14) and in planetary ionospheres have been observed.

4. Spectral Broadening

Broadening of a radio frequency carrier can be caused by propagation if the source-plasma-observer are in relative motion (Ref. 7-18). The physical idea is that the received signal is composed of "rays" that are scattered off of the irregularities. If these irregularities are moving transverse to the source-observer line, then some of the received rays will have come from plasma blobs with a velocity component toward the receiver; that is, they will appear blue-shifted with respect to the carrier. Similarly, some rays will be scattered off of blobs moving away from the observer and appear red-shifted. The net effect is to produce a carrier with a finite line width. The radial dependence of spectral broadening caused by the solar wind is shown in Fig. 7-6 (Ref. 7-17). Spectral broadening caused by scattering in a planetary ionosphere has also been observed (Ref. 7-19).

5. Angular Broadening

Irregularities in an intervening plasma cause a loss of transverse coherence in the wave due to scattering. The result is that an initial plane wave is scattered into a bundle of rays with finite angular width (Ref. 7-18). This phenomenon is most pronounced at lower radio frequencies (cf. equation for refractive index fluctuation, above). Observations of this effect have been made in the solar wind (Ref. 7-20), and at very low frequencies in the earth's ionosphere. Angular scattering causes pulse energy to arrive at the receiver over a finite time (some energy comes direct; some energy comes via a scattered path and arrives later). Thus angular scattering gives rise to pulse broadening and hence to a loss of coherence of a wideband signal.

C. COMMUNICATIONS LINK EFFECTS

The propagation effects discussed above can significantly affect earth-spacecraft communications links. Both data transfer (uplink commands and downlink telemetry) and radio metric data can be seriously affected. The influence is substantial when the propagation path comes close to the sun. (All outer planet space probes have periods when the spacecraft-earth propagation path comes close to the sun.)

Command and telemetry degradation due to phase scintillation is related to the receiver phase error produced by the receiver's inability to track the plasma phase scintillations with complete precision. The amplitude of the demodulated command or telemetry signal will fluctuate as the cosine of the receiver phase error. The impact of this amplitude variation on performance is determined by the statistics of the average of the cosine of the phase error over a data symbol. For telemetry data rates less than the loop bandwidth of the phase-estimating section of the receiver, this averaging can substantially reduce the data channel performance degradation. Thus, low-rate data channels (e.g., the command channel) suffer less degradation than the high-rate (telemetry) channels.

The magnitude of the phase error depends on both the magnitude and time scale of the phase scintillations. The magnitude of the phase scintillations can be quite large (see, e.g., Fig. 7-4). Expressed as a fractional frequency stability, the scintillation-induced variations are typically orders of magnitude worse than that of the ground-based hydrogen maser. However, these fluctuations occur on all time scales with the principal effect (in terms of phase variance) on the longer time scales (Fig. 7-5). Thus, the phase-estimating section of the receiver can follow most of the phase scintillation; only high-frequency components of the scintillations (those outside the loop bandwidth) will produce significant phase error. One method for reducing the impact of the phase scintillation is to increase the receiver carrier tracking loop bandwidth. This can reduce the scintillation-induced phase error to an acceptable level. However, increasing the loop-bandwidth proportionately increases the receiver rms phase error due to thermal noise in the receiver. Thus, additional signal power may be needed to maintain the phase error contribution due to receiver thermal noise within acceptable limits.

Amplitude scintillations can have a very severe impact on command and telemetry performance. One mechanism for this performance degradation is similar to that discussed above for phase scintillation. Unlike phase scintillation, however, amplitude fluctuations directly alter the signal levels seen at the telemetry detector. In addition the amplitude scintillations can adversely affect carrier tracking, increasing the receiver carrier-tracking loop phase error and creating, as discussed above, an additional source of telemetry degradation. Fortunately for telemetry purposes, solar wind scintillations at S-band are fairly weak unless the ray path comes close to the sun. (Fig. 7-3 shows the fractional intensity fluctuation, m, versus sun-earth-probe angle for a source far behind the sun. As outlined in the previous section, the geometry is crucial. Thus, for telemetry analysis of, say, a spacecraft embedded in the plasma, Fig. 7-3 would have to be scaled appropriately depending on the radio frequency of the link and on the source-sun-earth geometry.) Ionospheric amplitude scintillations are generally stronger at night than in the daytime. While they can be severe at VHF frequencies, the ionospheric amplitude scintillations are usually weak at Network allocation frequencies

(Ref. 7-14). Combinations of Faraday rotation fluctuations with amplitude scintillations have been observed in the transionospheric channel (Ref. 7-9), however. These have to be considered in frequency reuse schemes using polarization diversity. Scintillations can be important if the communication link uses bursts of telemetry that are short compared to a typical fade duration or if they require a coherence bandwidth that is larger than the channel will support due to scintillation. There are of course coding and diversity schemes for suppressing the scintillation effects. For example, amplitude scintillations are correlated over fairly short distances on the earth's surface. Thus one can get uncorrelated fluctuations by arraying antennas separated by a few Fresnel zone radii. Since the Fresnel zone size is wavelength and geometry dependent, the exact required separations have to be calculated for each situation, but would typically be in the range 10's to 100's of kilometers. Also, coding schemes which distribute the message over many independent amplitude fades can be employed to reduce the telemetry sensivity to amplitude scintillations. Appropriate coding can very substantially reduce the impact of the amplitude and phase scintillations on command and telemetry performance. Generally, the objective of such coding is to make the command or telemetry performance depend on the <u>average</u> of the amplitude variation seen by the telemetry detector, instead of the extreme of these variations. Time-diversity transmission, multiple transmission of the same data with time spacings greater than the correlation time of the amplitude variations seen by the telemetry detector, with suitable recombination in the telemetry detector is one possible technique. However, this requires a <u>very</u> large increase in the data channel symbol rate. It appears that suitable interleaving of a convolutionally encoded channel may also yield acceptable performance with no increase in the data channel symbol rate.

Spectral broadening can be characterized as a combination of amplitude and phase scintillation on short time scales (Ref. 7-18). Thus it can cause problems with carrier synchronization and with fluctuations in signal-to-noise ratios. Fortunately, spectral broadening is only important either very close to the sun (see Fig. 7-6) or during some planetary encounters (Ref. 7-19) when the earth-to spacecraft line is moving very rapidly.

Angular broadening can affect telemetry if power is scattered out of the beam of the receiving antenna, thus reducing the strength of the received signal. For single dish antennas operated at DSN microwave frequency allocations the effect is negligible, except very near the sun. However, angular scattering also causes pulse broadening and loss of coherence of the signal. Thus it needs to be considered in communications systems that require short bursts and/or large coherence bandwidths.

REFERENCES

7-1. Heald, M. A., and Wharton, C. B., Plasma Diagnostics With Microwaves, Wiley, New York 1965.

7-2. Denisse, J. F., and Delcroix, J. L., Plasma Waves, Interscience, New York 1963.

7-3. Stelzried, C. T., "A Faraday Rotation Experiment of a 13 cm Signal in the Solar Corona," Ph. D. thesis, University of Southern California, 1969.

7-4. Bauer, S. J., Physics of Planetary Ionospheres, Springer-Verlag, New York, 1973.

7-5. Anderson, J. D., et al., "Experimental Test of General Relativity Using Time-Delay Data from Mariner-6 and Mariner-7," Ap. J., 200, 221, 1975.

7-6. Shapiro, I. I., et al., "The Viking Relativity Experiment," J. Geophys. Res., 82, 4329, 1977.

7-7. Muhleman, D. O., Esposito, P. B., and Anderson, J. D., "The Electron Density Profile of the Outer Corona and the Interplanetary Medium From Mariner-6 and Mariner-7" Ap. J., 211, 943, 1977.

7-8. Muhleman, D. O., and Anderson, J. D., "Solar Wind Electron Densities from Viking Dual-Frequency Radio Measurements," Ap. J., 247, 1093, 1981.

7-9. Tyler, G. L., et al., "The Viking Solar Corona Experiment," J. Geophys. Res., 82, 4335, 1977.

7-10. Das Gupta, A., et al., "VHF Faraday Polarization Fluctuations and Strong L-band Amplitude Scintillations Near Appleton Anomaly Crests," Nature, 298, 354, 1982.

7-11. Tatarski, V. I. Wave Propagation in a Turbulent Medium, Dover, New York, 1961.

7-12. Coles, W. A., Rickett, B. J., and Rumsey, V. H., "Interplanetary Scintillation," in Solar Wind Three (C. Russel, ed.) IGPP Press, Los Angeles, Calif., 1974.

7-13. Armstrong, J. W., and Woo, R., "Solar Wind Motion Within 30 R_S: Spacecraft Radio Scintillation Observations," Astron. Astrophys., 103, 415, 1981.

7-14. Fremouw, E. J., et al., "Early Results From the DNA Wideband Satellite Experiment - Complex-Signal Scintillation," Radio Science, 13, 167, 1978.

7-15. Woo, R., and Yang, F-C ,"Measurements of the Magnetic Field Orientation in the Jovian Ionosphere Deduced from Pioneer 10 and 11 Scintillation Observations," J. Geophys. Res., 83, 5245, 1978.

7-16. Woo, R., et al., "Structure of Density Fluctuations Near the Sun Deduced from Pioneer 6 Spectral Broadening Measurements," Ap. J., 210, 568, 1976.

7-17. Woo, R., and Armstrong, J. W., "Spacecraft Radio Scattering Observations of the Power Spectrum of Electron Density Fluctuations in the Solar Wind," J. Geophys. Res., 84, 7288, 1979.

7-18. Woo, R., et al., "Probing the Solar Wind With Radio Measurements of the Second Moment Field," Ap. J., 218, 557, 1977.

7-19. Woo, R., and Armstrong, J. W., "Spectral Broadening Measurements of the Ionospheres of Jupiter and Saturn," Nature, 287, 309, 1981.

7-20. Woo, R., "Radial Dependence of Solar Wind Properties," Ap. J., 219, 727, 1978.

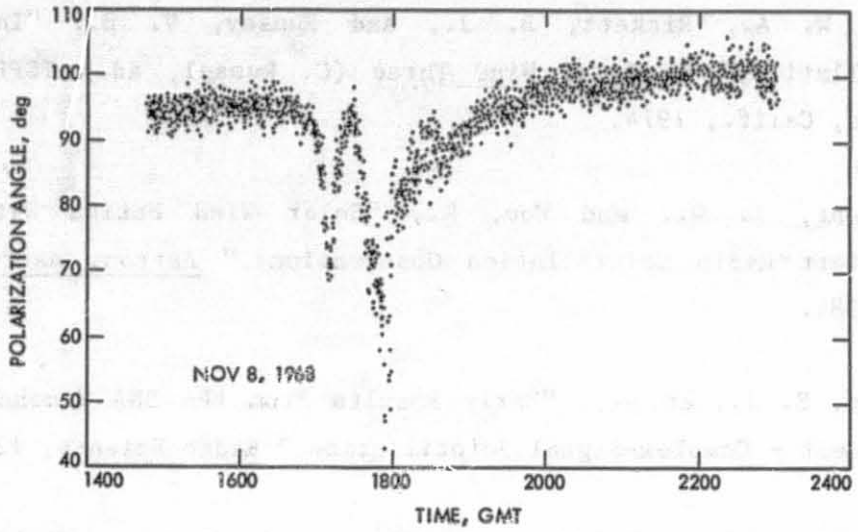

Fig. 7-1. Pioneer 6 polarization (10 second data points) versus time, November 8, 1968

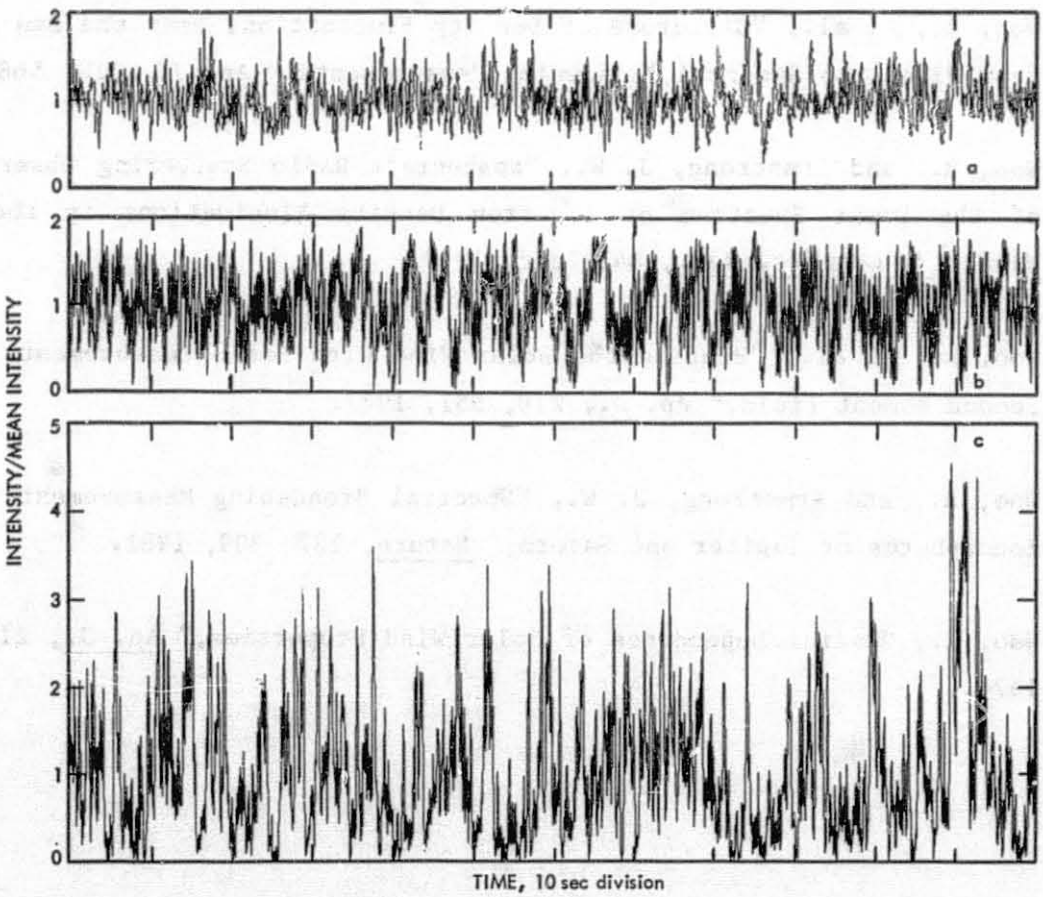

Fig. 7-2. Examples of S-band intensity scintillation as ray-path offset from sun decreases. Ray-path offsets (top to bottom) are 35, 20, and 10 solar radii

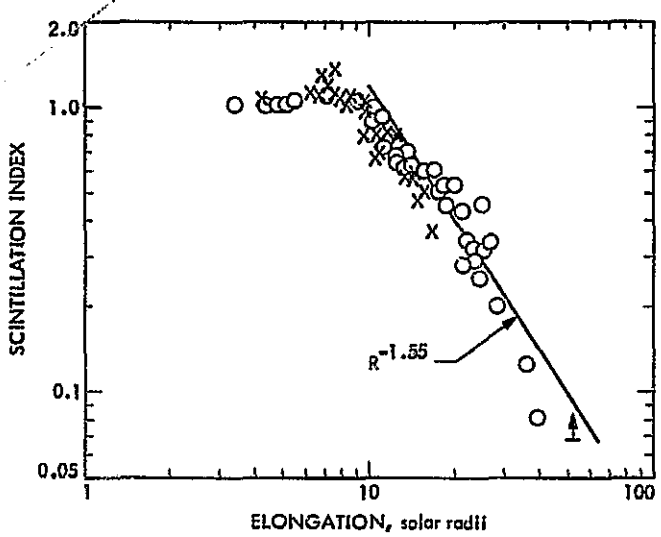

Fig. 7-3. Scintillation index (f ≈ 2.3 GHz) versus elongation (ε = 0 at sun's center). Circles: 1976-1978 data; crosses: 1979 data. Spacecraft radio source is about 2 AU from the earth

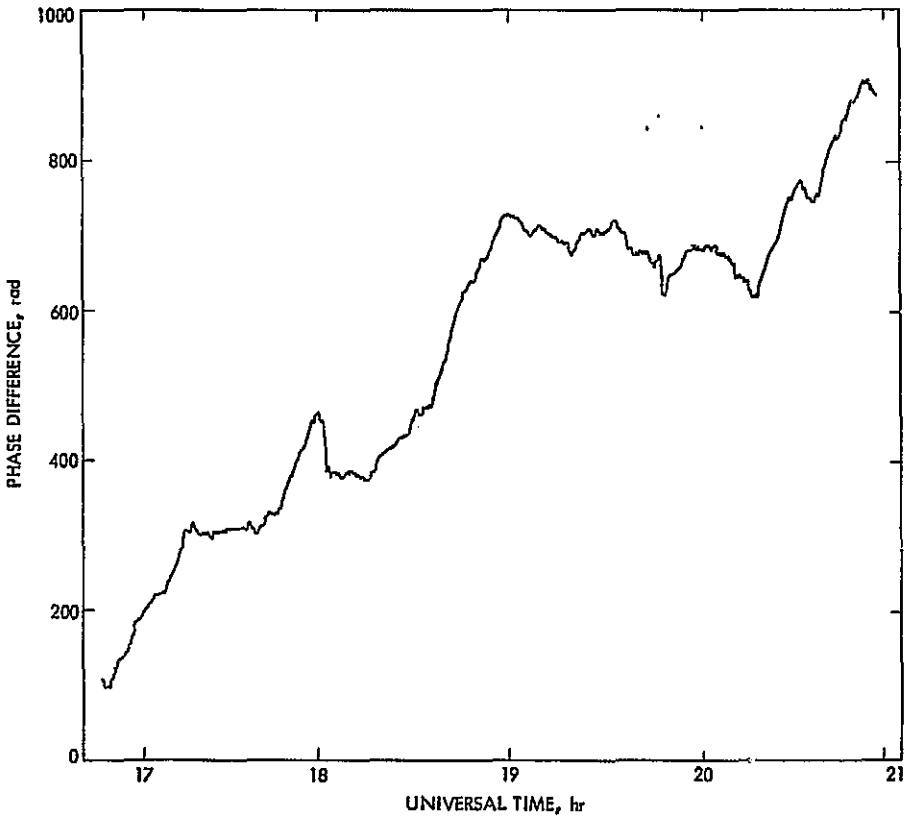

Fig. 7-4. Time history in UT of Mariner 10 S/X phase difference in radians (arbitrary zero) taken on May 1, 1974, when the solar elongation angle θ was 11.5 deg

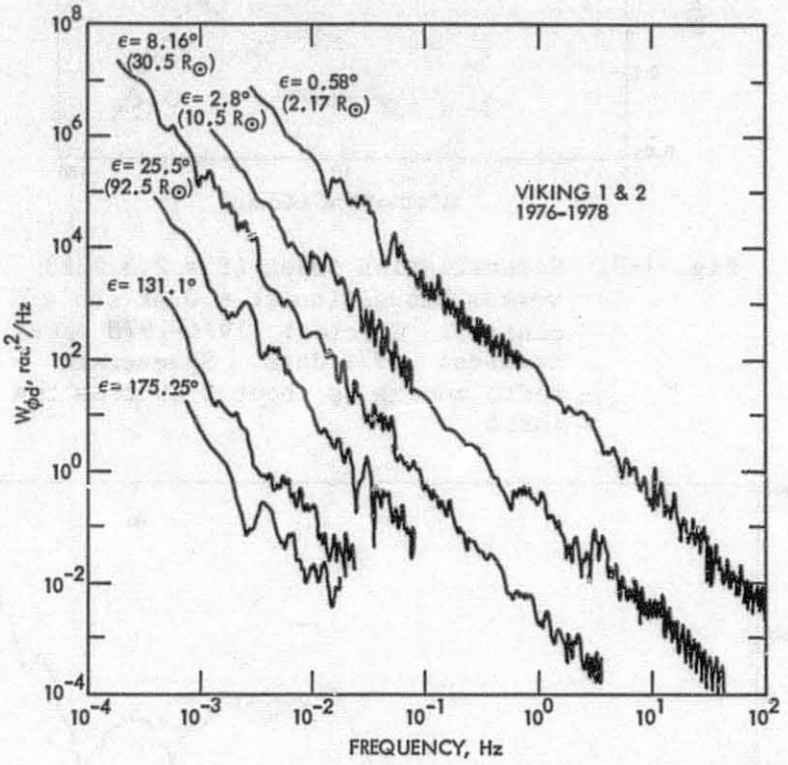

Fig. 7-5. Typical power spectra of the Viking phase difference scintillations observed over the entire solar elongation range. The spectra for $R \leq 30.5\ R_S$ are of open loop data, while the rest are of closed-loop data

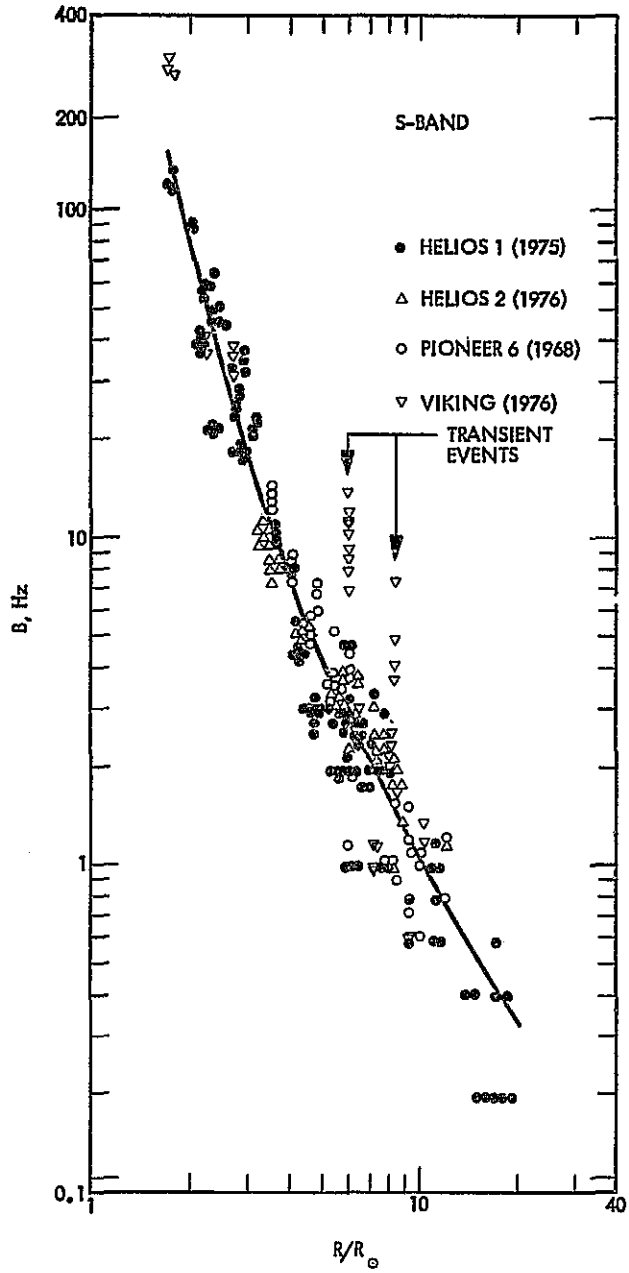

Fig. 7-6. Radial variation of spectral broadening bandwidth B at 2.3 GHz

VIII. ATMOSPHERIC EFFECTS

C. T. Stelzried and S. D. Slobin

A. INTRODUCTION

The earth's atmosphere (Ref. 8-1) consists mostly of the dry components oxygen (about 21% by volume), nitrogen (about 78% by volume) argon (about 1% by volume), and wet components (water vapor, clouds and rain). Water vapor at 100% relative humidity is approximately 1.7% by volume assuming the U.S. Standard Atmosphere, 15°C, at sea level.

A communications link through the atmosphere suffers attenuation from both the dry and wet components (Refs. 8-2 through 8-9). This results in a decreased signal-to-noise ratio (SNR) of the communications link due to both the signal attenuation and the increased noise temperature resulting from thermal emission.

B. THEORY

From the theory of radiative transfer (neglecting scattering,[1] and assuming hf << kT, Ref. 8-10), the sky noise temperature (atmosphere and cosmic background) contribution at the receiving system input is given by (Fig. 8-1[2])

$$T_{sky} = (T_s/L) + \int_0^{\ell} T(x)\,\alpha(x)\,e^{-\tau(x)}dx \text{ (kelvins)} \qquad (8\text{-}1)$$

where

$\alpha(x)$ = absorption coefficient of the atmosphere at x, nepers/m

x = slant distance along propagation path, m (x = 0 at surface[2])

---

[1] Scattering should be considered for rain at frequencies above about 10 GHz, and for clouds at frequencies above about 100 GHz (Refs. 8-11 and 12)

[2] It is sometimes convenient to integrate from the "top" of the atmosphere to the surface (Ref. 8-13).

ℓ = total slant distance along propagation path, m

T_s = source temperature (usually about 2.7 K, due to the cosmic background noise temperature), K

$T(x)$ = physical temperature of the atmosphere at x, K

L = total atmospheric absorption, ratio (≥ 1)
$= e^{\tau} = 10^{A/10}$

A = total atmospheric absorption, dB
$= 10 \log L = \tau\,(10 \log e) \approx 4.343\ \tau$

τ = total atmospheric absorption (optical depth), nepers

$$= \int_0^{\ell} \alpha(x)\, dx \approx 2.303\ A$$

$\tau(x)$ = atmospheric absorption between 0 and x, nepers

$$= \int_0^{x} \alpha(x')\, dx'$$

For an homogeneous, isothermal atmosphere, $\alpha(x) = \alpha_0$, and temperature $T(x) = T_p$. From Eq. (8-1),

$$T_{sky} = (T_s/L) + (1 - 1/L)T_p \qquad (8\text{-}2)$$

where

$L = e^{\tau} = e^{\alpha_0 \ell}$

T_p = equivalent atmospheric physical temperature, K
($\approx$ 260-280 K; Ref. 8-14)

Atmospheric loss (see Section E) can be determined from solving Eq. (8-2),

$$L = (T_p - T_s)/(T_p - T_{sky}) \qquad (8\text{-}3)$$

where T_{sky} is usually obtained from radiometric measurements. The total atmospheric loss in dB is given by

$$A = 10 \log L \qquad (8\text{-}4)$$

C. CHARACTERIZATION

Computed clear sky[3] atmospheric attenuation and noise temperature contributions in the zenith direction are shown in Fig. 8-2 and Table 8-1 as functions of frequency, surface water vapor density (i.e., absolute humidity), and station altitude. Microwave absorption is directly proportional to the total integrated water vapor content along the line of sight. For temperate latitudes in summer (20°C), the average surface water vapor density is about 7.5 g/m^3 (Refs. 8-15 and 8-16). At saturation (sea level, 20°C), the density is about 17 g/m^3; 3-5 g/m^3 may be more appropriate for arid regions such as Goldstone, California. Operating frequencies are usually chosen to be well away from the water vapor line (22.235 GHz). Minimum attenuation occurs with low humidity, low frequency, and high elevation angle (Fig. 8-1, $Z = 0^{\circ}$).

The effect of clouds and rain (Ref. 8-2) is to both further attenuate the signal and increase the atmospheric noise temperature. The calculated effect of a one- or two-cloud model (Ref. 8-17) is tabulated in Table 8-2 at S-, X-,

---

[3] "Clear sky" indicates an atmosphere containing only gaseous constituents (oxygen, nitrogen, and water vapor) with no liquid water (rain or clouds).

and K_a- bands. This is shown as a function of frequency in Fig. 8-3 for cloud water particle density of 0.5 g/m^3. Statistics of clear-sky and cloud noise temperature and attenuation at various sites in the United States, Alaska, and Hawaii are available in Ref. 8-18.

The combined effect (Ref. 8-19) of variations in clouds, rain, and clear sky surface water vapor density on the communication link performance can be determined experimentally. These effects are measured as a function of frequency, geographical location, and time of year. Figure 8-4 shows the cumulative distribution of X-band zenith atmospheric noise temperature increase above the clear sky baseline for Goldstone, California. Data for curves labelled by year were obtained with a noise adding radiometer. Also shown are curves for the CCIR arid region rain-only model (Ref. 8-21) and the very pessimistic Deep Space Network 810-5 Design Handbook (Ref. 8-22) cloud-only model. These curves are read (for example): "90-percent of the time the zenith noise temperature increase was 1 K or less for 1980." This is frequently designated as "90% weather."

There is a one-to-one correspondence between atmospheric attenuation increase and system noise temperature increase. From Eq. (8-2),

$$\Delta T_{op} = (L_0^{-1} - L^{-1})(T_p - T_s) \qquad (8\text{-}5)$$

where

ΔT_{op} = increase in system noise temperature due to atmospheric absorption increase from L_0 to L, K

$= T_{op} - (T_{op})_0$

T_{op} = system noise temperature assuming atmospheric absorption loss L, K

$(T_{op})_0$ = system noise temperature assuming a baseline atmospheric absorption L_0, K

L = atmospheric absorption, ratio ($= 10^{A/10}$)

L_0 = baseline atmospheric absorption, ratio ($= 10^{A_0/10}$)

T_s = cosmic background noise temperature, K

Atmospheric absorption and noise temperature are related as shown in Fig. 8-2 and Eq. (8-2) and an appropriate choice of $(T_p - T_s)$.

The increased noise temperature effects of water collecting on the antenna feed horn cover have been evaluated at X-band (Ref. 8-23). Special techniques are required to minimize the resulting increased noise temperature, especially with "weathered" plastic horn cover material (Ref. 8-24).

For "90% weather" and 30^o elevation angle pointing, the Goldstone atmospheric noise temperature contributions are tabulated in Table 8-3. The "90% weather" and 30^o elevation angle pointing conditions are useful for baseline system performance studies.

D. COMMUNICATIONS LINK PERFORMANCE

The signal-to-noise[4] ratio of a linear receiving system is given by (Ref. 8-25, hf << kT; otherwise see Ref. 8-26)

$$SNR = S_i/k(T_i + T_e)B \qquad (8\text{-}6)$$

where

S_i = input signal level, W

h = Planck's constant = 6.6262×10^{-34} J-s

k = Boltzman's constant = 1.3806×10^{-23} J/K

T_i = source input noise temperature, K

T_e = amplifier effective noise temperature, K

B = noise bandwidth, Hz $\left(= \frac{1}{G} \int_o^\infty G(f)\, df \right)$

---

[4] In the context of this section, signal power refers to the power in the carrier; therefore, the SNR is strictly the ratio of signal carrier power to noise power. Gulkis (Ref. 8-27) discusses noise power from a fluctuations viewpoint and provides insight into quantum and thermal noise for linear and incoherent amplifiers.

$G(f)$ = available power gain, ratio

G = maximum available power gain, ratio

f = operating frequency, Hz

It is instructive to consider this relationship for a receiving system degraded by an additional 0.1 dB of input absorption loss due to atmospheric changes. With high system noise temperatures ($T_{op} > 300$ K), this degrades SNR by $\approx$ 0.1 dB due to the additional direct signal attenuation. With low system noise temperatures ($T_{op} < 50$ K), this has a very much larger effect due to the increase in T_{op} caused by the added thermal noise contribution.

The degradation in signal-to-noise ratio is given by

$$\Delta \text{SNR} = \Delta A + 10 \log \left[T_{op} / (T_{op})_0 \right], \text{ dB} \qquad (8\text{-}7)$$

where

ΔA = increased atmospheric absorption, dB

$= (A - A_0)$

$= 10 \log (L/L_0)$

$A_0 = 10 \log L_0$

The increase in atmospheric attenuation may be inferred from measurements of increased system noise temperature. Thus, using Eq. (8-5),

$$\Delta A = 10 \log \left[\frac{T_p - T_s}{T_p - T_s + \Delta T_{op} \, 10^{A_0/10}} \right], \text{ dB} \qquad (8\text{-}8)$$

where ΔT_{op} is taken from Fig. 8-4 for a particular percent-weather, and A_0 is the baseline, or clear sky attenuation.

For the previous "90% weather" example (using A_0 = 0.04 dB at X-band), an increase of 1 K at zenith results from an attenuation increase of 0.016 dB.

Figure 8-5 indicates the degradation of SNR as functions of the baseline system temperature, baseline atmospheric absorption, and increase in atmospheric absorption. This analysis technique indicates a net improvement of better than 8 dB in sensitivity (90% of the time) for a 32-GHz receiving system relative to an 8.4-Ghz receiving system in the Goldstone environment (Ref. 8-28).

E. MEASUREMENT OF ATMOSPHERIC LOSS

It is shown in Section D that the receiving system sensitivity of a low noise system can be degraded severely, even with a relatively small amount of atmospheric loss.

It is frequently convenient to perform a radiometer tipping measurement to determine T_{atm} and the atmospheric loss. Assuming a flat earth with a stratified atmosphere

$$L = L_z^{\sec Z} \tag{8-9}$$

where

Z = zenith angle

L, L_z = atmospheric loss at zenith angle Z and zenith respectively, ratio (L, $L_z \geq 1$)

For the tipping measurement, the system temperature (T_{op}) is measured at zenith and Z. Assuming an antenna with no sidelobes and an infinitely narrow beamwidth, the change in T_{op} is given by

$$\Delta T_{op} = (L_z^{-1} - L_z^{-\sec Z})\,(T_p - T_s) \tag{8-10}$$

It is convenient to perform this measurement between zenith and Z = 60°.

Then

$$\Delta T_z = (L_z^{-1} - L_z^{-2})(T_p - T_s) \qquad (8\text{-}11)$$

A tipping measurement performed near the water vapor resonance (22.235 GHz) is convenient for monitoring atmospheric water vapor content in the antenna beam line of sight with a water vapor radiometer. The precipitable atmospheric water vapor content is monitored by repeated tipping measurements or by switching between horns mounted at suitable zenith angles. For clear sky conditions, this technique has the simplicity and accuracy of a relative measurement of ΔT_{op} as compared to the difficulty of the absolute measurements required for two-frequency instruments. Although the single-frequency water vapor radiometer should perform well in clear sky conditions, serious performance degradation occurs during cloudy weather. The primary effect of liquid water (clouds) in the troposphere is to increase the noise temperature. Most of the tropospheric delay is due to water vapor and very little is due to liquid water. Thus, two frequencies are needed to separate the vapor and liquid effects; only one frequency is needed if no liquid component is present.

REFERENCES

8-1. Smith, E.K. "Centimeter and Millimeter Wave Attenuation and Brightness Temperature Due to Atmospheric Oxygen and Water Vapor," Radio Science, Vol. 17, Nov.-Dec. 1982.

8-2. Ippolito, L.J., "Radio Propagation for Space Communications System," IEEE Proceedings, Vol. 69, No. 6, pp. 629-727, June 1981.

8-3. Crane, R.K., "Extinction by Condensed Water," Methods of Experimental Physics, Vol. 128, Academic Press, N.Y., 1976.

8-4. Straiton, Archie W., "The Absorption and Reradiation of Radio Waves by Oxygen and Water Vapor in the Atmosphere," IEEE Trans. Ant. and Prop., Vol. AP-23 pps. 595-597, July 1975.

8-5. Damosso, E.D., and De Pa[illegible]ova, S., "Some Considerations About Sky Noise Temperature at Frequencies Above 10 GHz," Alta Frequenza, Vol. XLV, No. 2, pp. 98-106, Apr. 1978.

8-6. Daywitt, W.C., "Atmospheric Propagation Equations Used in the NBS Earth Terminal Measurement System," NBSIR 78-883, NBS, Boulder, Colorado, Apr. 1978.

8-7. Hogg, D.C., "Effective Antenna Temperatures Due to Oxygen and Water Vapor in the Atmosphere," J. Appl. Phys., Vol. 30, No. 9, pp. 196-209, Feb. 1981.

8-8. Crane, R.K., "Fundamental Limitations Caused by RF Propagation," IEEE Proc., Vol. 69, No. 2, pp. 196-209, Feb. 1981.

8-9 Liebe, H. J., "Atmospheric EHF Window Transparencies Near 35, 90, 140, and 220 GHz," IEEE Trans. Ant. Prop., Vol. AP-31, Jan. 1983.

8-10. Chandrasekhar, S., Radiative Transfer, Dover Publications, N.Y., 1960.

8-11. Tsang, L., et al., "Theory of Microwave Emission from a Layer of Cloud or Rain," IEEE Trans. Ant. Prop., AP-25, No. 5, pp. 650-657, Sep. 1977.

8-12. Flock, W.L., Electromagnetics and the Environment: Remote Sensing and Telecommunications, Prentice-Hall, Inc., N. Y., 1979.

8-13. Waters, J.W., "Absorption and Emission by Atmospheric Gases," Methods of Experimental Physics, Vol. 128, Academic Press, N. Y., 1976.

8-14. Stelzried, C.T., "Atmospheric Noise Temperature Measurements," TDA Progress Report 42-63, Jet Propulsion Laboratory, Pasadena, Calif., pp. 87-96, June 1981.

8-15. Van Vleck, J.H., "Theory of Absorption by Uncondensed Gases," Propagation of Short Radio Waves (edited by D.E. Kerr), MIT Radiation Laboratory Series, Vol. 13, McGraw Hill, N.Y., 1951.

8-16. Bean, B.R., and Dutton, E.J., Radio Meteorology, Dover Publications, Inc., N.Y., 1968.

8-17. Slobin, S.D., Microwave Noise Temperature and Attenuation of Clouds at Frequencies Below 50 GHz, Publication 81-46, Jet Propulsion Laboratory, Pasadena, Calif., July 1981.

8-18. Slobin, S.D., "Microwave Noise Temperature and Attenuation of Clouds: Statistics of These Effects at Various Sites in the United States, Alaska and Hawaii," Radio Science, Vol. 18, No. 6, Nov./Dec. 1982.

8-19. Ippolito, L.J., et al., A Propagation Effects Handbook for Satellite Systems Design, NASA Reference Publication 1082, Dec. 1981.

8-20. Slobin, S.D., et al., "X-Band Atmospheric Noise Temperature Statistics at Goldstone, DSS 13, 1979 and 1980, and Clear Air Noise Temperature Models for Goldstone," TDA Progress Report 42-64, Jet Propulsion Laboratory, Pasadena, Calif., pp. 161-167, Aug. 15, 1982.

8-21. "Rain Attenuation Prediction", CCIR Study Group, WARC-79, Document P/105-E, Geneva, Switzerland, June 6, 1978.

8-22. "Deep Space Network/Flight Project Interface Design Handbook" Document 810-5, Rev. D, Vol. I, Jet Propulsion Laboratory, Pasadena, Calif., Oct. 15, 1981, (an internal document).

8-23. Slobin, S., Franco, M., and Clauss, R., "X-Band Noise Temperature Effects of Rain on DSN Antenna Feedhorns," TDA Progress Report 42-71, Jet Propulsion Laboratory, Pasadena, Calif., Aug. 15, 1982.

8-24. Hoffman, H., "Hydrophobic Coating for Antenna Weather Windows," Microwave J., pp. 43-48, Oct. 1979.

8-25. Haus, H.A., "Description of the Noise Performance of Amplifiers and Receiving Systems," Proc. IEEE, Vol. 58, No. 3, p. 436, Mar. 1963.

8-26. Stelzried, C.T., "Noise Temperature and Noise Figure Concepts: DC to Light," TDA Progress Report 42-67, Jet Propulsion Laboratory, Pasadena, Calif., pp. 100-110, Feb. 1982.

8-27. Gulkis, S., "Thermal Background Noise Limitations," TDA Progress Report 42-71, Jet Propulsion Laboratory, Pasadena, Calif., Nov. 15, 1982.

8-28. Clauss, P., Franco, M., and Slobin, S., "K_a-Band Weather Dependent System Performance Estimates for Goldstone," TDA Progress Report 42-71, Jet Propulsion Laboratory, Pasadena, Calif., pp. 60-65, Nov. 15, 1982.

Table 8-1. Clear sky zenith atmospheric noise temperature as a function of frequency and surface water vapor density W (Ref. 8-18)

Location and station altitude	Atmosphere components	2.3 GHz		8.5 GHz		21.0 GHz		32.0 GHz	
	O_2 + W(g/m^3)[a]	T,K	A,dB	T,K	A,dB	T,K	A,dB	T,K	A,dB
Sea level	O_2 + 0.0	2.12	0.035	2.29	0.038	3.23	0.053	6.38	0.106
H = 0.000 km	O_2 + 3.0	2.13	0.035	2.48	0.041	10.30	0.327	9.54	0.154
	O_2 + 7.5	2.15	0.035	2.78	0.045	20.50	0.327	14.29	0.228
	O_2 + 10.0	2.16	0.036	2.94	0.048	25.98	0.417	16.94	0.027
	O_2 + 15.0	2.18	0.036	3.28	0.053	36.52	0.597	22.24	0.355
DSS 14 Goldstone, Calif. H = 1.032 km	O_2 + 0.0	1.68	0.028	1.80	0.030	2.54	0.042	5.03	0.083
	O_2 + 3.0	1.69	0.028	1.98	0.032	9.95	0.157	7.87	0.127
	O_2 + 7.5	1.70	0.028	2.24	0.036	20.65	0.328	12.14	0.193
	O_2 + 10.0	1.71	0.028	2.39	0.038	26.37	0.423	14.52	0.230
	O_2 + 15.0	1.73	0.029	2.69	0.043	37.40	0.611	19.30	0.306

[a] W = surface water vapor density, exponential decrease with height, 2 km scale height.

Table 8-2. Sample cloud models and S-, X-, and K_A-band zenith atmospheric noise temperature contributions (Ref. 8-17)

Case	Lower Cloud				Upper Cloud				Remarks	S-band (2.3 GHz)		X-band (8.5 GHz)		K_a-band (32 GHz)	
	Density, g/m^3	Base, km	Top, km	Thickness km	Density, g/m^3	Base, km	Top, km	Thickness km		T,K	A,dB	T,K	A,dB	T,K	A,dB
1	-	-	-	-	-	-	-	-	Clear air	2.15	0.035	2.78	0.045	14.29	0.228
2	0.2	1.0	1.2	0.2	-	-	-	-	Light, thin clouds	2.16	0.036	2.90	0.047	15.92	0.255
3	-	-	-	-	0.2	3.0	3.2	0.2		2.16	0.036	2.94	0.048	16.51	0.266
4	0.5	1.0	1.5	0.5	-	-	-	-		2.20	0.036	3.55	0.057	24.56	0.397
5	-	-	-	-	0.5	3.0	3.5	0.5		2.22	0.037	3.83	0.062	28.14	0.468
6	0.5	1.0	2.0	1.0	-	-	-	-	Medium clouds	2.27	0.037	4.38	0.070	35.22	0.581
7	-	-	-	-	0.5	3.0	4.0	1.0		2.31	0.038	4.96	0.081	42.25	0.731
8	0.5	1.0	2.0	1.0	0.5	3.0	4.0	1.0		2.43	0.040	6.55	0.105	61.00	1.083
9	0.7	1.0	2.0	1.0	0.7	3.0	4.0	1.0		2.54	0.042	8.04	0.130	77.16	1.425
10	1.0	1.0	2.0	2.0	1.0	3.0	4.0	1.0	Heavy clouds	2.70	0.044	10.27	0.166	99.05	1.939
11	1.0	1.0	2.5	1.5	1.0	3.5	5.0	1.5		3.06	0.050	14.89	0.245	137.50	3.060
12	1.0	1.0	3.0	2.0	1.0	4.0	6.0	2.0	Very heavy clouds	3.47	0.057	20.20	0.340	171.38	4.407

NOTES:
1. Cases 2-12 are clear air and clouds combined
2. Antenna located at sea level
3. Heights are above ground
4. No cosmic background or ground contribution considered
5. T(K) is atmospheric noise temperature at zenith
6. A(dB) is atmospheric attenuation along vertical path from ground to 30 km above ground

Table 8-3. Tabulation of the Goldstone atmospheric noise temperature contribution for "90% weather" and 30° elevation angle pointing as a function of operating frequency (Ref. 8-28).

Frequency f, Ghz	Atmospheric noise temperature contribution T_{atm}, K
2.3	3.5
8.4	4.9
32	29

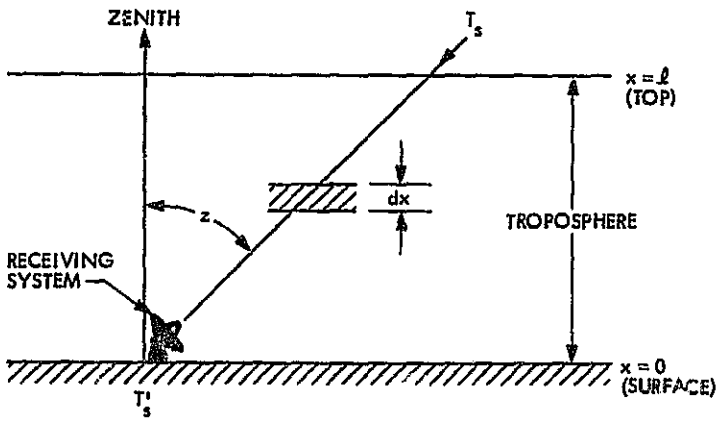

Fig. 8-1. Representation of a receiving system with signal propagating through lossy medium

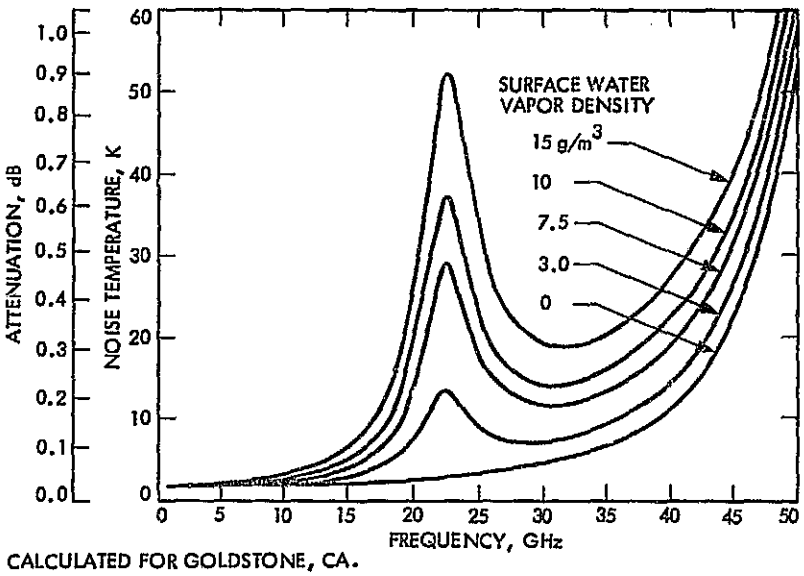

Fig. 8-2. Computed zenith clear sky atmospheric noise temperature and attenuation as functions of frequency and surface water vapor density

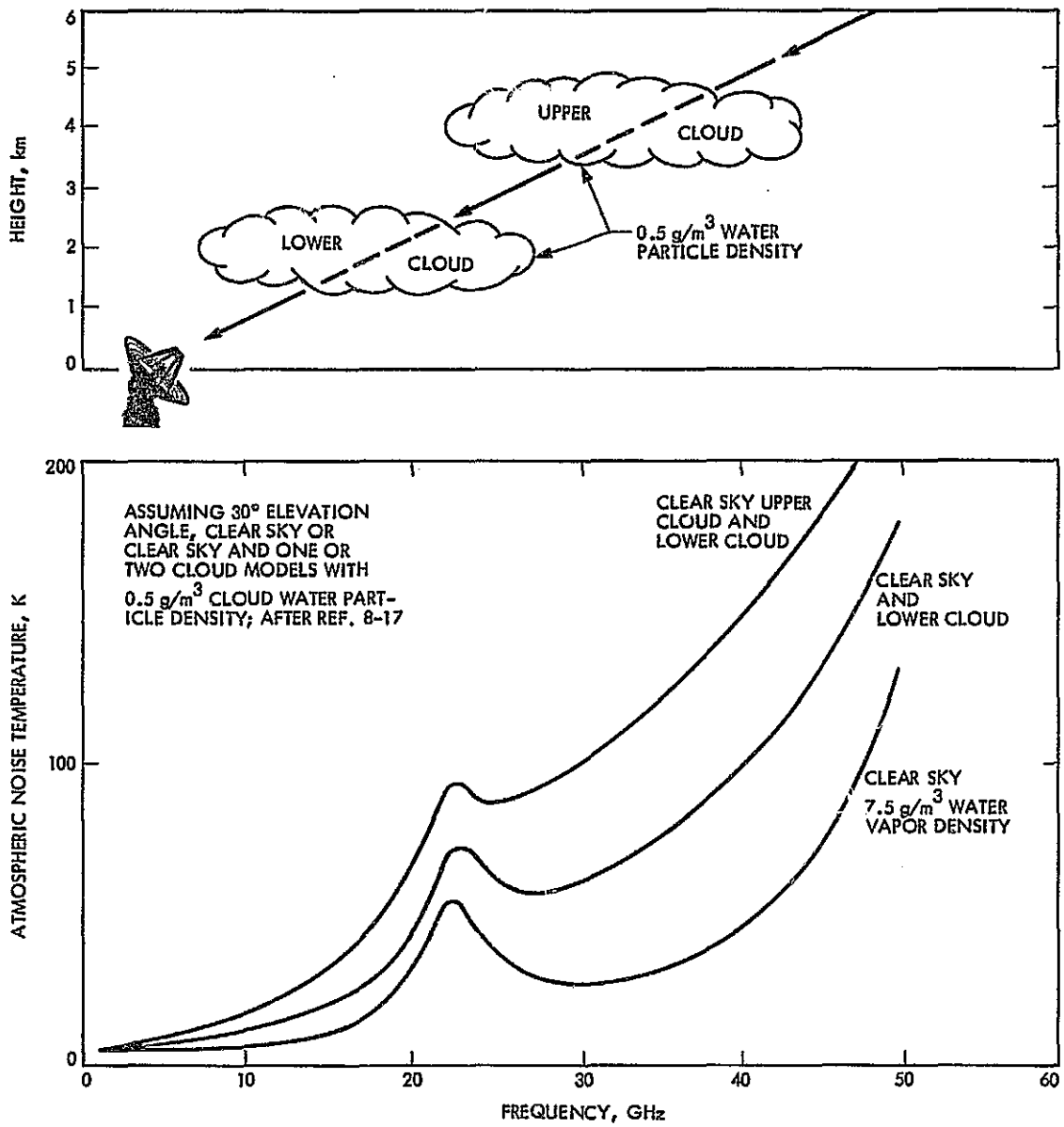

Fig. 8-3. Graph of atmospheric noise temperature vs frequency

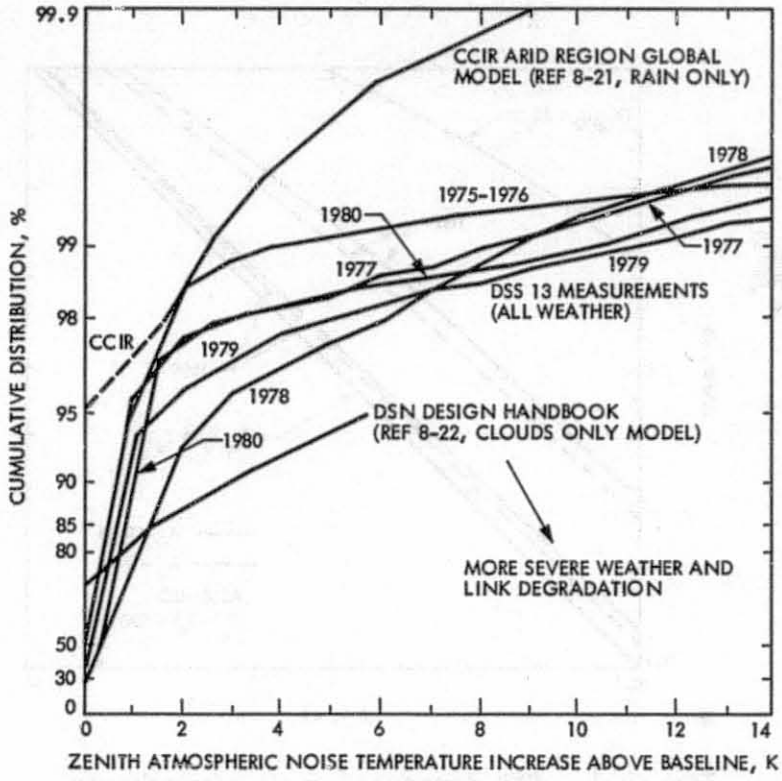

Fig. 8-4. Cumulative distribution of X-band, all weather, zenith atmospheric noise temperature increase above quiescent clear sky baseline at DSS 13, Goldstone, California (Ref. 8-20)

IX. COMMAND

N. A. Burow and M. K. Tam

A. INTRODUCTION

The Command System provides the means by which a project controls the activities of its spacecraft from the earth. This section presents an overview of the Multimission Command (MMC) System. The major components within the MMC System are discussed, with emphasis on the telecommunications-related implementations. Two versions of the spacecraft command detection system - the Viking Heritage command detector and the NASA standard command detector - are summarized. The former prevails in the existing flight projects and the latter will likely be adopted by the missions of the near future. (An in-depth discussion of these command systems is contained in Ref. 9-1). The preparation of Design Control Tables for the control of command link performance between Deep Space Stations and the spacecraft is also discussed.

B. MULTIMISSION COMMAND SYSTEM

The Multimission Command System (Ref. 9-2) extends from the point at which validated commands are entered at the Mission Operations Center (MOC) to the point on the spacecraft where commands, after error detection and correction, are distributed to spacecraft subsystems. Thus the MMC System includes the command functions performed by the MOC, the Deep Space Network (DSN), and spacecraft command detector and command decoder subsystems. The MMC System does not include the project-dependent Mission Sequence System where commands are formulated and validated, nor does it include the spacecraft subsystems which interpret and respond to the commands. The Command System, thus delimited, performs a multimission command delivery and accounting function. A block diagram showing the boundaries of the MMC System is given in Fig. 9-1.

The MMC System employs a store-and-forward method for delivery of command sequences to a spacecraft. The ability to store commands at various points in the command delivery system eliminates time criticality from the transport of commands. Large files of spacecraft commands may be generated by a project, sent by the MOC to the tracking station, and correct receipt at the

Deep Space Station verified before a command is to be "forwarded" to the spacecraft. This allows a project to prepare large files of spacecraft commands in advance and then to forward several files to the Station at the beginning of a spacecraft track.

The same store-and-forward concept is employed between the Station and the spacecraft. Commands may be radiated from the tracking station to the spacecraft, correct receipt at the spacecraft verified, and the commands stored on board the spacecraft for later execution. It should be noted that this store-and-forward mode of operation does not preclude near-real-time commanding of the spacecraft. The MMC store-and-forward operations are represented functionally in Fig. 9-2.

For discussion purposes, the command system may be divided into a ground segment and a spacecraft segment. The functional operations for these two portions are briefly described below.

1. Ground Command System Operations

Command sequences generated by the Projects for the different spacecraft are stored in command files at the MOC. Commands for a particular spacecraft are selected from the MOC command files, formatted into messages, and transmitted, via the Ground Communication Facility (GCF), to a specified tracking station. The command messages contain the commands to be radiated to the spacecraft, timing instructions to the DSS for the radiation of the commands, and error detection/correction coding. The Station verifies correct receipt of the command files or requests retransmission of files containing errors. The spacecraft commands are extracted from the messages by the tracking station Command Processor Assembly (CPA) and stored in the CPA until the time specified for their radiation to the spacecraft. When a command is to be radiated from the Station to the spacecraft it is placed in a queue in the CPA and sent to the Station Command Modulator Assembly (CMA). The CMA modulates the command bits onto a subcarrier, which then modulates the Station transmitter for radiation of the command to the spacecraft.

2. Spacecraft Command System Operations

The spacecraft portion of the Command System consists of two subassemblies: the command detector and the command decoder. Upon receipt of the composite command signal from the spacecraft receiver, the command detector removes the modulated subcarrier, detects the binary command bits, and presents the detected bit stream to the command decoder. The decoder then determines the validity of its input, and, if it is a valid command, decodes it and passes the decoded command to the addressed spacecraft subsystem. The decoder, therefore, depends only on command format and tends to be oriented toward a specific mission. The detector, on the other hand, is dependent on the uplink modulation scheme and tends to be less mission dependent.

C. DEEP SPACE NETWORK COMMAND SYSTEM CAPABILITIES

The capabilities of the Deep Space Network Command System that affect spacecraft designs are described in this section. More detailed information is contained in Refs. 9-3, 9-4, and 9-5.

The Deep Space Network Command System provides the capability for commanding one spacecraft from each Deep Space Station (DSS). The functions performed by the Network Command System include the following:

(1) Establishing the Deep Space Network configuration for the specified spacecraft.

(2) Receiving the command data from the MOC and storing it at the Station.

(3) Queuing command data to be radiated to the spacecraft.

(4) Radiating the command data to the spacecraft.

(5) Monitoring and reporting Deep Space Network Command System status and events.

A detailed diagram of the Command System (Mark III-80) is presented in Fig. 9-3.

The Command System at each Deep Space Station consists of a Command Processor Assembly (CPA) for software functions, a Command Modulator Assembly (CMA) for generating the command waveform, and the exciters, transmitters, and antennas for RF carrier modulation and transmission. (Note the redundancy of these units at each tracking station as shown in Fig. 9-3). The Command System produces a Pulse Code Modulation (PCM) nonreturn-to-zero (NRZ) data waveform. This waveform is used to bi-phase modulate a subcarrier in the phase-shift-keyed (PSK) mode or to switch between two subcarriers in the frequency-shift-keyed (FSK) mode. Data rates are variable from 1 bit per second to 128 bits per second. An upgrade to 2000 bps is planned (Ref. 9-6). PSK data rates can be either noncoherent or coherent with the subcarrier frequency. PSK and FSK subcarrier frequencies may be selected in the range of 100 Hz to 16 kHz, with a resolution of 0.1 Hz. PSK subcarriers may be either sinewave or squarewave. For FSK modulation, only sinewave subcarriers are available. The RF carrier may be modulated at modulation index angles from 0.1 to 1.5 radians peak, for both sinewave and squarewave subcarriers.

Command carrier power suppression and data power suppression as functions of modulation index angle are:

(1) Sinewave subcarrier:

$$\frac{P_C}{P_T}\,(\text{dB}) = 10 \log \left[J_0^{\,2}\,(\theta_D)\right] \tag{9-1}$$

$$\frac{P_D}{P_T}\,(\text{dB}) = 10 \log \left[2J_1^{\,2}(\theta_D)\right] \text{ (upper and lower sidebands)} \tag{9-2}$$

(2) Squarewave subcarrier:

$$\frac{P_C}{P_T}\,(\text{dB}) = 10 \log \left[\cos^2(\theta_D)\right] \tag{9-3}$$

$$\frac{P_D}{P_T}\ (\text{dB}) = 10 \log [\sin^2(\theta_D)] \quad \text{(all sidebands)} \qquad (9\text{-}4)$$

where

θ_D = command data modulation index in radians, peak

P_T = total power

P_C = carrier power

P_D = data power

J_0 = zero-order Bessel function

J_1 = first-order Bessel function

The nominal total radio frequency power output available for single-channel command modulation is 20 kW at the output of the transmitter. At the 64-meter antenna stations (Deep Space Stations 14, 43, and 63), an additional transmitter is available for emergency operation having a nominal carrier output power of 100 kW. Figure 9-4 shows Network command bit rate capabilities as a function of earth to spacecraft range, together with the bit rate requirements and capabilities of past and current spacecraft command detectors. More complete definitions of existing and planned Network command capabilities are contained in Refs. 9-5 and 9-6.

D. SPACECRAFT COMMAND SYSTEM CAPABILITIES AND PERFORMANCE

The capabilities and performance of the spacecraft command system are, in general, characterized by the choice of the command detector configuration and the link design. The following specifications are important factors for the hardware design of the command detector:

(1) Maximum bit rate.

(2) Minimum preamble to acquire command bit synchronization.

(3) Requirement for external data ambiguity resolution.

(4) Modulation characteristics.

(5) Subcarrier characteristics.

(6) Data transition dependency.

The performance of the command link is specified by the following parameters:

(1) Required per bit energy to noise spectral density ratio (ST_B/N_0) to achieve a given bit error rate (BER).

(2) Required duration (bit-times) to achieve bit synchronization, with an associated false acquisition probability at a given ST_B/N_0.

(3) Error statistics for in-lock and out-of-lock indications.

Past spacecraft missions have employed the following types of command detectors: a single-channel analog command detector, a two-channel PSK command detector, and a single-channel digital command detector (Viking Heritage). A new single-channel digital command detector (NASA standard) has been developed and will probably be used on new missions of the near future. Table 9-1 shows the general capabilities and performance of these four command detectors. Their usage in terms of past and expected future missions is also indicated. At present, only the two digital command detectors are in use. The operation of these two command detectors is summarized below.

1. Viking Heritage Command Detector Operation

The Viking Heritage command detector was originally developed for the Viking Mission, and was later adopted by the Voyager and Galileo Projects. The block diagram for the Viking Heritage command detector is presented in Fig. 9-5. It accepts a 512-Hz squarewave subcarrier modulated by the command data bits from the RF receiver output. The bit rate is defined by selecting the number of subcarrier cycles per bit (denoted by "M," where M is constrained to be an even integer). Command data bit rates in the range of 1 through 256 bps may be selected (hard wired prior to launch). These rates result from the use of the 512-Hz squarewave subcarrier and the requirement to have at least two subcarrier cycles per bit.

The Viking Heritage command detector first establishes two levels of synchronization, i.e., subcarrier synchronization and bit synchronization. To accomplish this synchronization, transmitted commands are prefixed by a length of unmodulated subcarrier, and then by a length of subcarrier modulated by the bit synchronization signal. The Viking Heritage command detector first establishes subcarrier synchronization by comparing the received unmodulated subcarrier with a local reference subcarrier signal. Then a local replica of the bit-sync modulated subcarrier is used as a reference to establish bit synchronization. After establishing these references the system can detect data. The functions of synchronization and data detection are performed by cross-correlation of the input signal with the appropriate local reference signal. The system requires a lock detector to ensure that the proper input signal is present. The inlock condition is determined by comparing the sum of the absolute values of five consecutive bits against a preset stored threshold value. A unique design feature of this system is the use of discrete step phase-tracking to compensate for small frequency offsets from Doppler shifts and/or oscillator instabilities. This phase-tracking is performed by accumulating a sum of samples taken near the transitions of the signal for an interval of one data bit period. The polarity of the sum determines the direction of the adjustment made to the demodulation reference.

As described above, the Viking Heritage command detector must detect and acquire both subcarrier and bit synchronization references in sequence before detecting data. To accomplish this synchronization in sequence, commands

transmitted from the Deep Space Stations are prefixed by a short burst of unmodulated subcarrier and followed by a short burst of subcarrier bi-phase modulated by the bit synchronization signal. During the data detection mode the command information bits are bi-phase modulated by the subcarrier and the bit synchronization signal. The composite signal transmitted by the Station for each mode described above can be written as:

$$2\sqrt{P_{tr}}\sin\left[\omega_c t + \theta_D\, Sq(\omega_s t)\right] \quad \text{for subcarrier detection and acquisition modes} \qquad (9\text{-}5)$$

$$2\sqrt{P_{tr}}\sin\left[\omega_c t + \theta_D\, BS \oplus Sq\,(\omega_s t)\right] \quad \text{for bit sync detection and acquisition modes} \qquad (9\text{-}6)$$

and

$$2\sqrt{P_{tr}}\sin\left[\omega_c t + \theta_D\, D(t) \oplus BS \oplus Sq\,(\omega_s t)\right] \quad \text{for data detection mode} \qquad (9\text{-}7)$$

where

ω_c = RF carrier frequency

ω_s = subcarrier frequency

θ_D = data modulation index

$D(t)$ = data bits

BS = bit synchronization squarewave of frequency ω_s/M or $1/T_B$

P_{tr} = transmitted power

$Sq(\omega_s t)$ = squarewave carrier of frequency ω_s.

The ratio of data power, P_D, to total received power, P_T, is determined by the modulation index as

$$\frac{P_D}{P_T} = \sin^2 \theta_D \qquad (9\text{-}8)$$

The ratio of carrier power, P_C, to total power with command modulation is given by

$$\frac{P_C}{P_T} = \cos^2 \theta_D \qquad (9\text{-}9)$$

where

θ_D, P_D, P_C, and P_T have been defined in Section C.

2. NASA Standard Command Detector Operation

The NASA standard command detector was developed as an integral part of the NASA standard transponder. It was designed to be in compliance with the NASA Planetary Program Flight/Ground Data System Standards (Ref. 9-7). The unit is operable in two modes - the NRZ mode without a subcarrier for Tracking Data Relay Satellite (TDRS) applications and the PSK mode with a 16-kHz sinewave subcarrier for near-earth and deep-space applications. This section is concerned only with the PSK mode. A total of nine command data bit rates are in-flight selectable. The allowable bit rates are specified as $2000/2^N$ bps, where N = 0, 1, 2, ..., 8.

Unlike the Viking Heritage system, the NASA standard command detector establishes subcarrier synchronization and bit synchronization simultaneously, eliminating the cumbersome multimode acquisition process required by the Viking Heritage system. For the NASA standard command detector, detections of subcarrier, bit synchronization, and data are performed simultaneously with a single correlation process. The subcarrier and bit synchronization phases are coherently related and are controlled by a quadrature subcarrier tracking loop and a data-transition bit synchronization loop, respectively.

A disadvantage of this subcarrier demodulation scheme is that the subcarrier reference has two stable lock points. As a result, the polarity of the detected data bits may be in-phase or 180° out of phase. This ambiguity of data polarity must be resolved in the decoding process. The decoding function is usually performed outside the command detector domain in a separate command decoder.

Functionally, the NASA standard command detector consists of a coherent automatic gain control (AGC) unit, a sample-and-hold (SH) circuit, an analog-to-digital converter (ADC), a second-order data-aided subcarrier tracking loop, a data transition bit synchronization loop, and a lock detector. Structurally, it consists of the signal conditioning assemblies (i.e., AGC, SH, and ADC), a read-only memory (ROM), a random-access memory (RAM) and a digital processing assembly employing a custom-LSI approach. Figure 9-6 illustrates the functional architecture of this command detector. A block diagram for the NASA standard command detector is shown in Fig. 9-7.

a. NASA Standard Command Detector Subcarrier Tracking. The NASA standard command detector utilizes a coherent sampling scheme to implement a second-order suppressed subcarrier data-aided tracking loop. The subcarrier tracking loop utilizes a perfect integrator and a quasi-continuously variable phase correction (resolution 1/64 of one subcarrier cycle). The maximum subcarrier phase correction step is 45 degrees. The entire tracking algorithm is stored in ROM, with ROM-resident loop coefficients selec d for the acquisition and the tracking phases so as to meet the acquisition time requirements and minimize steady-state phase jitter.

b. NASA Standard Command Detector Bit Synchronization Tracking. For bit synchronization tracking and data detection, the sampled values of the data channel are accumulated over a one-bit interval. The bit synchronization phase error is obtained by integration over a bit period centered on the expected data transition point. This process is called the "mid-phase accumulation," as distinguished from the "in-phase accumulation" performed for data detection.

c. NASA Standard Command Detector Lock Detector. The lock detector portion of the NASA standard command detector determines whether or not a command signal is present, and provides this decision to the command decoder. The lock detection algorithm and threshold coefficients are ROM-resident, providing complete flexibility in tailoring the detector to meet mission-specific acquisition and deacquisition performance requirements.

d. NASA Standard Command Detector Command Prefix. The NASA standard command detector does not require a fixed transmission procedure to acquire lock. However, to ensure that no valid command data bits are lost before in-lock indication is declared, a sequence of alternate 1's and 0's is transmitted prior to the command data bit stream to assist rapid acquisition of bit synchronization. A 132-bit preamble is required to meet the specified lock acquisition performance.

e. NASA Standard Command Detector Power Allocation. Since the NASA standard command detector assumes a sinewave subcarrier, the ratios of data power and carrier power to the total received power as a function of the modulation index are

$$\frac{P_C}{P_T} = J_0^2(\theta_D) \tag{9-10}$$

and

$$\frac{P_D}{P_T} = 2J_1^2(\theta_D) \tag{9-11}$$

where

θ_D, P_D, P_C, P_T, J_0 and J_1 have been previously defined in Section C.

3. Command Decoding

The functions of the spacecraft command detector are limited to demodulation and detection of the composite command signal. The contents of

the command sequence are transparent to the command detector. In order to process the command sequence and deliver the individual commands to the users, the detected command bit stream must be decoded and distributed. These functions are the responsibility of the spacecraft command decoder.

The proper decoding of the command sequence requires a complete understanding of the command structure, word format, and contents. These elements are mission dependent. Though the command decoding process is an important discipline of spacecraft system design, it is beyond the scope and purposes of this discussion. The only detector-related decoding problem is the data ambiguity inherent in the NASA standard command detector.

Since the NASA standard command detector may deliver either normal or inverted data bits, depending upon the axis at which the subcarrier is locked, care must be exercised to assure that the right commands are executed. (Note that the Viking Heritage command detector does not have this data ambiguity problem.) For an elaborate command decoding system utilizing a sophisticated computer, the data ambiguity may be simultaneously resolved when command frame synchronization is decoded. However, with a decoder of less sophistication, a real-time ambiguity resolver may be implemented.

To resolve the data ambiguity on a real-time basis, a sync word must precede the command bit stream but follow the alternate 1 and 0 preamble. Careful selection of the sync word will minimize the probability of error at a given length of the sync word. When the detector indicates an in-lock condition, the ambiguity resolver will first search for this sync word and then determine whether it is in its normal or inverted position. The subsequent command bits will then be accepted in the polarity as indicated by the sync word polarity decision. A seven-bit Barker code has been employed for such a sync word for near-earth application.

E. COMMAND CHANNEL DESIGN CONTROL

As a major function of the spacecraft telecommunications system, the command channel is subject to the provisions of the telecommunications design control policy (Ref. 9-8). This section identifies the parameters relating to

the command function and presents an example of the command channel design control table.

1. Carrier Channel

This paragraph presents the definitions of the parameters which affect the performance of spacecraft receiver carrier tracking.

a. Total Transmitting Power at Antenna. This parameter is the total power into a Station antenna. The nominal ground transmitted power is 20 kW. However, 100 kW (and possibly 400 kW) transmitted power may be used for emergency and other occasions.

b. Transmitting (Ground) Antenna Gain. This is the peak gain of a Station antenna including pointing and circuit losses, and wind and gravity deformation losses. Two antenna nets are normally in use: 34-m and 64-m antennas.

c. Space Loss. This is the loss due to the transmission medium. In a normal mission, space loss is a function of carrier frequency and spacecraft-Earth range. The absorption loss due to atmospheric and plasma effects represents additional losses and should also be taken into consideration.

d. Polarization Loss. This is the loss due to mismatch in polarization between the ground and the spacecraft antennas. A measure of ellipticity is used to determine the polarization loss.

e. Receiving (Spacecraft) Antenna Gain. This parameter represents the gain of the spacecraft antenna in the direction of the incoming signal. Traditionally, the value of this parameter is derived by factoring the expected loss due to antenna pointing error into the boresight antenna gain.

f. Spacecraft Circuit Loss. This is the loss due to transmission cables or waveguides from the spacecraft antenna terminal to the receiver input port.

g. Total Receiver Power (P_T). This is the realizable power at the receiver input port.

h. System Noise Spectral Density (N_0). This is Gaussian white noise power per unit frequency introduced by the environment, cabling, switches, antenna and receiver. This parameter is proportional to the spacecraft circuit loss and the effective system noise temperature. The latter is a function of the receiver noise figure, circuit loss, cable physical temperature and antenna noise temperature.

i. Total Receiver Power to Noise Spectral Density Ratio (P_T/N_0). This is the ratio of total received power to noise spectral density at the input of the detector.

j. Carrier Power to Total Received Power Ratio (P_C/P_T). This parameter reflects the allocation of power to the carrier as a fraction of the total power. It is determined by the modulation indices for the command signal and ranging signal (if present).

k. Carrier Threshold Tracking Bandwidth ($2B_{LO}$). This is the two-sided noise bandwidth of the receiver carrier tracking loop at threshold P_T/N_0.

l. Signal-to-Noise Ratio in $2B_{LO}$. This is the signal-to-noise power ratio into the spacecraft carrier tracking phase-locked loop for a two-sided receiver noise bandwidth of $2B_{LO}$.

m. Threshold Signal-to-Noise Ratio in $2B_{LO}$. This is the minimum value of the signal-to-noise power ratio in $2B_{LO}$ acceptable for the required accuracy of carrier tracking.

2. Command Channel

This paragraph presents the definitions of the parameters relevant to command detection.

a. Bit Rate. This parameter refers to the number of command bits transmitted over a period of one second.

b. Command Data Power to Total Received Power Ratio (P_D/P_T). This power ratio reflects the allocation of power to the command channel as a fraction of the total power. It is determined by the modulation index for the command signal. The power available to the command detector can be readily computed from this allocation.

c. Command Detector Losses. This is the aggregate loss within the command detector. Factors contributing to the command detector losses include radio loss, waveform distortion loss, subcarrier demodulation loss, bit sync detection loss, and circuit loss.

d. Command Detector Per Bit Energy to Noise Spectral Density Ratio (ST_B/N_0). This ratio reflects the net energy over one bit period at the output of the command detector to the noise spectral density.

e. Threshold ST_B/N_0. This is the minimum acceptable value of the ST_B/N_0 to achieve a given bit error rate.

f. Performance Margin. This is the amount of command power in excess of the minimum acceptable value required to achieve the specified bit error rate as defined in E.2.e.

3. Command Function Design Control Table

Table 9-2 is a typical Design Control Table for the uplink command function. It consists of two parts - the carrier channel and the command channel. The signal-to-noise ratio in relation to the bandwidth for both channels must exceed their respective thresholds for the command link to be established.

REFERENCES

9-1. Burow, N. A., and Tam, M. K., "Command Systems," in Deep Space Telecommunications Systems Engineering, edited by J. H. Yuen, Jet Propulsion Laboratory, Pasadena, Calif., July 1982.

9-2. "Multimission Command System Requirements for the 1977-1987 Era," Document 633-2, Jet Propulsion Laboratory, Pasadena, Calif., June 3, 1977 (an internal document).

9-3. Thorman, H. C., "DSN Command System Mark III-80," TDA Progress Report 42-57, Jet Propulsion Laboratory, Pasadena, Calif., pp. 35-42, June 15, 1980.

9-4. Thorman, H. C., "DSN Command System," TDA Progress Report 42-64, Jet Propulsion Laboratory, Pasadena, Calif., pp. 53-60, Aug. 15, 1981.

9-5. "Deep Space Network/Flight Project Interface Design Book," Document 810-5, Rev. D, Vol. I, Jet Propulsion Laboratory, Pasadena, Calif., Section CMD-10, Rev. A, "DSN Command System" Jan. 1, 1981 (an internal document).

9-6. "Deep Space Network/Flight Project Interface Design Book," Document 810-5, Rev. D, Vol. II, Jet Propulsion Laboratory, Pasadena, Calif., Section CMD-10 PC, "DSN Command System," Sep. 1, 1981 (an internal document).

9-7. "NASA Planetary Program Flight/Ground Data System Standards," NASA Document (unnumbered), Rev. 5, National Aeronautics and Space Administration, Washington, D. C., Section 3, "Command Standard," June 1, 1977.

9-8. "Policy for the Design of Deep Space Telecommunications Systems," Document 601-12, Jet Propulsion Laboratory, Pasadena, Calif., Sep. 1975 (an internal document).

Table 9-1. Capabilities and performance summary of four spacecraft command detectors

Parameter	2-channel PN detector	Single-channel analog detector	Single-channel digital detector (Viking Heritage)	Single-channel digital detector (NASA-standard)
Modulation format	PSK data PCM sync	PSK	PCM	PCM
Data rate, bps	1	4	Selectable up to 256	Variable in binary steps up to 2,000
Subcarrier waveform, Hz	Sinewave	Sinewave	512 squarewave	16,000 sinewave
Data transition dependency	None	Dependent	None	During acquisition
Multiple data rate capability	None	None	1 to 256 bps	7.8 to 2,000 bps
External ambiguity resolving requirement	None	None	None	Yes
Command ST_B/N_0, dB @ BER = 10^{-5}	11.7 $P_{sync}=2\ P_{data}$	10.9	10.5	10.5
Maximum acquisition time (in bit periods, T_B) @ threshold ST_B/N_0	511	360	90	132
Lock detector probabilities =				
P (in/noise	$<1.5\times10^{-2}$	$<10^{-3}$	$<10^{-5}$	$<10^{-4}$
P (out/signal)	$<1.6\times10^{-3}$	$<2\times10^{-6}$	$<10^{-5}$	$<2.5\times10^{-9}$
Past and expected missions	Mariner Venus '62, Mariner Mars '69 and '71, and Mariner Venus Mercury '73	Helios	Viking Orbiter '75, Voyager, and Galileo	All missions using standard deep space transponder

Table 9-2. Typical command design control table
Part 1. Uplink carrier

	Design	Fav tol	Adv tol	Mean	Variance
Transmitter parameters					
1) RF power, dBm	73.00	.00	.00	73.0	.00
Power output = 20.0 kW					
2) Circuit loss, dB	.00	.00	.00	.0	.00
3) Antenna gain, dBi	60.60	.30	-.70	60.3	.08
Elev angle = 10.00 deg					
4) Pointing loss, dB	-.10	.05	-.05		
Path parameters					
5) Space loss, dB	-267.19			-267.2	.00
Freq. = 2115.00 MHz					
Range = 2.581 + 08 km					
= 1.73 AU					
6) Atmospheric attenuation, dB	-0.02	.00	.00	.0	.00
Receiver parameters					
7) Polarization loss, dB	-.10	.05	.05		
8) Antenna gain, dBi	34.50	.40	-.40	34.4	.03
9) Pointing error, dB	-.06	.03	-.03	-.1	.01
Limit cycle, deg	.20	-.20	.00		
Angular errors, deg	.00	.00	.00		
10) Rec circuit loss, dB	-1.50	.50	-.50	-1.5	.08
11) Noise spec dens, dBm/Hz	-169.26	-.21	.87	-168.9	.03
Operating temp, K	860.00	-40.00	190.00		
Hot body noise, K	.00	.00	.00		
12) Carr thr noise BW, dB-Hz	12.55	-.97	.79	12.5	.13
Total power summary					
13) Rcvd power, p_T, dBm (1+2+3+4+5+6+7+8+9+10)				-101.1	.21
14) Rcvd P_T/N_0, dB-Hz (13-11)				67.9	.24
15) Ranging suppression, dB	.00	.00	.00	.0	.00
16) Command suppression, dB	-3.06	.10	-.10	-3.1	.00
17) Carr pwr/tot pwr, dB, (15+16)				-3.1	.00
18) Rcvd carr pwr, dBm, (13+17)				-104.1	.21
19) Carr SNR in $2B_{LO}$, dB, (18-11-12)				52.3	.37
					3S = 1.8

Table 9-2. Typical command design control table (contd)
Part 2. Command channel

	Design	Fav tol	Adv tol	Mean	Variance
Data channel performance					
20) Data bit rate, dB	14.95	.00	.00	14.9	.00
Bit rate = 31.3 bps					
21) Data pwr/total pwr, dB	-3.35	.10	-.10	-3.3	.00
22) Data pwr to rcvr, dBm (13+15+21)				-104.4	.21
23) S_T/N_0 to rcvr, dB				49.6	.25
24) System losses, dB	-3.00	.50	-.50	-3.0	.04
Radio loss, dB	.00	.00	.00		
Demod, detect loss, dB	.00	.00	.00		
Waveform dist loss, dB	.00	.00	.00		
25) S_T/N_0 output, dB (23+24)				46.6	.29
26) Threshold S_T/N_0, dB	9.60	.00	.00	9.6	.00
Threshold bit error rate	1.00-05				
27) Performance margin, dB (25-26)				37.0	.29
					3S = 1.6

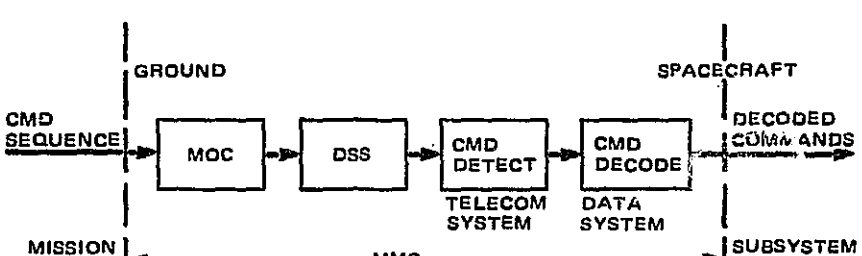

Fig. 9-1. MMC System uplink block diagram

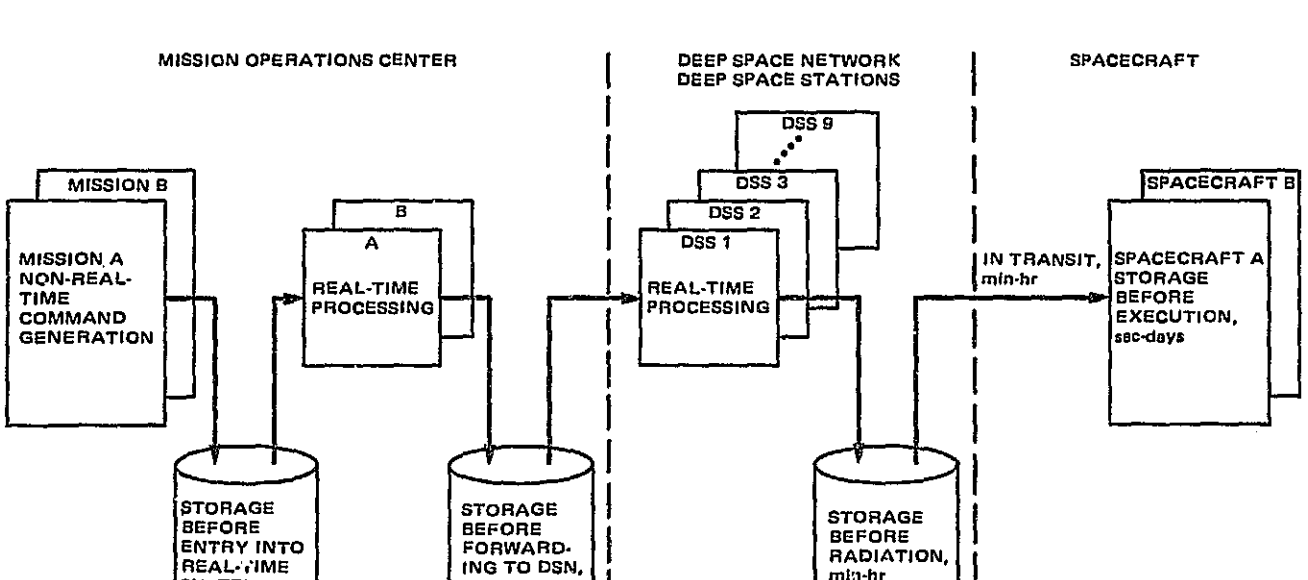

Fig. 9-2. MMC System "store and forward" operations (with typical storage times)

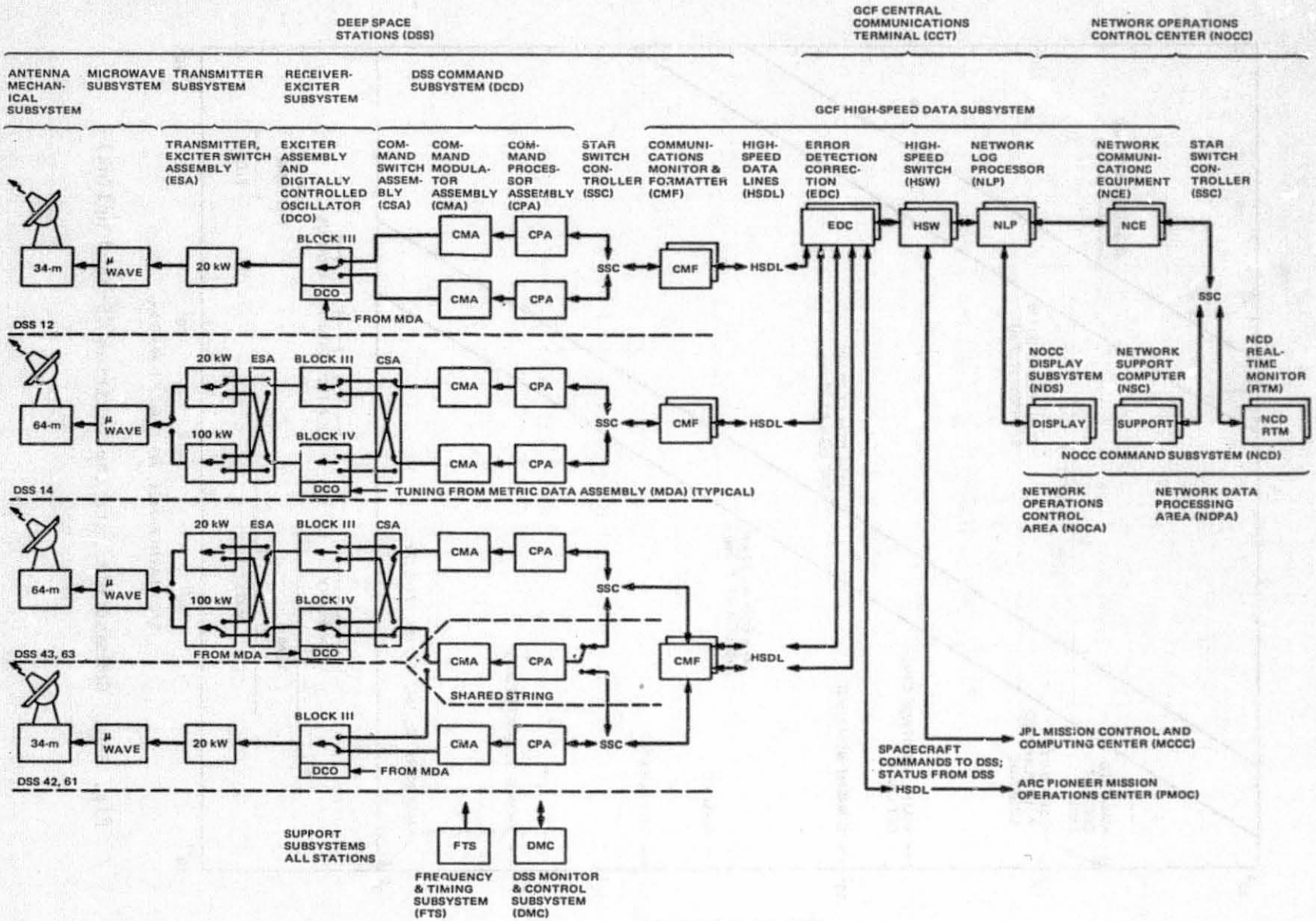

Fig. 9-3. Deep Space Network Command System Mark III-80

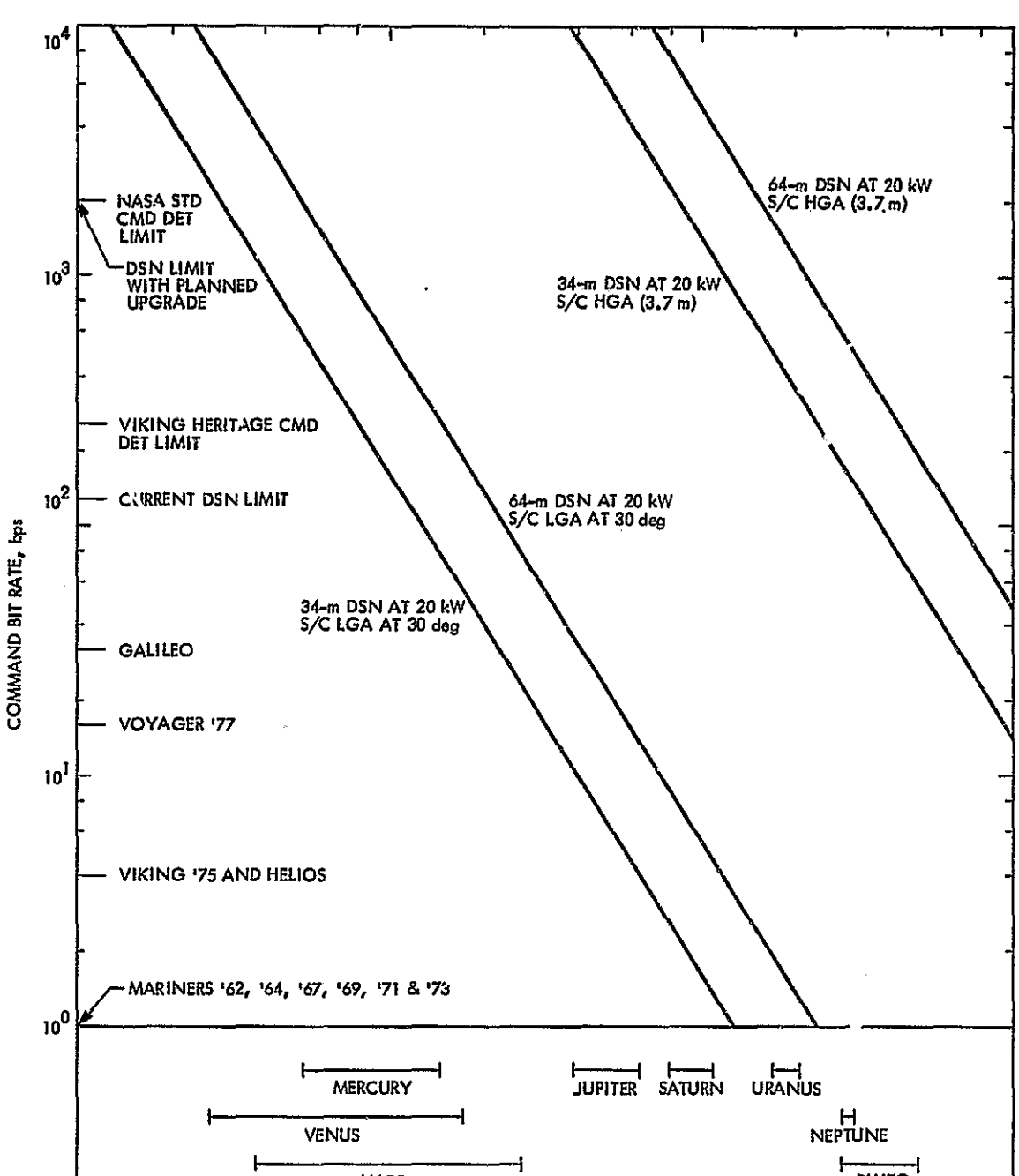

Fig. 9-4. Command bit rate capabilities (S-band uplink)

C-25

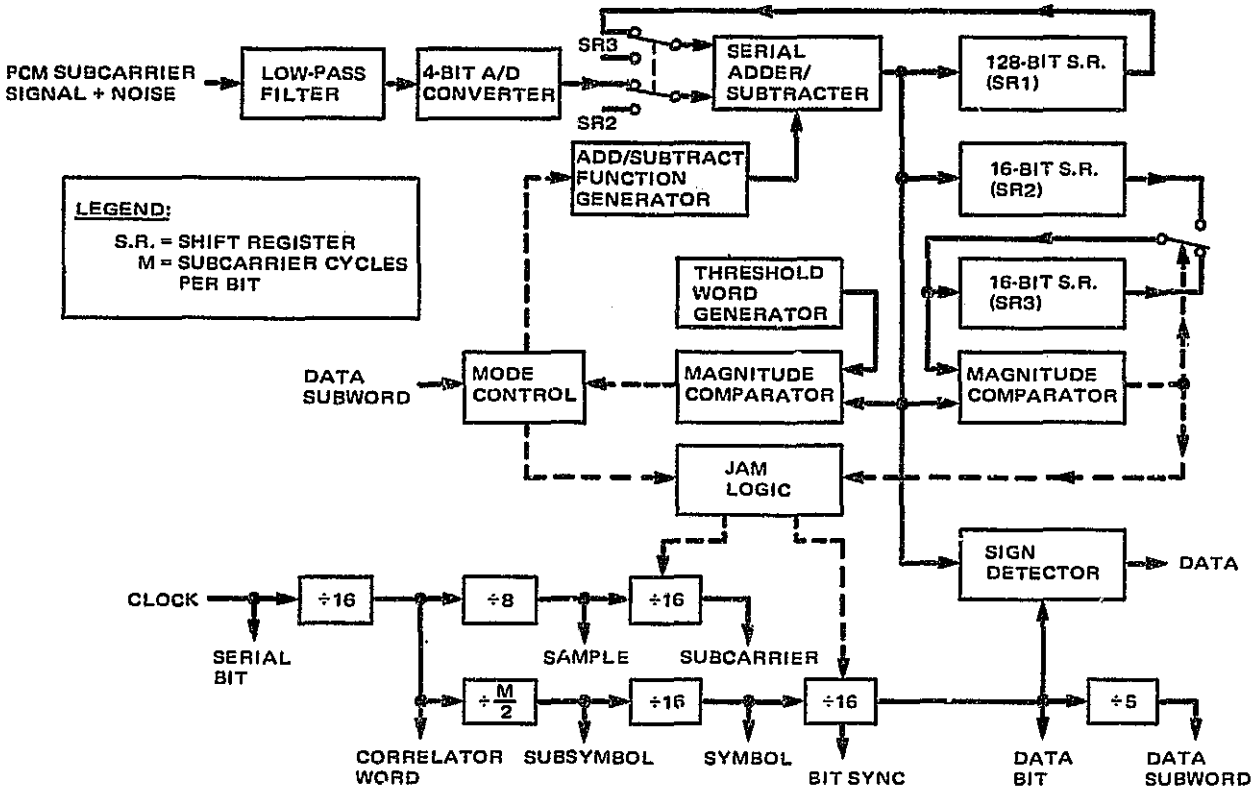

Fig. 9-5. Viking Heritage command detector block diagram

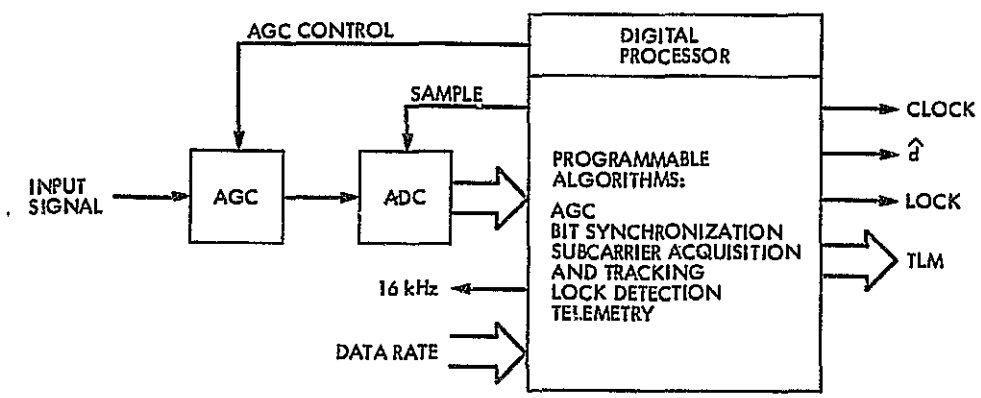

Fig. 9-6. NASA standard command detector functional architecture

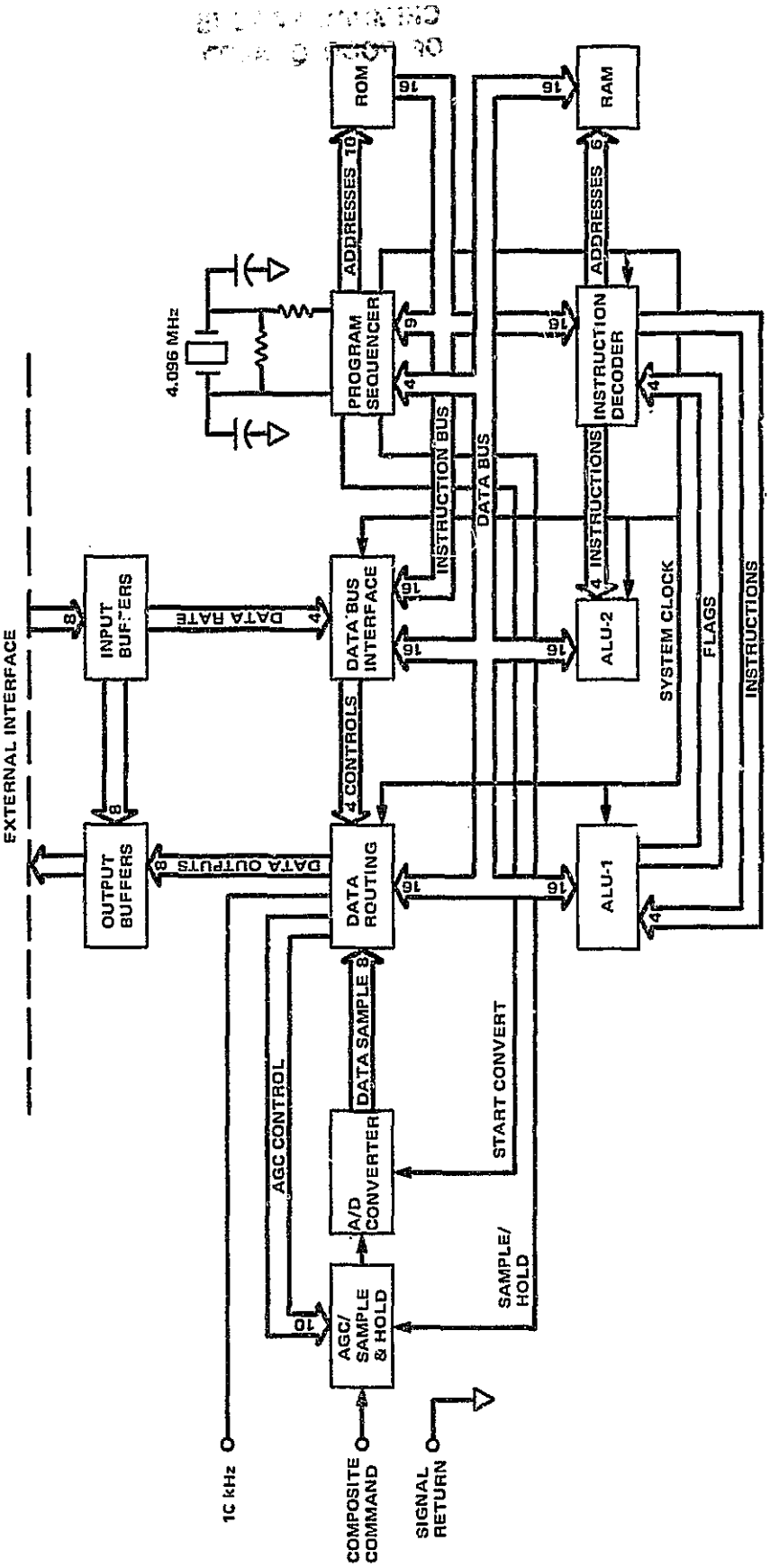

Fig. 9-7. NASA standard command detector block diagram

X. NEW DIRECTIONS: 1982-2000

N. A. Renzetti, J. W. Layland, C. T. Stelzried, and A. L. Berman

A. NETWORK OBJECTIVES

The major objective of the Deep Space Network in the period 1983-2000 is the fulfillment of the extremely diverse telecommunications requirements of the known and anticipated users. Deep space exploration projects will continue to occupy a dominant role, although in the mid-1980s, with the completion of the Networks Consolidation Program, high earth orbiter projects will become substantial users of the Network. Also playing an increasingly important role in the Network of the next decade will be non-flight projects, such as Geodynamics, Radio Astronomy, Radar Astronomy, and the Search for Extraterrestrial Intelligence (SETI).

The major challenge in meeting the primary Network objective of the next decade will be that of providing increased performance as required by users at costs which can be borne by NASA in an environment of limited resources. Emphasis will be on increased commonality, flexibility, and automation to reduce maintenance and operations costs, and lower mission costs.

More specific goals during the next decade to meet the overall Network objectives are:

(1) Addition of new wider bandwidth and effective aperture capabilities to accommodate higher bit rates and increasing spacecraft range.

(2) Development of new techniques and equipment to enable high precision deep space and orbital spacecraft navigation.

(3) Improvement in frequency and timing to support more sophisticated radio science experiments.

(4) Implementation of state-of-the-art frequency, bandwidth, aperture, and timing to augment the Network role in support of non-flight projects.

(5) Development of the use of K-band and optical, to meet increased link performance and reduce spectrum crowding.

(6) Development of long-lead-time advanced technology for Network requirements anticipated for future projects, which will only be designed to (then) existing and proven technology.

B. NEW REQUIREMENTS

New directions for the Network are determined by new requirements which are generated by existing and approved projects, and by the anticipated requirements of future planned projects. Figure 10-1 presents the Approved Program mission set, while Fig. 10-2 presents the Advanced Planning mission set, which is subject to change as preproject planning evolves.

The Voyager 2 1986 Uranus and 1989 Neptune encounters are examples of new requirements being generated by existing missions. These two encounters were not firmly planned and approved until well into the Voyager mission, and because of the tremendous spacecraft-earth distance, will require enhanced communications link performance beyond the capability of the present Network. This new link performance requirement will be met via the technique of arraying multiple antennas, both Network and non-Network. Arraying technology has been under development by the Network for a number of years, and will be described in greater detail in the following subsection.

A second example of new requirements being generated by existing projects is Pioneer 10, which will be at communications threshold at the beginning of 1990. Science interest in Pioneer 10 is high since it is the only spacecraft which will exit the solar system through the tail region of the heliosphere. Figure 10-3 illustrates the Pioneer 10 link conditions over the next 10

years. At the current time, it is expected that a Pioneer 10 telecommunications requirement beyond 1990 will be met either through the upgrading of the Network 64-m antennas, or via antenna arraying techniques.

The Galileo spacecraft, a Jupiter orbiter with a planned May 1986 launch, will be the first deep space probe to carry X-band uplink capability. This implementation of an operational X-band uplink capability represents a most significant benchmark in the NASA Planetary Program, as there are a number of X-band telecommunications drivers which will act synergistically to move the Planetary Program in the direction of routine X-band uplink and downlink telecommunications links. Foremost in the long-term view, the S-band frequency spectrum allocation among all categories of users is and will continue to become increasingly crowded and impinged upon by a myriad of interfering sources. Hence, the move of Planetary Program telecommunications to the far less crowded X-band frequency allocation will greatly relieve the congestion being experienced in the S-band frequency allocation. In addition, there are very substantial technical enhancements to be reaped by the move to both uplink and downlink X-band telecommunications, including improvements in uplink performance and reductions in solar plasma and ionospheric phase scintillation, which will improve near-sun commanding and telemetry and radio science experiments, and enable the exciting search for the existence of gravitational waves. S-band downlink would, in the above scenario, most likely be retained for occasional use because of its great value in providing (with X-band) dual-frequency charged particle calibrations to Radio Science and Navigation.

For X-band uplink[1], assuming equal Network and spacecraft antenna efficiencies and sizes, the improved uplink performance is given by the square of the frequency ratio $(7.2/2.1)^2$, or about 10.7 dB. This allows uplink communications with the spacecraft at smaller sun-earth-probe angles, at lower power levels, and to far greater spacecraft-earth distances, all other things being equal.

[1] X-band uplink is presently implemented on the Goldstone Station 13 research antenna and is planned for the Network 34-m operational antennas in 1987.

Phase scintillation on the uplink is also reduced by the ratio of the frequencies squared, or by a factor of approximately 13. This will greatly enhance certain radio science experiments, where solar plasma and ionospheric phase scintillation become a limiting error source. Foremost in this class of experiments is the search for gravitational waves, which requires a total system frequency stability better than $(W\ f/f)\ Z\ 1 \times 10^{-15}$. Currently S-band phase scintillation on the uplink is the measurement sensitivity limiting source, and the move to X-band uplink will improve the sensitivity of the gravitational wave search by a straightforward factor of about 13.

Finally, the reduction of phase scintillation on the uplink improves both telemetry reception and navigational data quality, as in the current S-band uplink/X-band downlink spacecraft telecommunications systems, the relatively large S-band phase scintillation is multiplied by the ratio of X-band to S-band (8.4/2.1) frequencies in the two-way link.

The Venus Radar Mapper (VRM), Mars Geoscience Climatology Orbiter (MGCO) and Mariner Mark II (Refs. 10-1, 2) missions all plan to capitalize on the X-band uplink implementation. The VRM and MGCO missions plan precision gravity mapping of Venus and Mars respectively; the X-band uplink will greatly enhance these radio metric data measurements. Some of the planned Mariner Mark II missions will utilize the X-band uplink in combination with X-band downlink to simplify the spacecraft design.

According to plans, the Russian Venera spacecraft will deposit balloons in the Venus atmosphere. Precision tracking of balloon L-band transmitters will provide atmospheric wind measurements. The Network plans to participate in this experiment and will add an L-band receive capability on the ground 64-m antennas to enable this. This capability will also be used when the Venera spacecraft continues on to Halley's comet. Precision tracking in the vicinity of Halley's comet combined with Venera comet tracking data will provide increased comet orbital data. This effort, named Pathfinder, will enhance the follow-on comet encounter by the European Space Agency's Giotto Mission.

Plasmas in the near earth regions will be investigated with the OPEN (Origin of Plasmas in the Earth's Neighborhood) missions. The OPEN missions are designed to operate with the planned Mark IVA Network limitations of 250 kb/s[2]. Anticipated approval for higher data rates beyond this limitation to 600 kb/s[3] would allow enhanced scientific results.

Conventional Very Long Baseline Interferometry (VLBI) exploits the longest baselines available on the surface of the earth. Longer baselines, necessary to investigate unresolved radio sources, require a radio telescope in space (Ref. 10-3). Both Tracking Data Relay Stations (TDRS) and a free flying satellite are under consideration for use as an orbiting radio telescope. In these configurations, the orbiting radio telescope and the Network provide the data collection for the extended baseline. It is proposed that the orbiting radio telescope provide the wide band data collection (about 50 Mb/s) to the TDRS White Sands receiving station. Some proposals assume a direct link (about 10 Mb/s) to the Deep Space Network for real-time data performance monitoring.

The Network will be required to handle a wide variety of spacecraft missions under varying conditions, from launch to end of mission. This requires configuration flexibility, high sensitivity, and large dynamic range capability. High reliability, maintainability, and low operational costs are all additional extremely important requirements the Network must meet.

C. FUTURE PLANS

Future plans are based upon achieving the goals and meeting the needs of the next generation of flight projects in as cost-effective and innovative a fashion as possible. This includes the ability to array Network and non-Network antennas to provide enhanced link performance for critical mission phases such as the Voyager Uranus and Neptune encounters.

---

[2] This requires 500 ks/s for R = 1/2 coding

[3] This requires 2.4 Ms/s for the anticipated Manchester modulation and R = 1/2 coding.

The Network will support both U.S. and non-U.S. missions as appropriate. Deep Space Network stations and three 26-meter stations which are now part of the Ground Spaceflight Tracking and Data Network (GSTDN) will be integrated to provide a consolidated network for tracking both deep space probes and high earth orbiters. Figures 10-4 and 10-5 show the planned consolidated Mark IVA Network configurations for 1985 and 1987.

In the MK IVA era the telemetry system of a Network signal processing center comprises four groups of equipment which are selectable for mission and antenna front-end requirements. These four groups are illustrated in the telemetry configurations shown in Figs. 10-6 and 10-7. Telemetry groups 1 and 2 (Table 10-1) with the newly designed baseband assembly (BBA) have the capability to perform real-time baseband arraying with up to six separate antennas simultaneously. Telemetry groups 3 and 4 (Table 10-2) using the symbol synchronizer assembly (SSA) from the MK III era cannot perform baseband arraying. The Maximum Likelihood Convolutional Decoder (MCD) will be modified to extend the indicated 250 kb/s designed limit to include the 300 kb/s required for OPEN missions. The Telemetry Processor Assembly (TPA) limits the overall telemetry system data rate performance to 600 kb/s for record only and 200 kb/s real-time (limited by the local area network).

Figure 10-8 shows the baseline 1989 network and candidate non-NASA antennas for future arraying plans. These areas are discussed further in the following section.

The receiving system figure of merit ($M=G_R/T_{op}$) is a key parameter for defining system sensitivity used in telemetry link performance calculations. The reader may wish to refer to Sections I, II, and III for detailed discussions and for past and present capabilities.

Table 10-3 and Fig. 10-9 show the planned improvement in the Network receiving system figure of merit over the next two decades. This includes upgrading the present (1982) 64-meter antennas which now operate at X-band (8.4 GHz) with about 50% efficiency (M = 72 dB) to 70 meter diameter with about 66% efficiency (M = 74 dB) as shown in Fig. 10-10, and subsequently

increasing the frequency capability to 32 GHz (Ref. 10-4). The ability to array the large antennas together (Ref. 10-5), demonstrated at the Voyager Saturn encounter, will be expanded and made fully and conveniently operational so that combinations of any or all of the X-band antennas can be arrayed as needed for flight project support. The optimum anticipated improvement of the Australian array, consisting of Station 43 (64-m), Station 42 (34-m), Station 45 (34-m), and the Parkes Radio Astronomy Observatory, is about 3.7 dB relative to the Network 64-meter antenna alone.

It is clear from Figs. 10-9 and 10-10 that providing the significantly higher frequency capability to possibly 32 GHz offers the most substantial performance increase available for the foreseeable future. Changing frequencies requires complementary spacecraft work, and will not happen in the near future. The planned upgrade of the 64-meter antennas provides improvements to existing spacecraft telecommunication links, such as with Voyager and Pioneers, as well as future spacecraft using existing technology.

D. VOYAGER: COMMUNICATING TO URANUS AND NEPTUNE

The August 1981 flyby of Voyager 2 past Saturn provided data into the Network at a rate of 44.8 kbps. As analyzed in Section II, this link at peak performance carried a margin of almost 3 dB into a single Deep Space Network 64-meter antenna. The array, consisting of the 64-meter antenna and one 34-meter antenna, was in fact used to provide adequate immunity to weather-induced link degradation, and to extend coverage to lower elevations. Due to the increased distance, the signal level at the Voyager 2 flyby of Uranus in 1986 will be more than 6 dB lower than it was at Saturn, and the signal level at the Neptune encounter will be some 3.5 dB lower still.

The Voyager project has two general requirements for these outer planet encounters: (1) to acquire nearly continuous measurement of the fields and particles surrounding the target planet, and (2) to acquire imaging data which is adequate to develop a basic characterization of the planets, their satellites, and rings. The software of the control computers onboard the Voyager is being changed during the flight to Uranus to include image data compression

to partially compensate for the decreased signal strength. With compression, image data can be acquired at 14.4 or 8.4 kbps, which is comparable to uncompressed data at 29.9 or 19.2 kbps, respectively. Since the data compression requires both onboard computers to be operating, there is some significant risk that the data compression will not be available when needed.

At Uranus, the arrayed 1985 configuration of the Network will support the 14.4-kbps data rate for Voyager into the Goldstone or Canberra Complexes with adequate margin. The Voyager closest approach to Uranus will occur over Australia. Arrangements are in process to array the Parkes Radio Astronomy Observatory with the Canberra Complex for the most important days of the Uranus encounter. This interagency array will support the higher fallback data rate of 29.9 kbps, as well as a 21.6-kbps data rate which will combine the compressed imaging with replay from the tape recorder, thus substantially increasing the number of images which can be returned at encounter.

At Neptune, the signal from Voyager will be some 3.5 dB weaker than at Uranus, and the improvements from data compression which helped to provide the required science return from Uranus may no longer be operative. As noted above, the planned development of the Network to 1989 will make available at each longitude an arrayed configuration of a high-efficiency 70-meter antenna and two 34-meter antennas to meet the basic requirements of the Voyager Neptune encounter. This configuration will support the 8.4 kbps compressed imaging at both Goldstone and Canberra, and will also support an intermediate compressed imaging data rate of 11.2 kbps. It also gives good support of the required general science coverage. Assuming that equitable arrangements can be made to use the Parkes Observatory again for Neptune, the arrayed configuration of the Canberra Complex plus Parkes will be able to support the preferred data rate of 14.4 kbps. The 14.4-kbps data rate can also provide a limited quantity of uncompressed imaging if needed.

Discussions have begun with other large radio observatories of the world to enlist their help in supporting the science objectives of the Voyager at Neptune. These include the NRAO Very Large Array in Soccoro, New Mexico, the 64-meter antenna facility in Japan, and the 100-meter telescope in Bonn, Germany. It is hoped that by 1989 the organizational and technical

arrangements will be in place to support the Voyager with an American array consisting of the Goldstone Complex and the VLA (configured for 2.5 equivalent 64-meter antennas) and an Asian array consisting of the Canberra complex, the Parkes Observatory, and the Japanese 64-meter antenna. These arrays would be capable of supporting the Voyager at either the 19.2-kbps fallback data rate, or the 21.6-kbps combined playback and compressed imaging data rate. The potential European array of the Madrid Complex with the Bonn observatory would be capable of supporting either 8.4 or 11.2 kbps data return from Neptune. Thus with the help of the world's large radio telescopes, a scientific return from the Voyager encounters at Uranus and Neptune which rivals that achieved at Saturn appears to be within our reach.

REFERENCES

10-1. Morrison, D., and Hinners, N., "A Program for Planetary Exploration," Science Vol. 220, May 6, 1983.

10-2. Neugebauer, M., "Mariner Mark II and the Exploration of the Solar System," Science Vol. 219, Feb. 4, 1983.

10-3. Preston, R. A., et al., "The Future of VLBI Observatories in Space," Proceedings of CNES Conference of VLBI Techniques, Toulouse, France, Sep., 1982.

10-4. de Groot, N., "Developments Related to Future Use of the 32-GHz Allocation for Deep Space Research," TDA Progress Report 42-73, Jet Propulsion Laboratory, Pasadena, Calif., May 15, 1983.

10-5. Stelzried, C. T., Berman, A. L., and Noreen, G. K., "Antenna Arraying Performance for Deep Space Telecommunications Systems," TDA Progress Report 42-72, Jet Propulsion Laboratory, Pasadena, Calif., Feb. 15, 1983.

Table 10-1. Telemetry subsystem channel capabilities for Telemetry Groups 1 and 2

Functions	Channel 1	Channel 2
Subcarrier demodulation	Approximately 10 kHz to 2 MHz, square wave	Approximately 10 kHz to 2 MHz, square wave
Baseband combining	Up to six receivers	N/A
Sequential decoding	k=24, 32; r=1/2; frame length: variable; 6 s/s to 10 ks/s	N/A
Maximum likelihood convolutional decoding	k=7; r=1/2 or 1/3; 10 b/s to 250 kb/s	N/A
Block decoding	Reed-Muller 32/6; up to 2 kb/s	N/A
Symbol rate	4 s/s to 500 ks/s	6 s/s to 250 ks/s
Uncoded rate	6 b/s to 250 kb/s	6 b/s to 250 kb/s
Data format	NRZ-L, NRZ-M, BiØ-L on carrier	NRZ-L, NRZ-M, BiØ-L on carrier

Table 10-2. Telemetry subsystem channel capabilities for Telemetry Groups 3 and 4

Functions	Channel 1	Channel 2
Subcarrier demodulation	Approximately 512 kHz to 1 MHz	Approximately 512 kHz to 1 MHz
Baseband combining	N/A	N/A
Sequential decoding	k=24, 32; r=1/2; frame length: variable; 6 s/s to 10 ks/s	N/A
Short constraint length convolutional decoding	k=7; r=1/2 or 1/3; 10 b/s to 125 kb/s	N/A
Block decoding	Reed-Muller 32/6; up to 2 kb/s	N/A
Symbol rate	6 s/s to 250 ks/s	6 s/s to 250 kb/s
Uncoded rate	6 b/s to 32 kb/s	6 b/s to 32 kb/s
Data format	NRZ-L, NRZ-M, BiØ-L on carrier	NRZ-L, NRZ-M, BiØ-L on carrier

Table 10-3. Tabulation of the Deep Space Network predicted downlink performance figure of merit ($M=G_R/T_{op}$) to 1989.

Parameter	Calendar year				
	1985	1986	1989	1989	Post 1990
Frequency f, GHz	8.42	8.42	8.42	8.42	32
System noise temperature[a] T_{op}, K	22	--	20	--	45
Antenna diameter D_R,m	64	--	70	--	70
Antenna gain G_R,dB	72	--	74	--	84
Figure of merit ($M=G_R/T_{op}$),dB	59	63[b]	61	65[c]	67

[a] Assumes "90% weather" (see Section VIII) and 30° elevation angle.

[b] Assumes arrayed Network Australian 64-m antenna, two 34-m antennas, and Australian (Parkes) 64-m antenna.

[c] Assumes arrayed Network Australian 64-m antenna, two 34-m antennas, and Australian (Parkes) and Japanese 64-m antennas.

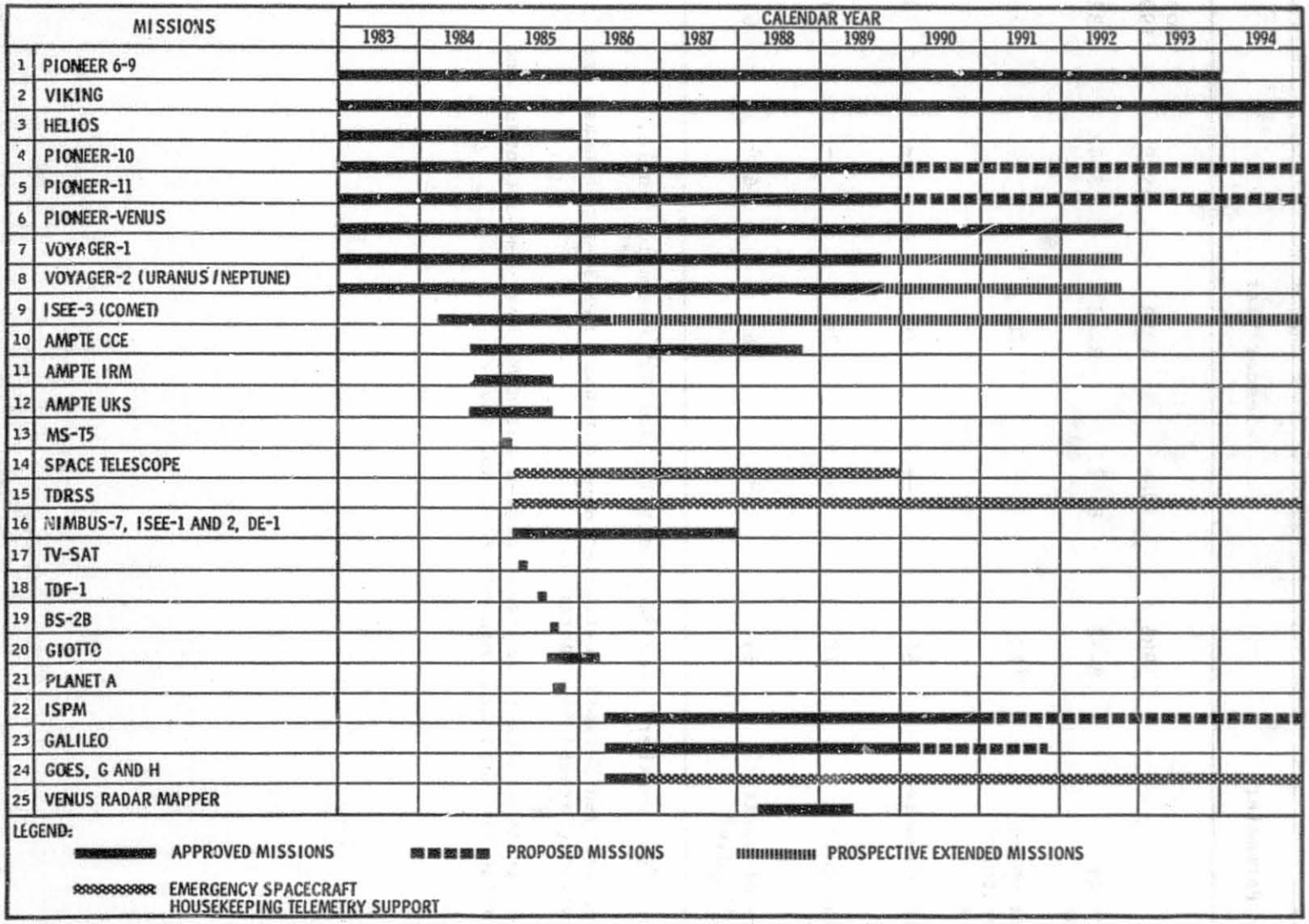

Fig. 10-1. Consolidated network approved program mission set

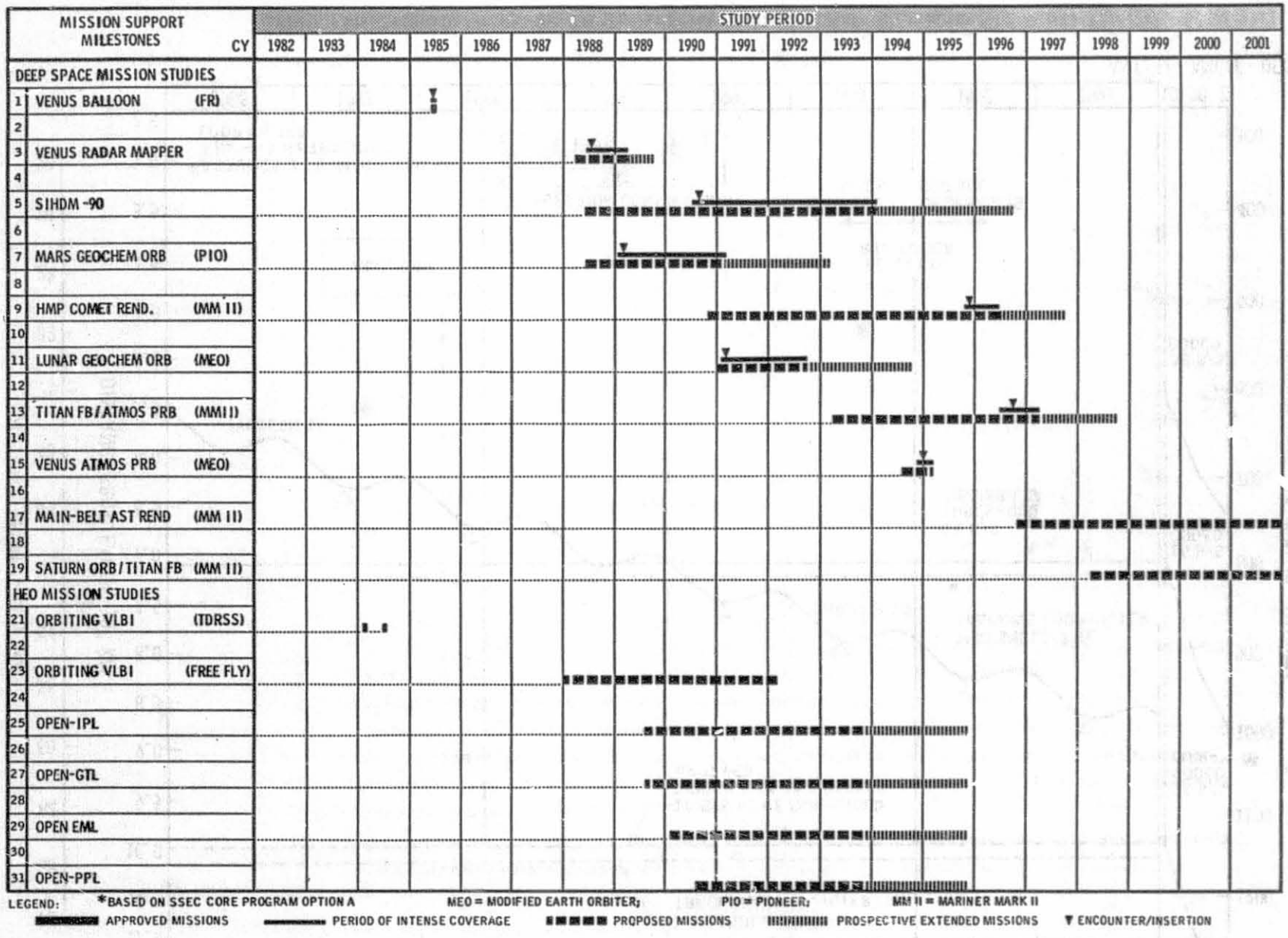

Fig. 10-2. Deep Space Network advanced planning mission set

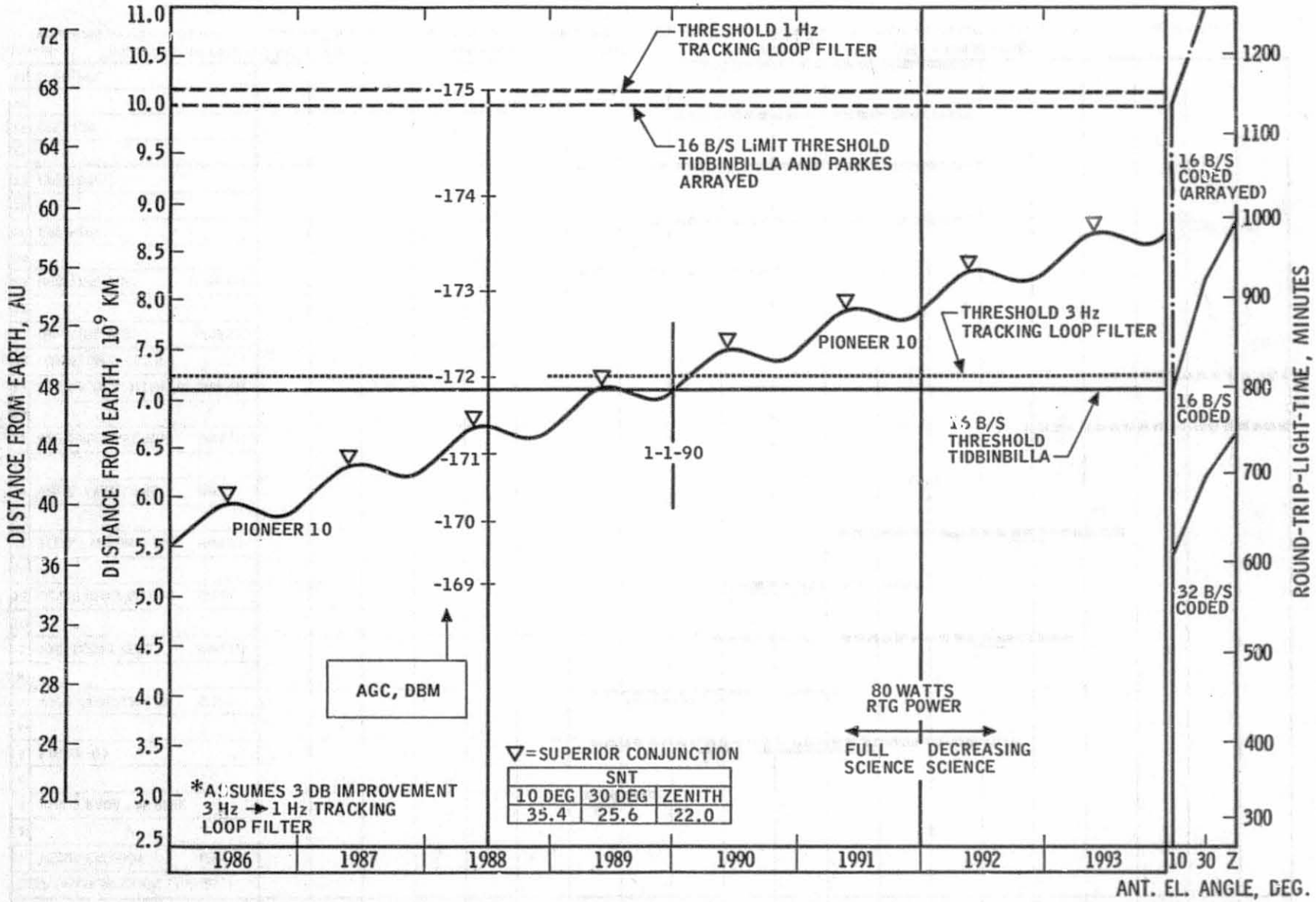

Fig. 10-3. Pioneer 10 future network link performance

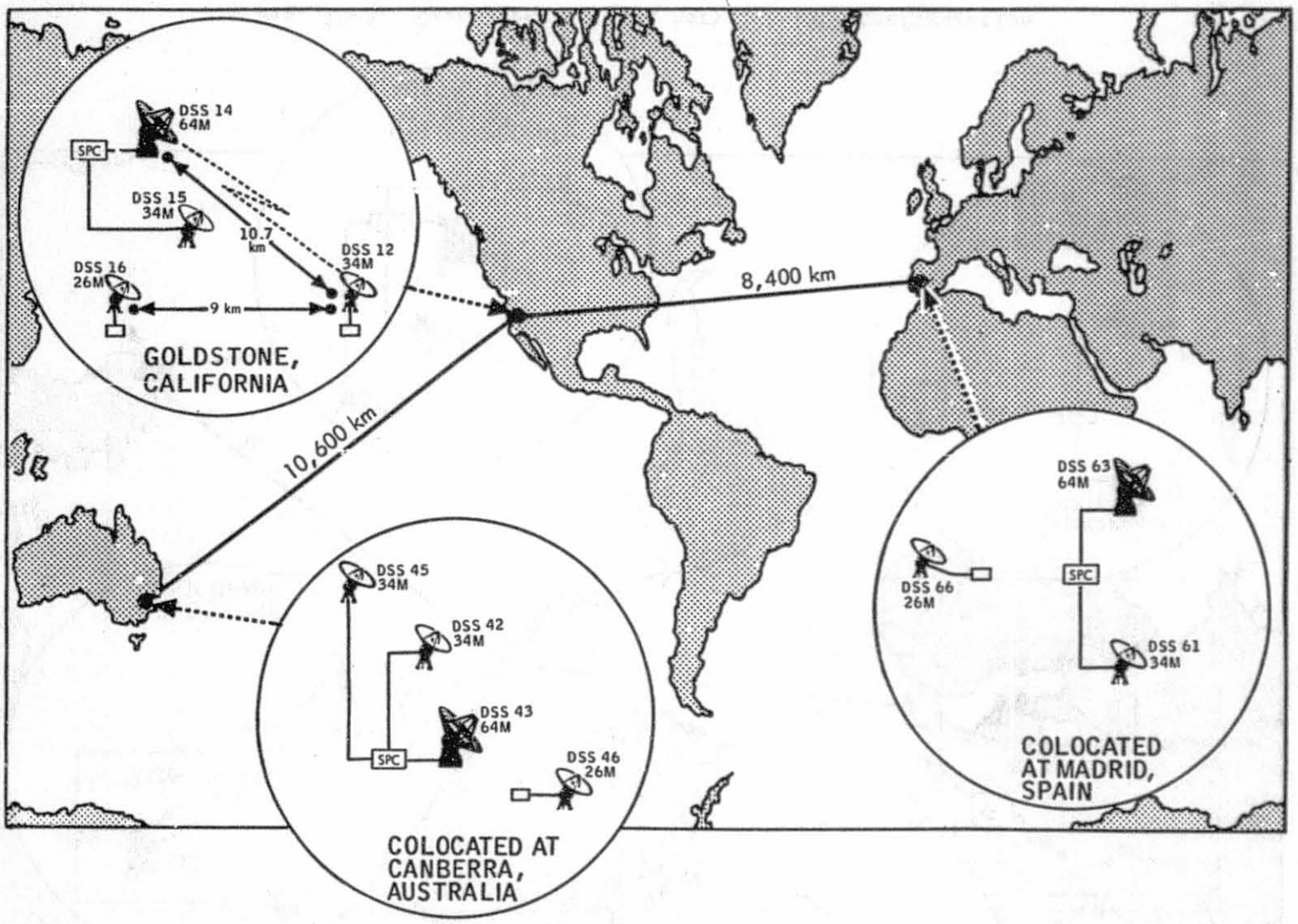

Fig. 10-4. Deep Space Network Mark IVA-1985 configuration

Fig. 10-5. Deep Space Network Mark IVA-1987 configuration

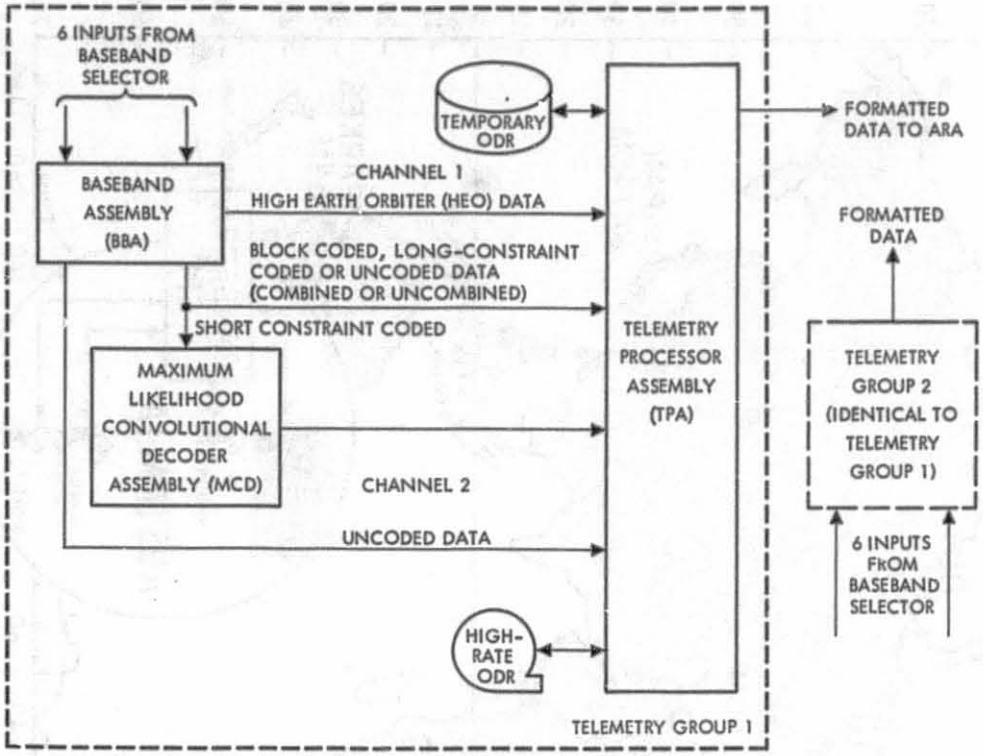

Fig. 10-6. Block diagram of telemetry groups 1 and 2 (post 1984)

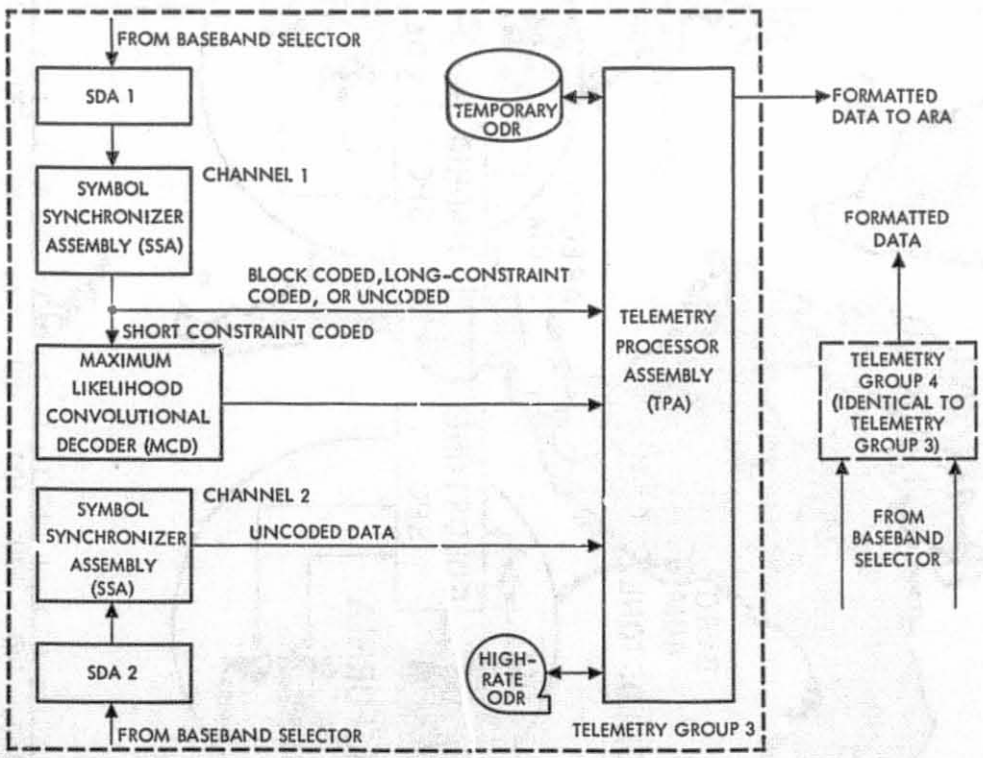

Fig. 10-7. Block diagram of telemetry groups 3 and 4 (post 1984)

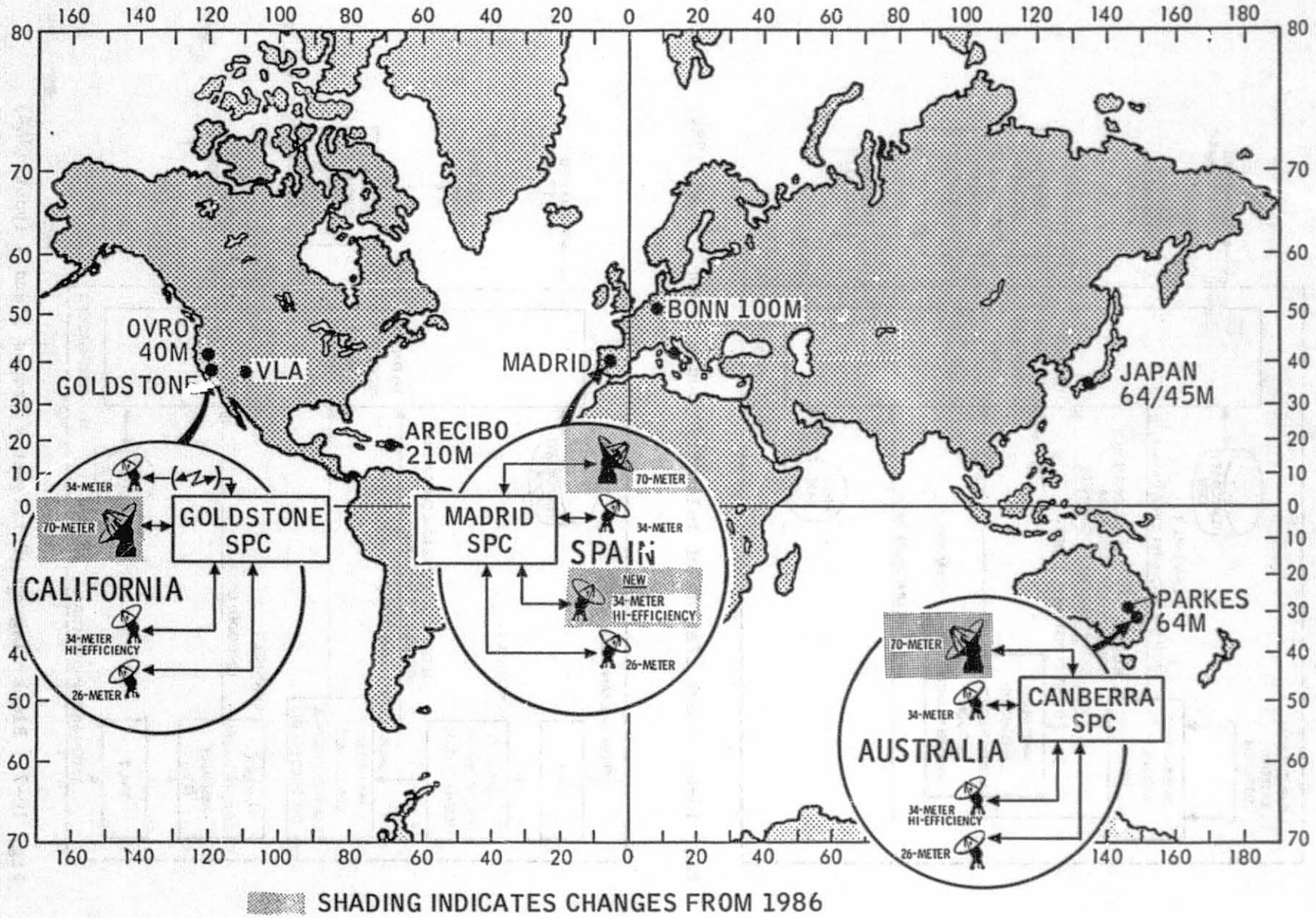

Fig. 10-8. Baseline 1989 network configuration and candidate observatories siting

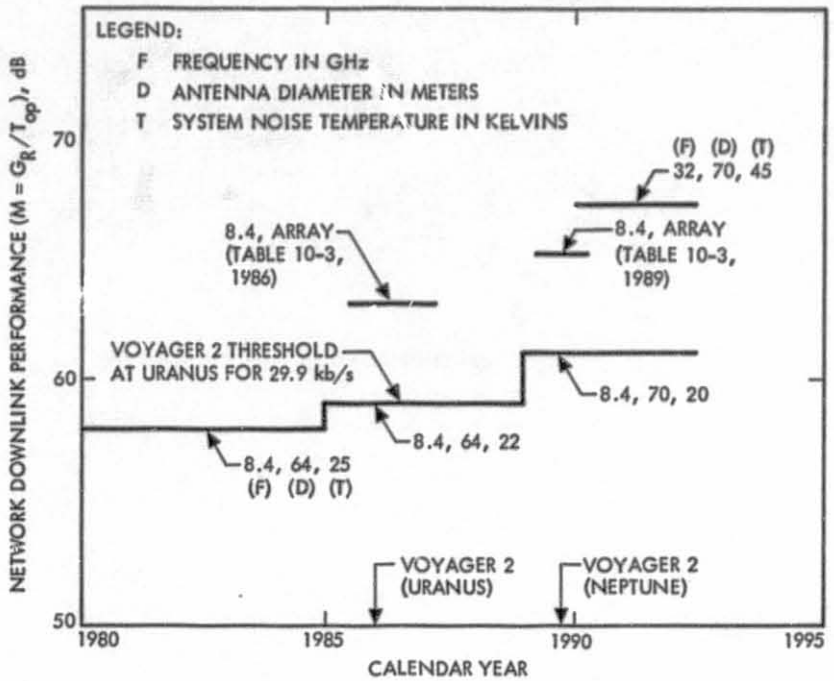

Fig. 10-9. Profile of the Deep Space Network downlink performance ($M=G_R/T_{op}$) from 1982 to 1990 (from Tables 2-1 and 10-3)

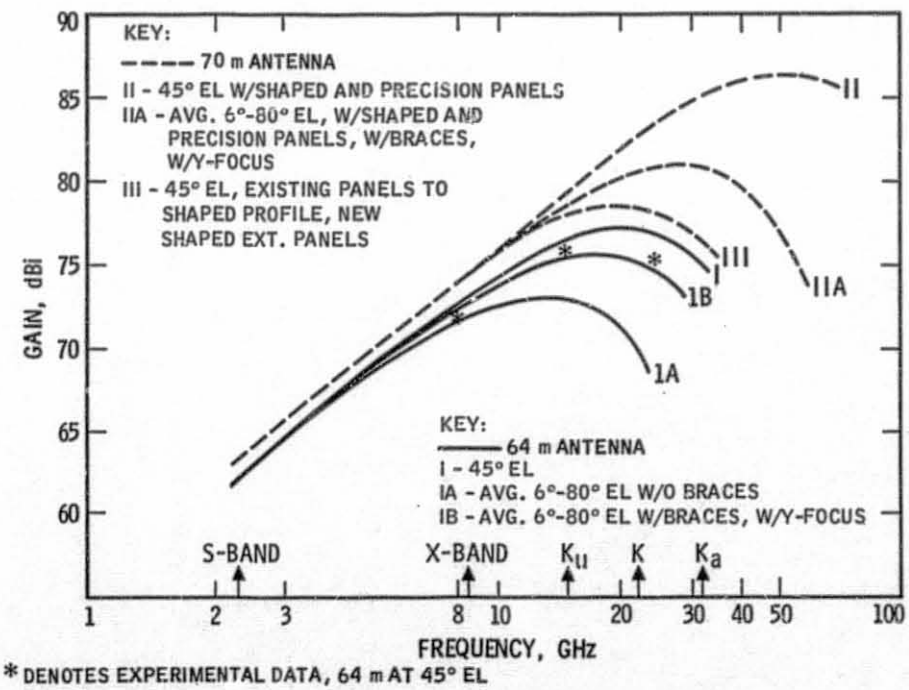

Fig. 10-10. Projected performance of the Deep Space Network 64-m-diameter antenna upgrade options